Exploring oleic acid for *anopheles arabeinsis* mosquito larvicidal applications

by

Farirai Ashly Matshaba

Dissertation submitted in partial fulfilment of the requirements for the degree of

MEng Chemical Engineering

In the Faculty of Engineering, Built Environment, and Information Technology

University of Pretoria, South Africa

2022

DECLARATION

I, **Farirai Ashly Matshaba, student number 19402882**, do hereby declare that this research is my original work. To the best of my knowledge and belief, it has not been previously in its entirety or in part submitted and is not currently being submitted either in whole or in part at any university for a degree or diploma, and that all references are acknowledged.

SIGNED on the 21st of October 2022.

F.A. Matshaba

EXPLORING OLEIC ACID FOR *ANOPHELES ARABIENSIS* MOSQUITO LARVICIDAL APPLICATIONS

Author: Farirai Ashly Matshaba

Supervisor: Focke,Walter Wilhelm

Degree: MEng Chemical Engineering

Department: Chemical Engineering

ABSTRACT

Malaria is a major economic and medical burden in countries where it is endemic. The world health organization (WHO) recommends indoor residual spraying (IRS) of insecticides and sleeping under insecticide treated nets (ITNs) to prevent malaria transmission. Larviciding is being considered as an additional control measure. Oleic acid (cis–9–octadecanoic acid), a plant-derived fatty acid has been found to be effective larvicide for *Aedes* and *Culex* mosquito species. However, it had not yet been explored against *An. (anopheles) arabiensis*, the principal malaria vector in South Africa. This presented the research opportunity which was pursued and reported on in this study.

Initial laboratory bioassays were performed to determine the efficacy of oleic acid on 3rd and 4th *An. arabiensis* instar. Statistical analysis indicated that oleic acid, as a free-standing oil, had an LC_{50} of 13 ppm and an LC_{90} of 31 ppm after 48 h exposure at 95% confidence interval. Rancimat analysis showed that both curcumin and eugenol, natural antioxidants, provided effective protection for oleic acid against oxidative degradation. Curcumin proved to be a better antioxidant than eugenol. The induction period (IP) exceeded 15 h at a dosage of 0.25 wt.%. The corresponding value for eugenol was IP $\approx$ 7 h at 0.75 wt.%.

Attempts were made to develop dosage forms for the oleic acid. These included, two porous matrices, i.e., activated charcoal and spent-coffee biochar. The latter was prepared by pyrolysis at 500 ℃. SEM revealed a highly porous biochar with a honeycomb-like structure.

Raman analysis confirmed successful carbonization as the spectrum was similar to that recorded for the activated charcoal. Both matrices were impregnated with oleic acid in a vacuum chamber. It proved possible to impregnate spent coffee biochar with up to 60 wt.% oleic acid. In the case of activated charcoal, a loading of up to 50 wt.% proved possible.

Oleic acid was also intercalated into layered double hydroxide (LDH) by hydrothermal reconstruction of calcined LDH. Intercalation of oleate anions into Mg/Al LDH was confirmed by XRD, FTIR, and TGA analysis. TGA analysis showed a loading corresponding to 25 wt.% oleate in the LDH. The XRD diffractogram proved intercalation of the oleic acid since the d-spacing increased from 0.76 nm for pristine LDH, to 3.65 nm for the intercalate. SEM showed that the plate-like morphology of the LDH was recovered following intercalation.

Oleic acid was also incorporated into thermoplastic starch by twin screw extrusion. This was a nanocomposite containing nanocellulose and nano-clay at 5 wt.% nano-clay. The inclusion of the nano-clay was necessary to incorporate the oleic acid into the thermoplastic starch during processing. Loadings of up to 10 wt.% oleic acid were achieved using this extrusion-based process. FTIR confirmed the presence of oleic acid in the extruded starch strands.

Lastly, 35 wt.% oleic acid-in-water emulsions were prepared using a modified sorbitan monooleate-based emulsifier. The average particle size was determined to be 211 ± 80 nm. The emulsion was relatively stable as the zeta potential was -56 ± 10 mV, measured after four weeks of ageing.

The utility of these dosage forms was evaluated using large glass containers filled with 3 L of water. Sufficient dosage form was added to release up to 500 ppm of oleic acid into the water. Water was sampled from the bottom of the containers and laboratory bioassays were performed on a weekly basis. Only in the case of the oleic acid-in-water emulsion was an acceptable mortality of the larvicides attained, i.e., > 90%. However, it took three weeks before this was achieved. None of the other dosage forms proved effective. Potential reasons for this failure are discussed.

Keywords: oleic acid, arabiensis, larvicidal, bioassay, spent coffee grounds, porous, antioxidant, emulsion, layered double hydroxide, mosquito

DEDICATION

To my young brother Tino, always remember, *your fears are just clues of unclaimed opportunities, pursue your fears with unfeigned determination and zest!*

ACKNOWLEDGEMENTS

I would want to sincerely appreciate the unequalled guidance, support, and mentorship from my supervisor Prof. W W Focke throughout the duration of my study. This work also took collective effort and workmanship from selfless individuals, and it thus suffice to acknowledge their varying contributions not in any specific order.

To my parents and siblings, thank you all for your emotional support.

TABLE OF CONTENTS

LIST OF FIGURES

LIST OF TABLES

LIST OF SYMBOLS AND ABBREVIATIONS

WHO	World Health Organization
IRS	Indoor residual spraying
ITNs	Insecticide Treated Nets
An.	Anopheles
Ae.	Aedes
LC$_{50}$	Lethal concentration for 50 % mortality
LC$_{90}$	Lethal concentration for 90 % mortality
DDT	Dichloro-diphenyl-trichloroethane
FAME	Fatty acid methyl ester
BDE	Bond dissociation enthalpy
LDH/s	Layered Double hydroxide/s
FTIR	Fourier-transform infrared spectroscopy
SEM	Scanning Electron Microscopy
TGA	Thermogravimetric analysis
XRD	X-Ray Diffraction
OA	Oleic acid
SMO	Sorbitan monooleate
SCGs	Spent coffee grounds
PSCG	Pyrolyzed Spent Coffee grounds (Spent coffee biochar)
AC	Activated charcoal
ICP	Inductively coupled plasma spectroscopy

DISSERTATION OUTLINE

This research work comprises of five chapters. Contributions and insights from previous research are acknowledged as references. To help further understand this work, supplementary material is included at the end as appendices.

Chapter 1: This serves as the prelude to this work which outlines the aim and objectives of this research. In a nutshell, it addresses why, and how this research was conducted.

Chapter 2: To successfully conduct this research, a focused study on the review of literature considered vital for this work is covered in this section. The approach in this literature review was to determine existing literature, critique it, and establish gaps and find ways to exploit the information. This section commences with malaria vectors, mosquito lifecycle, malaria vector control, and larviciding as a supplementary control measure. Plant-based oils as mosquito larvicides were covered leading to oleic acid being singled out as an environmentally safe, sustainable, and economic option. No previous work has been done utilizing oleic acid as a larvicide for *An. Arabiensis* the principal malaria vector in South Africa. Natural antioxidants, eugenol and curcumin were identified as potential oleic acid antioxidants. The section concludes by considering literature on LDHs, porous matrices, starch, and emulsion-based systems.

Chapter 3: This section covers the experimental design and framework i.e., raw materials, synthesis methods and the characterization techniques utilized. An interesting finding of note was that organoclay addition at 5 wt.% prevented oleic acid exudation during twin screw extrusion of thermoplastic starch-nanocellulose reinforced nanocomposites.

Chapter 4: The findings from this work are presented in this section. The findings are discussed and validated with previous work where applicable. Key findings and contributions of this work are reported here. They include the larvicidal efficacy of oleic acid against *An. arabiensis* larvae; the complex porous morphology of spent coffee biochar; the antioxidant effect of curcumin, and the residual effect of the emulsion-based slow-release delivery system.

Chapter 5: In this section the results are summarized, the main conclusions are presented and recommendations for future extension of the work are made.

CHAPTER 1: INTRODUCTION

1.1 Background

Mosquitoes serve as vectors of deleterious pathogens to humans causing diseases like malaria, West Nile virus, yellow fever, Chikungunya, dengue, filariasis and Zika virus. In 2020, the global malaria death toll was 627 000 with more than half of the deaths recorded from Africa (World Health, 2021). The World Health Organization (WHO) recommends indoor residual spraying (IRS) of synthetic insecticides and sleeping under insecticide treated nets (ITNs) to interrupt malaria transmission. Alongside prompt and effective treatment, these strategies have averted many malaria cases and fatalities across the African continent. However, synthetic insecticides present an environmental challenge and insecticidal resistance is a growing concern (Ranson & Lissenden, 2016). Furthermore, some mosquito species like *An. arabiensis* are exophagic. Hence, outdoor biting defines the limit of what is achievable with IRS and ITNs (Kibret & Wilson, 2016; Mburu *et al*, 2019). The challenges and limitations of synthetic insecticides necessitates supplementary measures for malaria vector control.

Larviciding is an established supplementary vector control method which, when effectively utilised, lowers adult mosquito populations (Fillinger & Lindsay, 2011; World Health, 2013). Plant essential oils have been investigated as potential mosquito larvicides mainly against *Aedes* and *Culex* species (Benelli *et al*, 2017; Pavela, 2015; Senthil-Nathan, 2020). A review by Pavela *et al* (2019b) presents more than 400 plant extracts as mosquito larvicides and 29 highly potent with LC_{50} (lethal concentration for 50 % mortality) below 10 ppm. The efficacy of plant extracts varies with the geographic origin, type, and part of the plant, as well as the solvent used for extraction (Farag *et al*, 2021; Ghosh *et al*, 2012; Johnson *et al*, 2018; Sigamani *et al*, 2020). There may be some challenges to industrialise some of these plant extracts.

Oleic acid (cis–9–octadecanoic acid) is a naturally abundant mono-unsaturated fatty acid which is a main constituent of many vegetable oils. This food-based additive has been proven to have high larvicidal potency. Oleic acid (OA) tests against *Culex quinquefasciatus, Ae. aegypti* and *An. stephensi* proved effective with LC_{50} below 10 ppm (Chellappandian *et al*, 2022; de Melo *et al*, 2018; Rahuman *et al*, 2008). In addition, oleic acid also possesses ovipositional repellent activity against *Culex quinquefasciatus* (Hwang, Schultz & Mulla,

15

1984) and was established to be safe to non-target mosquito predators (Chellappandian *et al*, 2022).

There is a knowledge gap on the larvicidal potency of oleic acid against *An. arabiensis*, the principal malaria vector in South Africa. Furthermore, none of the work on laboratory bioassays of oleic acid considered residual capacity, a prime factor to establish its suitability for field evaluations (Shaalan *et al*, 2005). However, oleic acid is prone to oxidative degradation and is less dense than water. When applied as a free-standing oil, it will float on the surface affecting other organisms on the air-water interface (World Health, 2013).

The controlled release of oleic acid in aqueous environments has not yet been reported. This aspect was addressed to ensure the efficacy of oleic acid for larvicidal applications, over extended periods of time. Therefore, various slow-release mechanisms were considered. Porous matrices i.e., activated charcoal and spent coffee grounds (SCGs) biochar can be impregnated with oleic acid and utilised as slow-release matrix for larvicidal bioassays. This study included the possibility of using SCGs as a reservoir for the active. It is a highly abundant renewable by-product of coffee brewing that is disposed of in landfills (McNutt & He, 2019). The oxidative stability of oleic acid can be improved by adding natural antioxidants (Varatharajan & Pushparani, 2018). Layered double hydroxides (LDHs) can intercalate oleate anions and thereby improve the oxidative stability (Blasi *et al*, 2021). The stability of LDHs is pH dependent. Therefore, it was anticipated that as it decomposes in water, it will slowly release the intercalated anions.

Oleic acid can also be trapped in water soluble polymers. Presently, thermoplastic starch/nanocellulose reinforced biodegradable polymer matrix was considered. This choice was informed by oleic acid being known to form inclusion complexes with starch which protects against thermal and oxidative degradation (Marinopoulou *et al*, 2016b). Such nanocomposites are easily prepared by twin screw extrusion. The pellets obtained from such a process will dissolve in water to progressively release the oil.

Emulsion-based systems provide another alternative. Interestingly, oleic acid-based emulsifiers are available (e.g., sorbitan monooleate) and suitable for the preparation of emulsion based larvicidal systems. Formulation of emulsions is less energy intensive and allow formulation of concentrated delivery systems which makes it economically attractive.

16

1.2 Aims

To establish the larvicidal efficacy of oleic acid on *An. arabiensis* using LC_{50} and LC_{90} as the measure. To develop an oleic acid-based slow-release system as a larvicide with residual efficacy exceeding four weeks.

1.3 Objectives

- Identify and investigate potential oleic acid natural antioxidants.
- Conduct laboratory bioassays according to WHO guidelines to establish the LC_{50} and LC_{90} of oleic acid as a free-standing oil on *An. arabiensis* 3rd and 4th instar larvae.
- Explore a range of possible oleic acid-controlled release delivery systems including:
  - Porous carbon matrices i.e., activated carbon and spent coffee biochar
  - Oleic acid intercalated layered double hydroxides (LDHs).
  - Thermoplastic starch/nanocellulose reinforced nanocomposite
  - Oleic acid emulsions
- Characterize raw materials and prepared samples using X-Ray diffraction (XRD), Fourier transform infrared spectroscopy (FTIR), Raman spectroscopy, scanning electron microscopy (SEM), thermogravimetric analysis (TGA), optical microscopy and the particle size analysis and zeta potential.
- To determine the residual efficacy of oleic acid-controlled release delivery systems by performing laboratory bioassays for a period of five weeks.

CHAPTER 2: LITERATURE REVIEW

2.1 Malaria vectors

Malaria is caused by protozoan *Plasmodium spp.* parasite transmitted through the bites of infected female *Anopheles* mosquitoes. There are four species of plasmodium: *P. malariae, P. vivax, P. ovale and P. falciparum* (Becker *et al*, 2010). Out of more than 400 different species of A*nopheles*, only 30 are malaria vectors (World Health, 2020). Members of the A*nopheles gambiae s.s, Anopheles arabiensis* (of the *An. gambiae* complex) and *Anopheles funestus* are undoubtedly the most prevalent vectors which cause the high morbidity and mortalities in Southern Africa due to malaria infections (Brooke *et al*, 2013; Mharakurwa *et al*, 2012; Nkya *et al*, 2022; Service, 1980).

2.1.1 The lifecycle of a mosquito

Mosquitoes pass through four stages in their life cycle from eggs hatching into larvae, then pupae which metamorphosise and emerge as adult mosquitoes. The first three stages are waterborne whilst the last and troublesome adult stage is terrestrial. **Figure 2.1** shows the stages of the mosquito lifecycle.
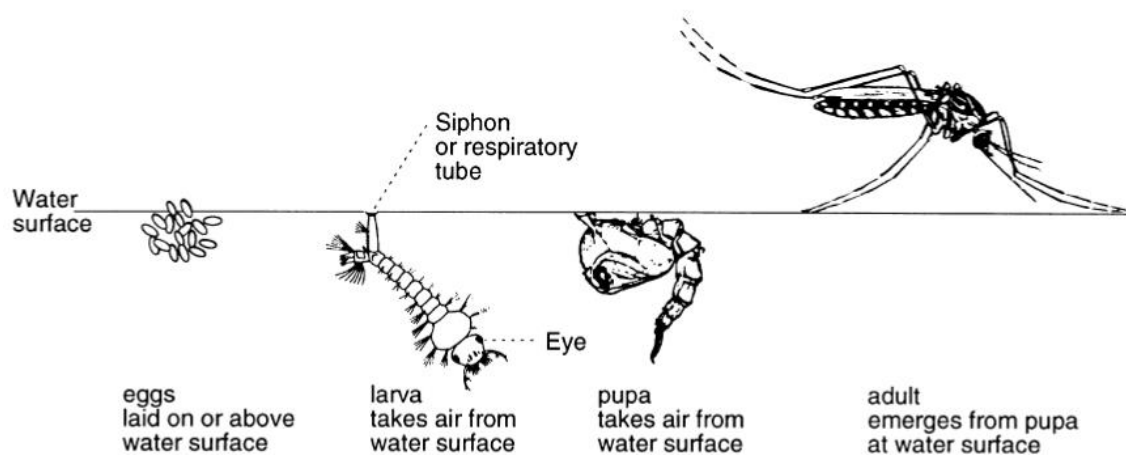
Figure 2.1: Mosquito life cycle reprinted from Rozendaal (1997) with permission from World Health Organisation

a. Eggs

The female mosquito lays eggs on the water surface either singly (*Anopheles*) or in attached groups called rafts (*Culex, Uranotaenia, Coquillettidia, Orthopodomyia* and subgenus *Culiseta*) (Becker *et al*, 2010). A gravid adult female *anopheles* mosquito lays on average 30-

18

300 eggs per oviposition which occurs two to four days (or more for cool temperatures) after getting a protein blood meal (Service, 1980). The hatching process is dependent on temperature conditions with larvae hatching after a day or two.

b. Larvae

Mosquito larvae are also known as wigglers (Karunamoorthi, 2011) from their characteristic behaviour of diving into deeper parts of water when disturbed. *Anopheles* larvae do not have a respiratory tube and to breathe they lie parallel to the water surface. Mosquito larvae develop through four instars or stages before reaching the pupal stage. Larvae instar can be identified through the size of the head capsule as a morphometric indicator (Becker *et al*, 2010).

c. Pupae

The pupae are comma shaped also referred to as tumblers due to rolling or tumbling action escaping to deeper water when disturbed (Foster & Walker, 2022). No feeding occurs during the pupal stage which usually last about two days with variations due to temperature (reduced at high temperature or extended at lower temperatures) after which the cuticle splits and an adult emerges (Becker *et al*, 2010).

d. Adult mosquito

The mosquito life cycle completes after a week though it may require more time in cooler temperatures (10-14 days). Upon emerging, the male mosquito requires about 24 hours to rotate their hypopygium through 180° before they become sexually active (Becker *et al*, 2010). Hence, they are the first to emerge. Male mosquitoes survive only on sugary diet like nectar and lives for about 1 week. Though female mosquitoes can feed on sugary sources, their diet requires blood supplied protein to develop their eggs. Mating occurs shortly after emergence of female mosquito when it flies into a swarm of male mosquitoes. During their lifespan, female mosquitoes mate just once and store sufficient sperm to fertilize several egg batches (Dahalan *et al*, 2019).

The female mosquito antennae aid to locate blood meals (by the exhaled carbon dioxide and other trace odours) and aquatic places for oviposition (Singh *et al*, 2021). Female mosquitoes have a lifespan of one month or more. Their survival is subject to humidity, temperature, dodging blood host defense mechanisms and malaria insecticidal control measures. *Anopheles* mosquitoes rest with the abdomen suspended in the air. They possess long palps

are the same length as their proboscis which makes them look peculiar compared to other mosquitoes (Becker *et al*, 2010). The flight range of adult *Anopheles* mosquito is typically not more than three kilometres from the breeding site (World Health, 2005b).

2.2 Malaria epidemiology in South Africa

An. arabiensis of the *An. gambiae* complex (Brooke *et al*, 2013) is the principal vector for malaria transmission in South Africa though *An. funestus* group has been involved in epidemics and outbreaks (NICD, 2019). An entomological surveillance conducted in a rural village of Mamfene, Mkhanyakude district, KwaZulu-Natal province showed that *An. parensis* is the major vector of the *An. funestus* group (Burke *et al*, 2019a). *An. rivulum* and *An. vaneedeni* of the *An. funestus* group are postulated to play a minor role towards malaria transmission in South Africa (Burke *et al*, 2017; Mouatcho *et al*, 2018). *An. funestus* is also linked to pyrethroid resistance in South Africa (Hargreaves *et al*, 2000).

Malaria transmission is mainly reported in the low altitude areas of Mpumalanga, KwaZulu-Natal, and Limpopo provinces. Malaria cases and deaths in South Africa recorded from 2000 to 2018 are presented in **Figure 2.2** below. In South Africa, malaria is seasonal, being most prevalent from September to May. *P. falciparum* is the prime cause of severe malaria with fatalities (NICD, 2019; Raman *et al*, 2016). Burke, Brooke & Duncan (2019b) established that metabolic rates for both *An. arabiensis* and *An. Parensis* do not vary with seasonal changes. However, malaria transmission is low in winter, and this might be associated with lower population densities.
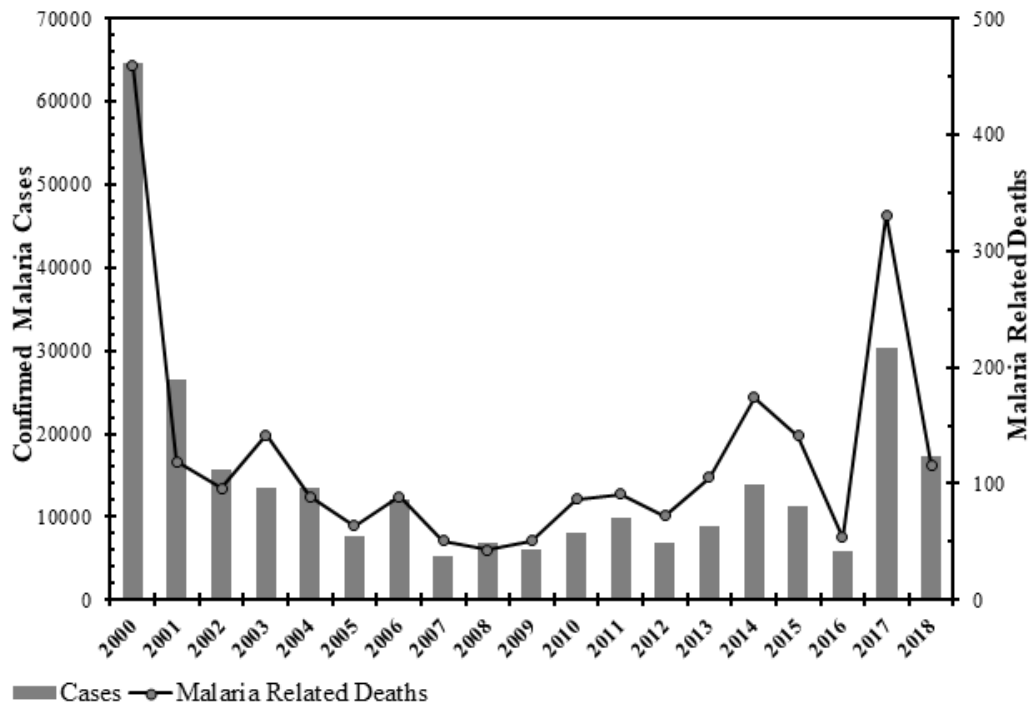
Figure 2.2: Total malaria cases and deaths from 2000 – 2018 in South Africa adapted from NICD (2019)

2.3 Mosquito vector control

Vector control is necessary to prevent the proliferation of malaria by the mosquito bites. The World Health Organization, (WHO) recommends indoor residual spraying (IRS) and sleeping under ITNs as the prime interventions to help prevent malaria transmission (World Health, 2019). IRS targets the mosquitoes which rests on walls after feeding. The chemical insecticides used for IRS include organophosphates, organochlorides, carbamates and pyrethroids (Ranson & Lissenden, 2016). The use of the organochloride, dichloro-diphenyl-trichloroethane (DDT) dates to 1945 and has been successfully used to reduce malaria transmission (Karunamoorthi, 2011). Mosquito bites can also be prevented using synthetic or natural repellents as well as insecticide vaporisers in the form of mosquito coils, electric liquid vaporiser and vapour emitting mats.

2.3.1 Larviciding

Larviciding constitutes the application of toxic agents (larvicides) to the breeding sites to combat mosquito larvae thereby reducing adult emergence. Larvicides can work as stomach poison upon ingestion, contact poison, growth regulator or a biological control agent (World Health, 2013). An effective larvicide should combine several modes of action i.e., tracheal

21

flooding, chemical toxicity to larvae and interference with the water surface properties (Corbet *et al*, 1995).

2.4 Plants extracts as potential larvicides

Much research has been conducted and is underway to explore the potential of plant-derived products as larvicides against different mosquito species. This is due to the health and environmental challenges posed by the repeated use of synthetic based products. Fenthion for one, proved to be an ecological risk to the Nile tilapia fish (Jayasundara & Pathiratne, 2008). In contrast, plants extracts are environmentally benign, safe to non-target aquatic species and rapidly degrade in the natural environment (Govindarajan *et al*, 2016a).

Plant extracts are multipurpose leading to cuticle disruption, fecundity reduction, and inhibiting respiration (Pavela, 2015). Exposure to extracts can also lead to weaker emerging adults laying fewer eggs with reduced hatching rates (Silva *et al*, 2019). A review by Pavela *et al* (2019b) suggests that more than 400 plant species have been investigated as potential mosquito larvicides. Out of these at least 29 proved to be highly effective for mosquito genera *Anopheles*, *Aedes* and *Culex* with LC_{50} less than 10 ppm. Only three studies by Karunamoorthi & Ilango (2010), Andemo *et al* (2014) and Muema *et al* (2016) covered *An. arabiensis,* the principal vector in South Africa and none reported an LC_{50} less than 10 ppm. Larvicidal effects of plants extracts on *An. arabiensis* were also covered in four articles (Edriss *et al*, 2013; Elimam *et al*, 2009; Mavundza *et al*, 2016; Mavundza *et al*, 2013). The best results from these previous investigations on *An. arabiensis* by Andemo *et al* (2014) reported an LC_{50} of 15 ppm.

Generally, most plant extracts with larvicidal potency emanate from the Lamiaceae, Apiaceae, Asteraceae, Piperaceae and Fabaceae botanical classes (Pavela *et al*, 2019b; Piplani *et al*, 2019). The response to plant extracts varies with mosquito species with *Aedes* being less vulnerable than *Culex* and *Anopheles* larvae (Elimam *et al*, 2009; Karthi *et al*, 2020; Shaalan *et al*, 2005). A study by Karthi *et al* (2020) also proved that the potency varies with the solvent used. Acetone extracts achieved best results with a composition comprising of eicosanoic acid, cis-9-hexadecenal, 1-hexyl-2-nitrocyclohexane, oleic acid and di-N-decylsulfone. Sigamani *et al* (2020) in their study, obtained better results from a chloroform extract compared to methanol although hexadecanoic acid, oleic acid and β-sitosterol were identified in both extract portions. Dey *et al* (2020) and Farag *et al* (2021) in their studies also

22

identified both hexadecanoic acid and oleic acid as constituents of their effective plant extracts compositions.

2.5 Essential oils as larvicides

Essential oils are concentrated lipophilic complex mixtures of volatile liquids which are products of secondary plant metabolism with a distinctive scent (Pavela, 2015; Yeshi & Wangchuk, 2022). Their constituents are, in the main, monoterpenes and sesquiterpenes with minor components which can be aliphatic compounds and phenylpropanoids (Benelli & Mehlhorn, 2018). The mode of action for essential oils is ascribed to neurotoxic action which is facilitated by the inhibition of the acetylcholinesterase (AChE) (Rattan, 2010). This results in accumulation of acetylcholine which triggers a state of perpetual stimulation and excitation resulting in death (Casida & Durkin, 2013).

As early as 1989, limonene, the chief ingredient of citrus essential oil, was shown to be an oviposition deterrent against *Culex quinquefasciatus* and was toxic to its 4th instar larvae with LC_{90} of 53.8 ppm after 24 hours (Kassir *et al*, 1989). In another study, R- and S-limonene demonstrated excellent larvicidal activity against the 3rd instar larvae of *Ae. aegypti* with LC_{50} of 27 and 30 ppm respectively (Santos *et al*, 2011). Cheng *et al* (2004) investigations of essential oils from leaves of C*innamomum osmophloeum* on *Ae. Aegypti*. It showed that the cinnamaldehyde chemotype was the most effective with LC_{50} of 36 ppm. Pure ingredients, cinnamaldehyde, eugenol, anethole and cinnamyl acetate had LC_{50} values of 29, 33, 42 and 33 ppm respectively. Thus, pure cinnamaldehyde proved slightly more effective than the cinnamaldehyde type EO.

However, it is not always the case that the pure ingredient will result in a higher efficacy. Pellets containing Insect Killer Highly Concentrate, (IKHC) reckoned to have geraniol as the main active ingredient proved more lethal than pure geraniol when tested with *Aedes albopictus* (Chuaycharoensuk *et al*, 2012). Mdoe *et al* (2014) investigated the same Essential oils of C*innamomum osmophloeum* against *An. gambiae s.s.* and concluded that mortality is concentration and time dependent. The abundant active ingredient was identified as trans-cinnamaldehyde constituting 70.2 % of the mixture. The LC_{50} values for laboratory and field studies were established to be in the range of 22 - 58 µg/ml and 12 - 64 µg/ml respectively.

Govindarajan *et al* (2016a) found that *Pinus kesiya* essential oil was safe against three aquatic non-target species. The main constituents were identified as α-pinene, β-pinene, myrcene and germacrene D. In a different study, Govindarajan *et al* (2016b) also investigated *Plectranthus*

23

barbatus essential oil and their chief isolates on *An. subpictus* larvae. The key isolates, eugenol, α-pinene and β-caryophyllene were more effective than the EO against 3rd instar with LC$_{50}$ of 25, 32 and 42 µg/ml respectively. Larvicidal activity of different monoterpenes were also investigated on 3rd instar of *An. gambiae s.s.* by Kweka *et al* (2016). Perillyl alcohol and isopulegol had the best results with LC$_{50}$ values after 24 h of 18 and 49 mg/L respectively. Limonene had low toxicity with LC$_{50}$ value of 270 mg/L after 24 hours. Essential oils of clove and cinnamon were investigated against 3rd instar of *An. gambiae* by Thomas *et al* (2017). Their chemical compositions are shown in **Table 2.1**. Cinnamon EO had better efficacy than clove EO with LC$_{50}$ value of 12 compared to 18 µg/ml.

Table 2.1: Chemical composition of the cinnamon and clove essential oil (Thomas *et al*, 2017)

Cinnamon essential oil		Clove essential oil	
Compound	Composition (%)	Compound	Composition (%)
Eugenol	96.5	Eugenol	99.14
β-Linalool	3.5	Methyl salicylate	0.13
		Phenol, 2-methoxy-4-(2-propenyl)-acetate	0.45
		Phenol, 2-methoxy-4-(2-propenyl)-	0.17
		Others	0.11

Pavela (2015) reviewed larvicidal essential oils with LC$_{50}$ ≤ 100 ppm and with known composition. Of the 122 plant species considered, none were tested on *An. arabiensis*. Only five articles reported larvicidal activity of essential oils on *An. arabiensis* (Damtie & Mekonnen, 2021; Karunamoorthi *et al*, 2014; Maharaj *et al*, 2012; Massebo *et al*, 2009; Nanyonga *et al*, 2012). The best results were reported by Karunamoorthi *et al* (2014) with an LC$_{50}$ of 14 ppm. Only Nanyonga *et al* (2012) reported the chemical composition of the essential oil they studied. It comprised monoterpenes, sesquiterpenes and 3.5 % hexadecanoic acid as the major fatty acid. In a study by Maharaj *et al* (2012), essential oils of *Toddalia asiatica* leaves from South Africa were proven to be most effective against *An. arabiensis* though their composition was not evaluated. In a different study by Liu *et al* (2013), *Toddalia asiatica* roots essential oils from China constituted of D-limonene, geraniol, and isopimpinellin as the principal components. It was established in the same study that the

24

isolated compounds in the order, D-limonene, geraniol, and isopimpinellin outperformed the essential oils of *Toddalia asiatica* roots on *Aedes albopictus* larvae.

2.5.1 Effect of chemical structure on the potency of essential oils

Various postulates have been put forward regarding the factors enhancing the potency of the compounds investigated as mosquito larvicides. Kweka *et al* (2016) alluded to the presence of a double bond, oxygen and their positioning affecting the potency of the chemical compound. Dias & Moraes (2014) in their review of essential oils as larvicides for *Ae. aegypti* highlighted several articles which proposes various factors. It is suggested that the toxicity of aromatic compounds exceeds that of aliphatic compounds. Furthermore, it was also suggested that hydrogenation of double bonds reduces lipophilic character. This limits passage through cuticle of larvae. An aliphatic aldehyde conjugated to an aromatic ring is deemed to be extremely potent (Dias & Moraes, 2014; Perumalsamy *et al*, 2015).

The number of conjugated double bonds strengthens potency (Santos *et al*, 2011) whilst hydroxyl groups reduce potency (Barbosa *et al*, 2012) as lipophilicity is key for larvicidal potency (Santos *et al*, 2011). This observation was derived from the investigation on 3rd instar larvae of *Ae. aegypti* which proved that p-cymene is more potent ($LC_{50} = 51$ ppm) than thymol ($LC_{50} = 81$ ppm) which possesses a hydroxyl group on its chemical structure (Santos *et al*, 2010). After investigating acyclic monoterpenes and their saturated derivatives against 4th instar *Culex pipiens* larvae, Michaelakis *et al* (2014) concluded that linear isomers are more toxic than their corresponding branched-chain alcohols. To determine synergistic and antagonistic behaviour between plant isolates, their chemical structures should be considered. However, it is quite clear that the efficacy of essential oils as mosquito larvicides varies with the mosquito species.

2.6 Challenges of plant extracts and essential oils as larvicides

Plant extracts and lipophilic essential oils (Pavela *et al*, 2019a) are hydrophobic (Reis *et al*, 2022) therefore are poorly water soluble. In addition, essential oils are highly volatile with very low residual capacity when exposed to the natural environment. Moreover, the efficacy of the plant extracts as larvicides varies with plant type and parts, climatic and environmental conditions (Ghosh *et al*, 2012) as well as the extraction solvent used (Farag *et al*, 2021; Johnson *et al*, 2018; Sigamani *et al*, 2020). The composition of essential oils also varies, and they are produced from plants at very low yields. Hence, they tend to be very expensive

25

(Pavela, 2015). Plant oils which can be utilised as a larvicide must be safe to the environment and non-target species and be economically viable. Preferably they should have a high boiling point. With these considerations as a benchmarking standard, oleic acid seems a viable option.

2.7 Oleic acid as a mosquito larvicide

Oleic acid (cis–9–octadecanoic acid), is a naturally abundant unsaturated fatty acid and main constituent of many vegetable oils including olive oil, canola oil, and peanut oil (Huang *et al*, 2020; Stolp & Kodali, 2022). Oleic acid bioassay tests against *Culex quinquefasciatus, Ae. aegypti* and *An. stephensi* proved it to be effective with LC_{50} below 10 ppm (Chellappandian *et al*, 2022; de Melo *et al*, 2018; Rahuman *et al*, 2008). An $LC_{50} < 10$ ppm is impressive which meets the benchmark of the 29 plant extracts considered effective in the review by Pavela *et al* (2019b).

Figure 2.3 below shows that relative to their saturated equivalents, unsaturated fatty acids are more potent against *Culex quinquefasciatus* (de Melo *et al*, 2018). According to Perumalsamy *et al* (2015) larvicidal potency of oleic acid is attributed to acetylcholinesterase (AChE) inhibition. In addition, oleic acid also possesses ovipositional repellent activity against *Culex quinquefasciatus* (Hwang *et al*, 1984). It was established to be safe to non-target mosquito predators (Chellappandian *et al*, 2022). To the best of our knowledge no research was conducted on the larvicidal potency of oleic acid against *An. arabiensis*. Furthermore, none of the work on laboratory bioassays of oleic acid considered residual capacity, a prime factor to establish its suitability for field evaluations (Shaalan *et al*, 2005).
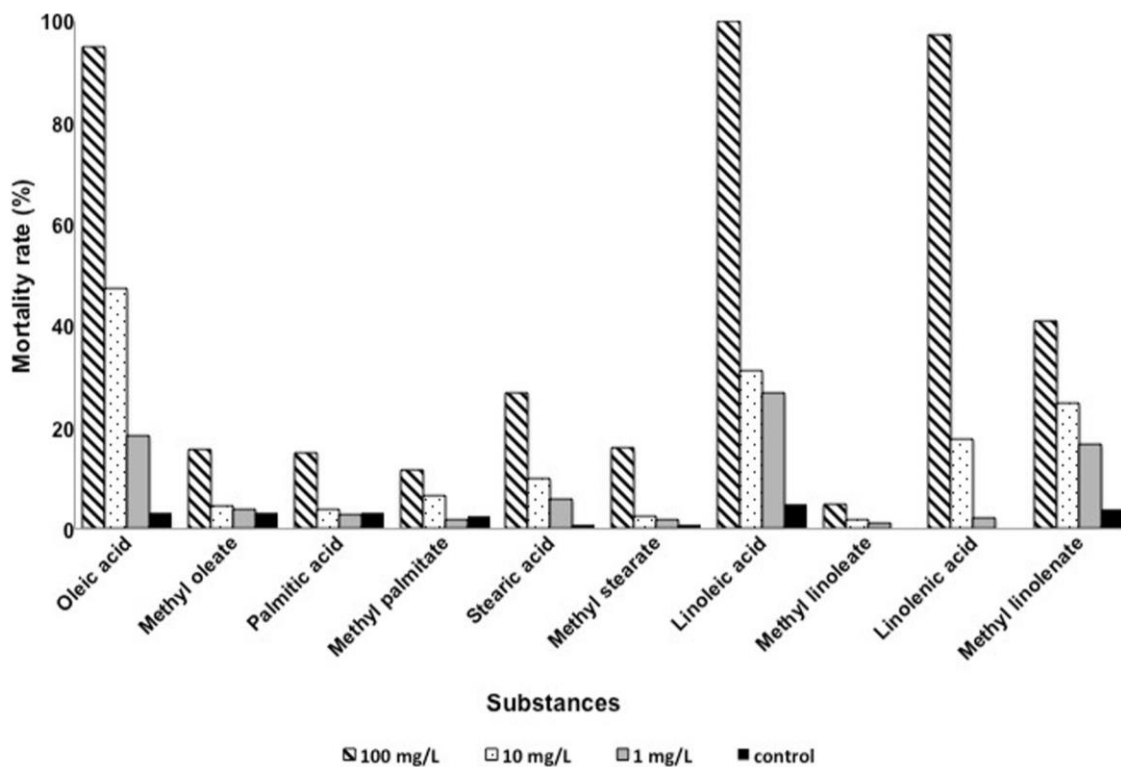
Figure 2.3: Effects of fatty acids and methyl esters on mortality (%) of 4th instar larvae of *culex quinquefasciatus* after 24 h exposure, reprinted from de Melo *et al* (2018) with permission from Elsevier

A technical grade of oleic acid can be easily acquired at an economical price. However, oleic acid is prone to oxidative degradation due to the presence of an unsaturated *cis* double bond (Kumar, 2017). Additionally, it is less dense than water. When applied as a free-standing oil, it will float affecting other organisms on the air-water interface (World Health, 2013). Various approaches can be considered to improve oleic acid availability, oxidative stability, and thereby prolong its residual capacity. Included are the use of natural antioxidants, intercalation in layered double hydroxides, trapping the oil in porous matrices, microencapsulation etc. (Blasi *et al*, 2021; Maia *et al*, 2019; Marinopoulou *et al*, 2016a; Pavela *et al*, 2019a; Varatharajan & Pushparani, 2018). Subsequent sections will explore these ideas in more detail.

2.7.1 Oxidative stability of oleic acid

Oleic acid (cis–9–octadecenoic acid) is an unsaturated fatty acid containing one C=C double bond (C18:1) which makes it susceptible to oxidative degradation when exposed to environmental stressors. Oleic acid degrades via an autocatalytic oxidation reaction resulting in discoloration of the oil, increase in viscosity and acidity as well as an increase in rancidity.

27

The autocatalytic oxidation reaction scheme is a multi-step process as shown in **Figure 2.4** (Kumar, 2017; Sharma *et al*, 2019b).

Initiation

$$RH \xrightarrow{\text{initiator}} R\bullet + H\bullet$$

Propagation

$$R\bullet + O_2 \xrightarrow{\text{fast}} ROO\bullet$$
$$ROO\bullet + RH \xrightarrow{\text{slow}} ROOH + R\bullet$$

Branching

$$ROOH \longrightarrow RO\bullet + OH\bullet$$
$$RO\bullet + RH + O_2 \longrightarrow ROH + ROO\bullet$$
$$OH\bullet + RH + O_2 \longrightarrow H_2O + ROO\bullet$$

Termination

$$ROO\bullet + ROO\bullet \longrightarrow ROOR + O_2$$
$$ROO\bullet + R\bullet \longrightarrow ROOR$$
$$R\bullet + R\bullet \longrightarrow R\text{-}R$$
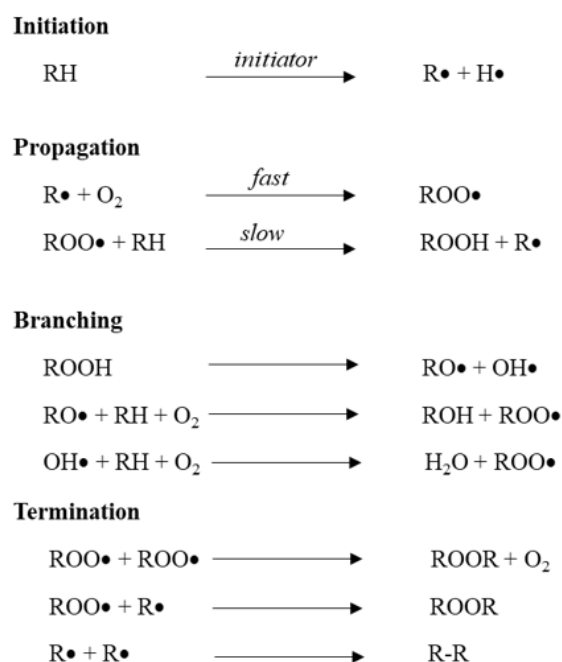
Figure 2.4: Auto-oxidation mechanism adapted from Sharma *et al* (2019b)

Free radicals are initiated by hydrogen abstraction from oleic acid through external factors such as heat and UV light (Pantoja *et al*, 2013). The free radicals rapidly react in oxygen forming peroxyl radicals which further react with oleic acid forming hydroperoxides. Hydroperoxides, after reaching a certain concentration, results in auto-catalysis, a spontaneous rapid oxidation process (Sharma *et al*, 2019b). The time required to reach this condition is commonly referred as the induction period, IP (Pullen & Saeed, 2012). The reaction only terminates after all the sample is oxidized and free radicals react to form a more stable product.

2.7.2 Antioxidants mechanisms

Antioxidants are chemical compounds which aid to interrupt, suppress and lower the rate of the oxidation process (Westhuizen, 2017). Antioxidants can be classified as either primary or secondary antioxidants. Primary antioxidants are chain breakers, free radical scavengers or quenchers which interrupts the peroxyl radical abstracting hydrogen from the propagation stage (Pisoschi *et al*, 2021). Primary antioxidants are therefore hydrogen donors (Yaakob *et al*, 2014). Primary antioxidants mainly comprise of phenolic compounds and amines. Secondary antioxidants interrupt the branching or autocatalysis stage as they form stable

28

products by decomposing hydroperoxides. Secondary antioxidants can be divalent sulphur compounds or trivalent phosphorus compounds. According to Varatharajan & Pushparani (2018), some of the key considerations when selecting antioxidants includes solubility, low bond dissociation enthalpy, high molecular weight, presence of polyhydroxy groups among others. Antioxidants can be either synthetic or naturally sourced products. Only natural antioxidants will be considered as they are environmentally safe.

2.7.3 Natural antioxidants

Plant based materials with high contents of phenolic compounds can act as natural antioxidants (Varatharajan & Pushparani, 2018). Natural antioxidants can therefore be obtained from leaves, fruits, seeds, and stems of different plants (Embuscado, 2015). They can be classified as phenols, anthraquinones, flavonoids, steroids, alkaloids, terpenoids, and their steric structures (Liu, 2022). Resveratrol, a polyphenol, dosed at 0.06 % (v/v) improved the induction period of high oleic acid peanut oil by 70 % (Huang *et al*, 2020). Eugenol and curcumin have been singled out as potential phenolic natural antioxidants since they are available in large quantities and inexpensive. In addition, curcumin is also reported to have larvicidal potency activity for *culex pipiens* (Sagnou *et al*, 2012) and for *Ae. aegypti* (de Souza *et al*, 2020) thus both curcumin and eugenol possess larvicidal potency.

a. Curcumin as a natural antioxidant

Curcumin is extracted from *Curcuma* herbs and the chief curcuminoid of *Curcuma Longa* (turmeric) rhizome (Jiang *et al*, 2021). Curcumin exists as either *enol*, (CUE) or *keto* (diketone) (CUK) form depending on the environment as shown in **Figure 2.5**. According to Rathore *et al* (2020), in non-polar and hydrophobic organic solvents, curcumin is entirely present in *enol* form. In contrast, in a polar water environment, it is in the *keto* form. Curcumin has a bond dissociation enthalpy, (BDE) of 329.9 kJ.mol^{-1} (Kirschweng *et al*, 2017) which is more than 40 kJ.mol^{-1} lower than the BDE of hydroperoxide free radicals (376 kJ.mol^{-1}) a condition stipulated for a good antioxidant according to Varatharajan & Pushparani (2018).
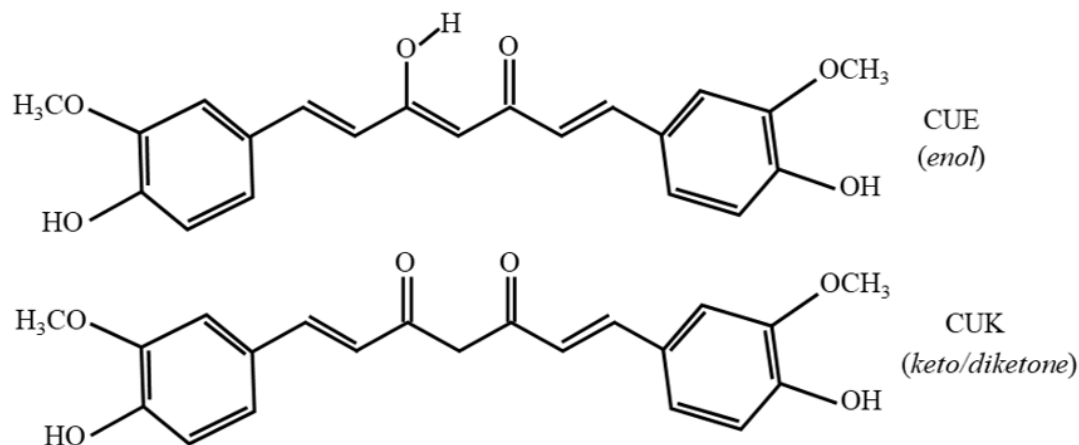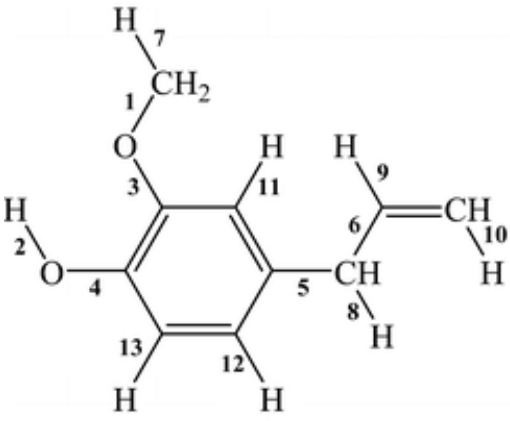
Figure 2.5: Structural isomers of curcumin, enol CUE and keto (diketone), CUK adapted from Galano *et al* (2009)

Curcumin as an antioxidant offered up to 6.8 h induction time at 600 mg.kg^{-1} dosage for fatty acid methyl esters obtained from residual cooking oil (Serqueira *et al*, 2015). In a different study by de Sousa *et al* (2014), curcumin at 500 ppm maintained an induction period of 6 h after 30 days of storage for methyl soybean biodiesel whilst at 1000 ppm the induction period was increased by up to 83 %.

b. Eugenol as a natural antioxidant

Eugenol is a phenylpropanoid mainly extracted from clove essential oils. According to Ledesma *et al* (2013), the phenolic hydrogen on eugenol as shown in **Table 2.2**, has a BDE of 87.8 kcal.mol^{-1}. This is equivalent to 367.4 kJ.mol^{-1} which is less than that of the hydroperoxides, 376 kJ.mol^{-1} (Kirschweng *et al*, 2017) hence eugenol can also be utilised as a natural antioxidant. Eugenol at 1.5 wt.% improved ethylic biodiesel induction period of up to 6 h (de Souza *et al*, 2018). In a study by Ramos *et al* (2021), eugenol as an antioxidant maintained an IP of 10.73 h at a dosage of 15 g.kg^{-1} for a commercial biodiesel after 150 days of storage.

30

Table 2.2: Chemical structure and bond dissociation energies, D_0 of Eugenol (Ledesma et al, 2013)

Structure	Bond	D_0 (kcal mol^{-1})
	1	52.2
	2	87.8
	3	97.2
	4	112
	5	82.1
	6	83.2
	7	102
	8	79.1
	9	112
	10	116
	11	117
	12	118
	13	119

2.7.4 Experimental determination of oxidative stability

There are number of parameters used to evaluate the oxidative stability of biodiesel or oils namely, acid number, viscosity, density, iodine value, induction period, peroxide value, FAME content and oil stability index among others (Yaakob *et al*, 2014). According to Pullen & Saeed (2012), the techniques used to determine the oxidative stability can be classified centred on what is measured i.e., primary or secondary oxidation products, physical properties, initial fatty oil composition (compositional analysis). The Rancimat method is an accelerated oxidation test. It is the most used standard for oxidative stability of biodiesel (Bär *et al*, 2021). The Rancimat method can therefore be utilized to evaluate the oxidative stability of oleic acid.

2.7.5 The Rancimat Method

This is a quick standard oxidation ageing experiment used to investigate the oxidative stability of biodiesel, fats, and oils. A fixed mass of the sample is placed in a reaction vessel maintained at specific temperature. Air is bubbled through the sample to initiate the oxidation

31

process. The air escapes the reaction vessel with entrained primary and secondary oxidation products mainly formic acid and acetic acid (Yaakob *et al*, 2014). Air leaving the reaction vessel is passed through deionized water in the measuring vessel as shown in **Figure 2.6**. The conductivity in the measuring vessel is continuously monitored by the conductivity cell. The induction period, IP is automatically determined by the Rancimat software from the second derivative of the conductivity versus time curve.
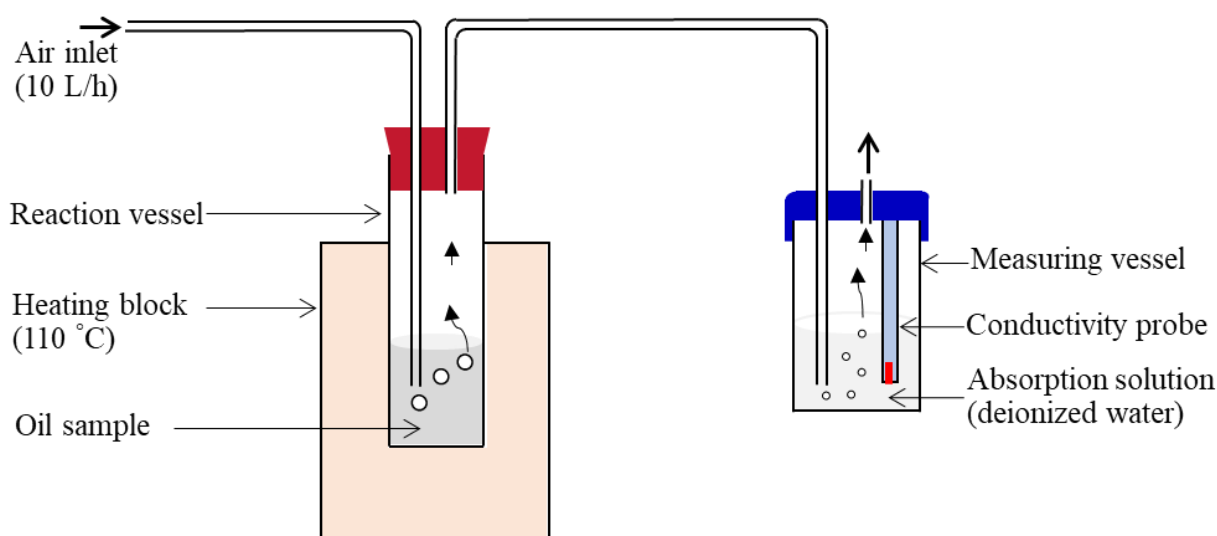
Figure 2.6: Components of the Rancimat instrument adapted from Sharma *et al* (2019b)

2.7.6 Estimation of oleic acid solubility in water

Oleic acid has very low solubility in water and is generally considered insoluble therefore a specific value could not be obtained from literature. However, ternary phase diagrams constituting of oleic acid, water and alcohol have been previously reported (Rahman, Rahman & Nabi, 2003; Santos *et al*, 2015; Zhang & Hill, 1991). Zhang & Hill (1991) measured tie lines at very low concentrations of ethanol at different temperatures. This makes their data convenient for estimating the solubility of the oleic acid in water at different temperatures. Their values, when plotted as the weight fraction of oleic acid against the mass fraction of water (only considering water and ethanol) in the aqueous phase produces straight lines as shown in **Figure 2.7**.
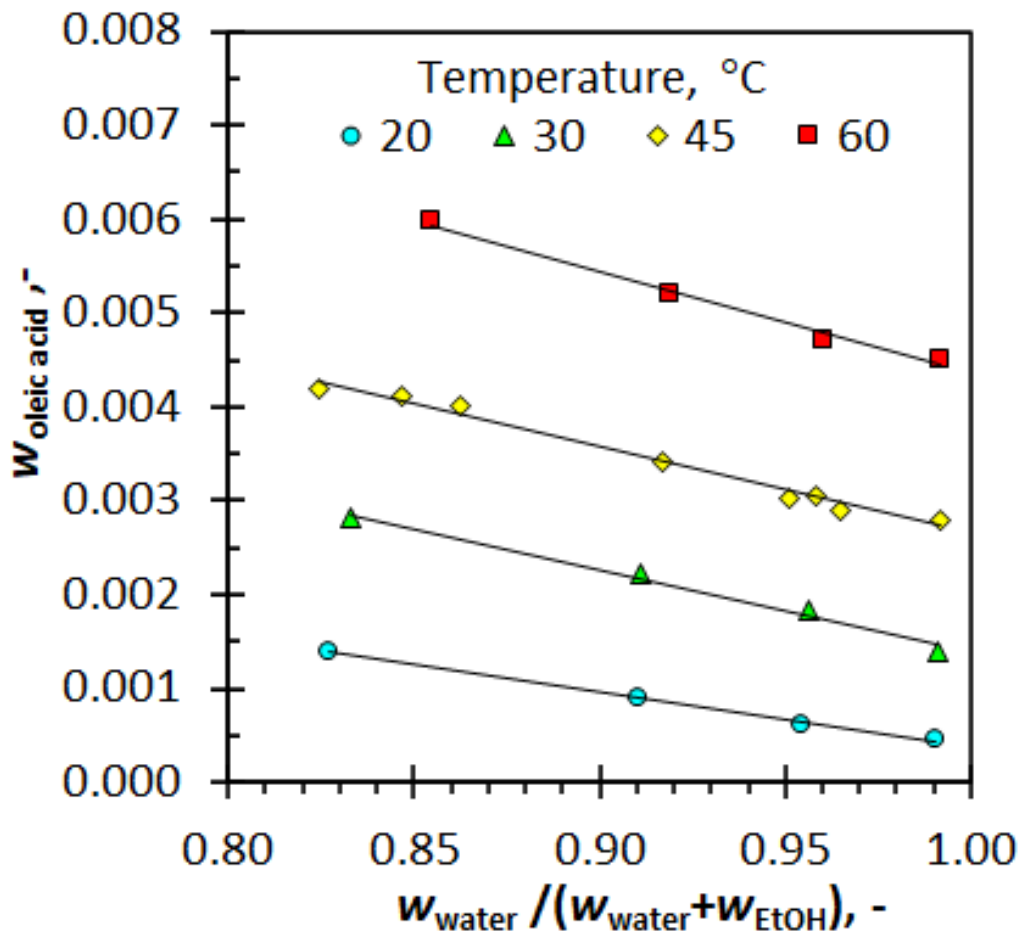
Figure 2.7: Mass fraction of oleic acid ($w_{oleic\ acid}$) against that of water with very low levels of ethanol (w_{water} / w_{water} + w_{EtOH}). Data plotted obtained from work by Zhang & Hill (1991)

A crude estimation of the solubility of oleic acid in water can then be determined by extrapolation of the lines to pure water. Oleic acid solubility in water increases linearly with the temperature as shown in **Figure 2.8**. The red mark shows the estimate at 25 °C the temperature maintained at the insectary used for the laboratory bioassays.

33
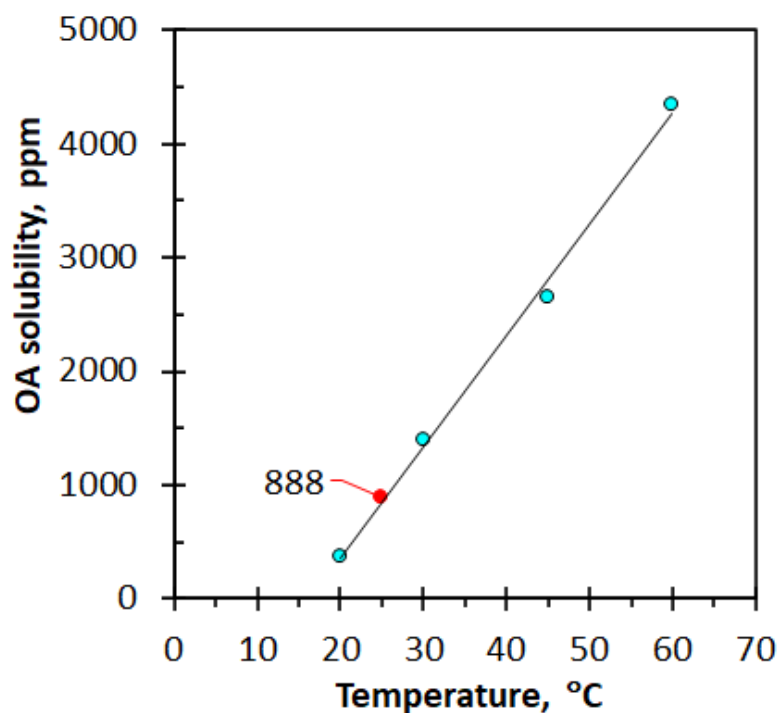
Figure 2.8: Estimated oleic acid solubility in water as function of temperature

The estimated oleic acid solubility at 25 ℃ of 888 ppm is considered as a crude estimate as the data utilised was extracted from a ternary phase diagram containing ethanol and water. The crude approximation is however way more than the LC_{50} values of oleic acid as a mosquito larvicide reported in literature of < 10 ppm (de Melo *et al*, 2018; Rahuman *et al*, 2008). However, a study by Vorum *et al* (1992) states that oleate solutions have a tendency to aggregate at concentrations less than 1 µM in phosphate buffer solution at a pH of 7.4. This suggests that the solubility of oleic acid might be very low.

2.8 Layered double hydroxides, (LDHs)

Layered double hydroxides, (LDHs) also known as anionic clays, lamellar double hydroxides or hydrotalcite like compounds belong to a family of inorganic crystalline materials. The history of the first natural LDH, hydrotalcite dates to 1842 where it was discovered in Sweden (Cavani *et al*, 1991). Due to their outstanding properties, easy of synthesis furthered by the advent of nanotechnology and the quest to develop new environmentally benign materials with novel properties, LDHs have attracted enormous attention in academia and industrial research. LDHs have been explored for their innovative application in the fields of agriculture, catalysis, photochemistry, adsorption, electrochemistry, polymer processing, drug delivery and controlled release and cosmetics among others (Benício *et al*, 2015;

34

Boumeriame *et al*, 2022; de Sousa *et al*, 2021; Donato *et al*, 2012; Fan, 2014; Huang *et al*, 2016; Kang *et al*, 2015; Kleyi *et al*, 2021; Ng'etich & Martincigh, 2021)

2.8.1 Structural arrangement of LDHs

LDHs are two dimensional (2D) nanostructured anionic clays. In principle, LDHs consists of mixed metal hydroxides layers of bivalent and trivalent cations located in brucite-like $[Mg(OH)_2]$ layers stacked by charge compensating interlayer anions and water (Kesavan Pillai *et al*, 2020). The general schematic representation of LDH structure is depicted in **Figure 2.9** with the insert showing the top layer structure. The brucite-like LDH sheets are made up of sharing edges of divalent metal hydroxide tetrahedra and the octahedral trivalent metal hydroxide (Cavani *et al*, 1991).

The hydroxide layer has a resultant positive charge as the divalent cations are substituted by the trivalent cations (Nhlapo *et al*, 2008). This net positive charge is compensated by the anions present in the galleries as illustrated in **Figure 2.9.** Their size and relative orientation determines the interlayer (basal) spacing. Water of crystallisation also occupies the interlayer space. The layered structure is maintained by Van der Waals and hydrogen bonding between the hydroxyl groups and the interlayer anions such as carbonate anions.
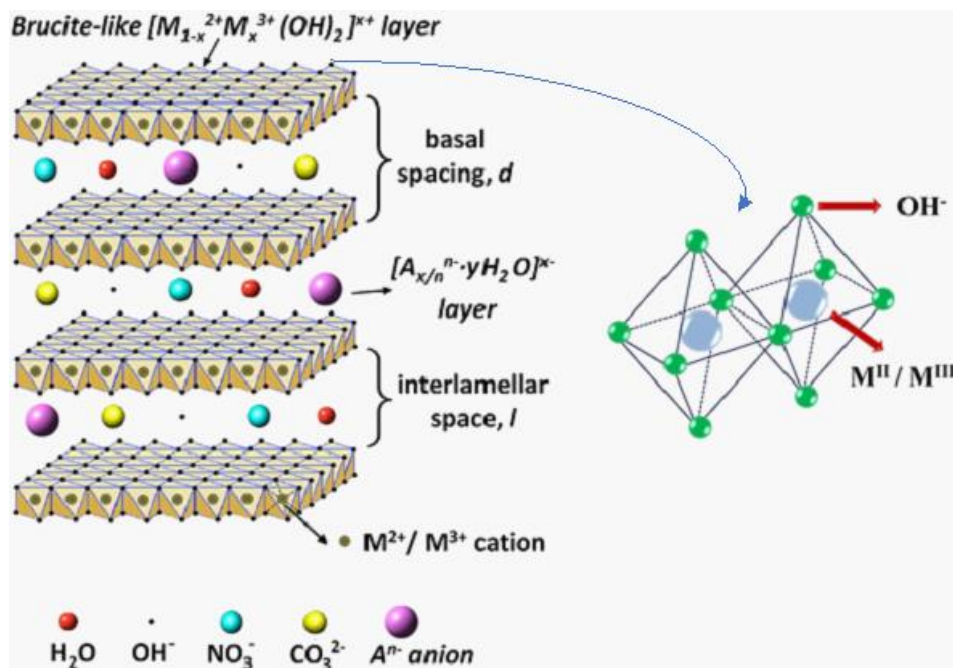
Figure 2.9: Generic schematic representation of LDH reprinted from Mittal (2021) with permission from Elsevier

The structural formula for LDH can be generalised as; $[M^{2+}_{(1-x)}M^{3+}_x(OH)_2]^{x+}[A^{n-}_{x/n}].mH_2O$, where M^{3+} and M^{2+} represents trivalent and divalent cations respectively, A^{n-} are organic or inorganic interlayer anions, $x = M^{3+}/[M^{2+} + M^{3+}]$ molar ratio ($0.2 < x < 0.33$) (Cavani *et al*, 1991; Nhlapo *et al*, 2008). The resulting $M^{2+}:M^{3+}$ ratio is therefore within the range of 2:1 – 4:1 (Theiss *et al*, 2016). However, LDH with monovalent and tetravalent cations have been reported (Poonoosamy *et al*, 2018; Zhao *et al*, 2014).

The trivalent cation radius should be almost the same as the divalent radius in order to form a stable LDH (Ng'etich & Martincigh, 2021). However, Saliba & Al-Ghoul (2016) managed to synthesise a stable cadmium-aluminium layered double hydroxide (Cd/Al LDH) though cadmium has an ionic radius significantly different from that of aluminium. The LDH cation layers are not interlinked, hence the interlayer anion can be exchanged thereby accommodating guest anions for varying applications (Theiss *et al*, 2016).

2.8.2 Layered double hydroxides synthesis

Several forms of LDHs can be synthesised either directly from solutions or indirectly using preformed LDH as the precursor. The direct synthesis methods consist of sol-gel synthesis, salt-oxide, hydrothermal synthesis, induced hydrolysis, and coprecipitation whilst the indirect synthesis methods include anion exchange and hydrothermal reconstruction method. Of these, the most commonly used methods are coprecipitation, anion exchange and hydrothermal reconstruction (Benício *et al*, 2015; Bini & Monteforte, 2018; Chaillot *et al*, 2021; Conterosito *et al*, 2018; Khorshidi *et al*, 2022; Mallakpour *et al*, 2020; Mishra *et al*, 2018; Mittal, 2021). These were considered in the present study.

    a. Coprecipitation

This is by far the most utilised method to synthesize various types of LDH (Chaillot *et al*, 2021; Ng'etich & Martincigh, 2021). This entails, slow addition of the metallic solution mixture containing M^{2+} and M^{3+} cations to a basic solution with the desired interlayer anion. The mixed metal cations solutions added should have the desired $M^{2+}:M^{3+}$ cation ratio desired in the final product (Theiss *et al*, 2016). The pH is controlled during the process by addition of an alkaline base to facilitate the precipitation of the LDH. Usually, it is NaOH though KOH and NH4OH can also be used. Basic pH is necessary but it varies with the metallic composition of the LDH (Roy *et al*, 1992).

36

Coprecipitation at low supersaturation is preferred to high supersaturation as it gives better product quality with high crystallinity (Chaillot *et al*, 2021). Low supersaturation is facilitated by slow addition (dropwise) of mixed M^{2+}/M^{3+} solution at up to 1 mL.min^{-1} (Benício *et al*, 2015). The process is conducted under an inert atmosphere and carbonate-free distilled water to avoid the formation of undesired impurities. The process is refluxed or aged at a specific temperature with constant stirring for hours to improve the quality of the final product to attain LDH with improved crystallinity and crystal size distribution (Khorshidi *et al*, 2022).

The precipitate is separated from the spent liquor through centrifugation or by a filtration process. The separated precipitate residue is rinsed to remove the by-product salt before drying to obtain the LDH final product. Reaction temperature, pH, metal precursor concentrations, ageing time and conditions affect the properties of the final product (Bukhtiyarova, 2019). Coprecipitation is a single step process which enables synthesis of large quantities for commercial applications (Kameda *et al*, 2009). Generally, LDH synthesized by the coprecipitation exhibits good structural organization and high purity.

b. Anion exchange

The anion exchange is an indirect form of LDH synthesis where pre-formed LDH with a different anion synthesised mainly by co-precipitation is added to a concentrated solution of the desired guest anion. The anion exchange process is determined by the strength of the electrostatic forces between the positively charged layers and the interlayer counter balancing anions (Daud *et al*, 2019). According to the findings of Miyata (1983) the ion-exchange of the anions follow the sequence $CO_3^{2-} > SO_4^{2-} > OH^- > F^- > Cl^- > Br^- > NO_3^- > I^-$. These findings illustrate that the divalent ions have the highest affinity to the LDH interlayer compared to monovalent ions with the carbonate ion being the strongest.

According to Sasai *et al* (2019), carbonate ions forms exceptionally strong hydrogen-bonded network with the hydrated water and hydroxyl groups in the LDH interlayer space. To use the anion exchange synthesis method, anions with weak LDH interlayer attractions like Cl^- and NO_3^- should be utilised. The metal cations involved should be stable at high pH values (Bini & Monteforte, 2018). However, anion exchange poses a processing challenge as neutral molecules and bulky anions are difficult to synthesize into the LDH interspaces via the ion-exchange method. In that case, the hydrothermal reconstruction method should be the preferred method (Kameshima *et al*, 2006).

37

c. Reconstruction route for LDHs (memory effect method)

The process entails a hydrothermal reconstruction of calcined LDH in the presence of desired guest anion solution in carbonate-free water. Carbonate based LDHs due to the favourable thermal behaviour during calcination are used as the precursor for the reconstruction method (Benício *et al*, 2015) although nitrate based LDHs can also be utilised (Kang & Park, 2022). During the hydrothermal reconstruction process, the calcined LDH is added to desired guest anion solution maintained at the desired temperature and aged under continuous stirring to ensure complete reconstitution. LDHs have very high affinity for carbonate anions. To prevent competitive carbonate intercalation which reduces product purity, carbonate-free water should be utilised, and the process performed under inert conditions (Bukhtiyarova, 2019).

Heat treatment of pristine LDH within the temperature range of 450-600 °C (Mittal, 2021) results in the loss of the interlayer water and anions forming mixed metal oxides (MMO) also known as calcined LDH or layered double oxide (LDO) (Nhlapo *et al*, 2008). The calcined LDH has an increased surface area and number of active sites. Since the LDH layers are not interlinked (Theiss *et al*, 2016), hydrothermal reconstitution of calcined LDH with desired anion solution results in a layered LDH structure. This property is known as the "memory effect" (Cavani *et al*, 1991; Mallakpour *et al*, 2020). The reconstruction process, "memory effect" is represented in **Figure 2.10**.
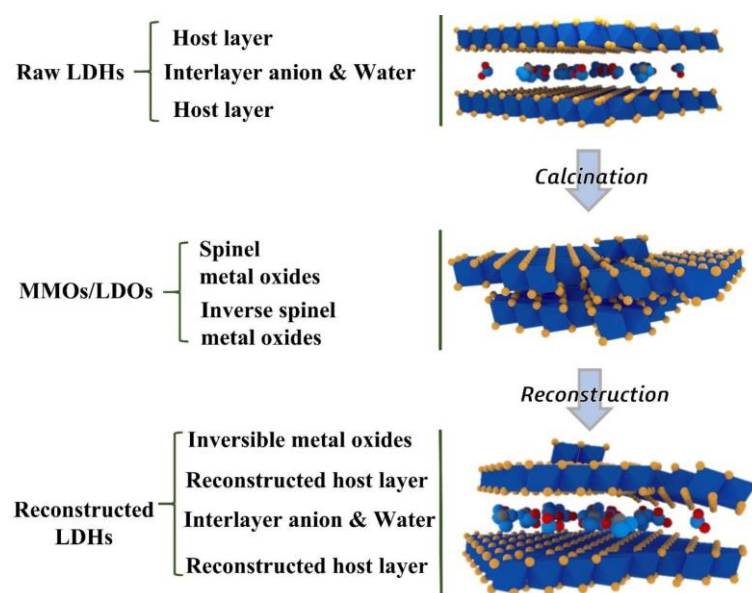
Figure 2.10: Reconstruction process of LDH by the "memory effect" reprinted from Ye *et al* (2022) with permission from Elsevier

Factors affecting the reconstruction process

The structural reconstruction process of calcined LDH varies based upon conditions such as calcining temperatures, rate, and the duration of heating (Mittal, 2021). According to (Carlino *et al*, 1996), rapid heating rate when calcining LDH reduces the quality of the final calcined product obtained hence they used a rate of 1 °C.min⁻¹ in their study. The time required for complete reconstitution of the calcined LDH is determined by the calcining temperature. Calcining below 550 °C requires 24 h, increasing to 3 days at 750 °C and only incomplete reconstruction is possible after 1000 °C (Rocha *et al*, 1999). **Figure 2.11** shows the effect of calcining temperatures on Mg/Al LDH morphology investigated by Li *et al* (2019a). As the calcining temperature increases from 350-1000 °C the particles become visibly thinner though the layered platelike hexagonal shape is continuously disrupted and no longer visible at 1000 °C. This justifies partial reconstruction results obtained by Rocha *et al* (1999) for - LDH calcined at 1000 °C.
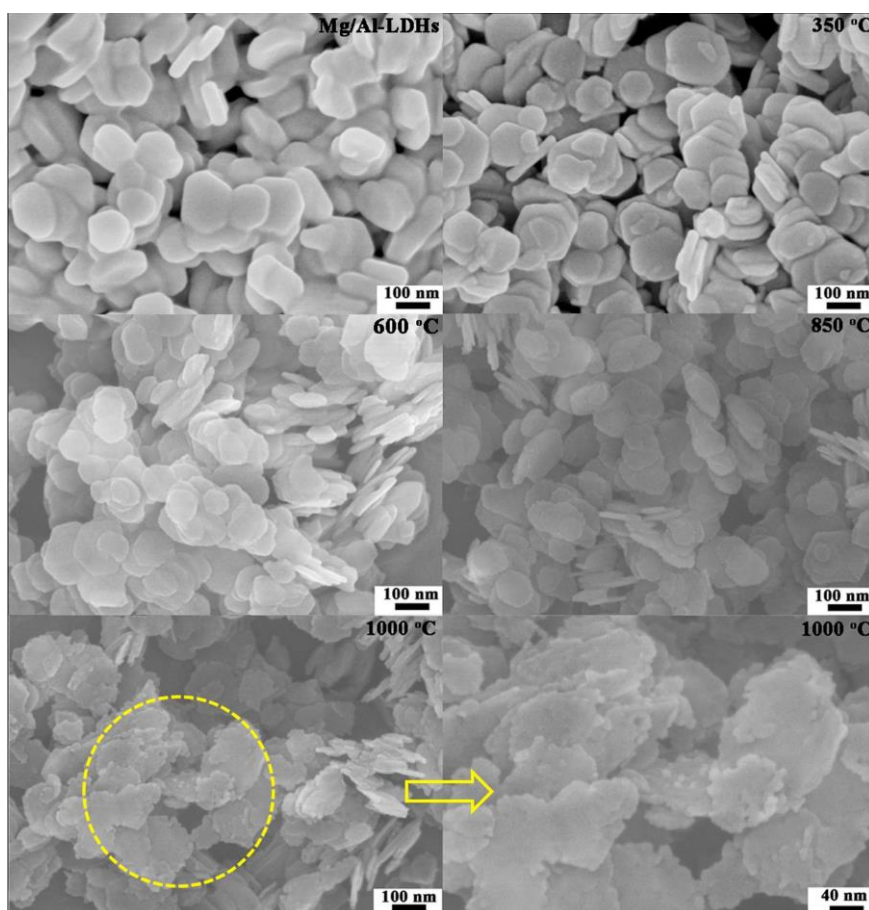
Figure 2.11: Effect of calcining temperature on MgA/Al LDH morphology reprinted from Li *et al* (2019c) with permission from Elsevier

Metal composition of the LDH also affects the "memory effect" as the resulting LDH will have varying thermal properties (Ye *et al*, 2022). Comparing NiAl and MgFe carbonate based LDHs, Meng & Yan (2017) established that in NiAl, carbonate decomposes at 365 °C with slight destruction on the layered structure at 800 °C. The MgFe carbonate LDH decomposition temperature was 380 °C and at 800 °C, the layered LDH structure is destroyed. The refluxing or ageing temperature also determines the intercalation process which varies from 60-80 °C (Bini & Monteforte, 2018; Celis *et al*, 2014; Rocha *et al*, 1999). Nhlapo *et al* (2008) established that the intercalation of lauric and stearic acids decreases and was incomplete below 60 °C and increases with temperature from 60-85 °C.

2.8.3 Layered double hydroxides as devices for controlled release

LDHs are natural alkaline and hence dissolve quickly and degrade in an acidic environment (de Sousa *et al*, 2021). The dissolution is pH dependent. Hence, this property can facilitate sustained delivery of intercalated anions. LDHs have therefore been investigated as release devices in drug delivery, cosmetic ingredients, and agriculture. They were proven to facilitate controlled release and in some cases even improve the dissolution rate and solubility of an active (Benício *et al*, 2015; de Sousa *et al*, 2021; Kesavan Pillai *et al*, 2020; Ng'etich & Martincigh, 2021; Rives *et al*, 2014). Kang *et al* (2015) investigated the release of ferulic acid intercalated into LDH via different synthesis methods. Their findings established similar cumulative release profiles of ferulic in deionised and saline water from LDH synthesised by the reconstruction method.

Methyl salicylate intercalated into MgAl LDH showed a sustained controlled release after 72 h in a phosphate buffer solution at pH of 7.4 (Mondal *et al*, 2016). In a study by Barahuie *et al* (2013), controlled release of protocatechuic acid intercalated into MgAl LDH showed pH dependent release in a phosphate buffer solution. 60 % of protocatechuic acid was released after 5 days at pH 7.4, 80 % after 2 days at pH 5.3 and 80 % released after 16.6 hours at pH 4.8. A study by Berber *et al* (2014) showed a controlled release of nitrates from MgAl nitrate based LDH which was also pH dependent. Two buffer solutions (pH 4 and 7) made from KCl, MgCl$_2$ and CaCl$_2$ solutions with their pH maintained by addition of HCl and NaOH solutions respectively were utilised.

40

2.8.4 Intercalation of oleate anions in LDH (LDH-oleate)

The oleate anion can be successfully intercalated into LDH using ion exchange (Blasi *et al*, 2021; Kameshima *et al*, 2006; Liu *et al*, 2006; Xu *et al*, 2004), coprecipitation (Manzi-Nshuti *et al*, 2009; Zhou *et al*, 2010a) and the hydrothermal reconstruction after calcination (Celis *et al*, 2014; Donato *et al*, 2012; Inomata & Ogawa, 2006; Kameshima *et al*, 2006; Yang *et al*, 2009). A summary which shows synthesis methods and source of the oleate ions which has been previously reported in literature is represented in **Table 2.3**.

Table 2.3: Previous studies of LDH-oleate synthesis

Source of oleate ions	Synthesis method	d-spacing/nm; LDH composition $M^{2+}M^{3+}$	References
Olive oil, 70-80 % oleate	Ion exchange	3.58; ZnAl 3.63; MgAl	(Xu *et al*, 2004)
Sodium oleate	Reconstruction after calcination at 600 °C	3.9; MgAl	(Inomata & Ogawa, 2006)
Sodium oleate	Ion exchange and reconstruction after calcination at 500 °C	3.9; MgAl	(Kameshima *et al*, 2006)
Potassium oleate	Ion exchange	#; CoAl	(Liu *et al*, 2006)
Sodium oleate	Coprecipitation	3.8; ZnAl 3.4; MgAl	(Manzi-Nshuti *et al*, 2009)
Oleic acid	Reconstruction after calcination at 500 °C	#; MgAl	(Yang *et al*, 2009)
Sodium oleate	Coprecipitation	3.8; MgAl	(Zhou *et al*, 2010a)
Sodium oleate	Reconstruction after calcination at 450 °C	4.7; MgAl	(Donato *et al*, 2012)
Sodium oleate	Reconstruction after calcination at 500 °C	3.85; MgAl	(Celis *et al*, 2014)
Sodium oleate	Ion exchange	3.08; MgAl	(Blasi *et al*, 2021)

Not reported

The successful intercalation of the oleate anion into the LDH interlayer can be validated through XRD, FTIR and TGA analysis. XRD analysis shows appearance of new peaks

41

towards lower 2θ field with increased d-spacing values showing expansion, FTIR results presents new oleate anion bands, and finally TGA shows the loss of the intercalated oleate anion. The amount intercalated can be determined by comparison of the residue with that or the pristine LDH (Inomata & Ogawa, 2006; Manzi-Nshuti *et al*, 2009; Yang *et al*, 2009). The intercalated oleate anion amount increased with increasing the Mg/Al ratio from 2-5 and the reconstruction method had better results compared to ion exchange (Kameshima *et al*, 2006). Different ageing temperatures have been reported varying from 60 °C (Celis *et al*, 2014) to 80 °C (Yang *et al*, 2009) with the latter reported to give nearly 100 % yield after 18 h.

The XRD measured d-spacing values varied within the range of 3.08 nm (Blasi *et al*, 2021) to a maximum of 4.7 nm (Donato *et al*, 2012). The oleate anion are arranged as bilayer and or micelle structures within the LDH interlayer (Donato *et al*, 2012; Kameshima *et al*, 2006). Xu *et al* (2004) postulates a different structural arrangement due to the kink in the oleate anion chain which reduces the d-spacing. This concurs with the findings of Celis *et al* (2014) who established different d-spacing values between *cis*-oleate anion and *trans*-elaidate anion. Though having same chemical composition, *cis*-oleate anion and *trans*-elaidate anion have different structural arrangements.

LDH intercalated with linear *trans*-elaidate anion had a d-spacing of 4 nm compared to 3.85 nm for the intercalated bent *cis*-oleate anion (Celis *et al*, 2014). The values of both Xu *et al* (2004) and Celis *et al* (2014) were different (3.63 and 3.85 respectively) for Mg/Al LDH-oleate. However, different synthesis methods and oleate anion source were used. According to Zhou *et al* (2010a), a d-spacing of 3.8 nm is intermediate to that of pure monolayer arrangement (1.8 nm) and bilayer arrangement (5 nm). It can therefore be inferred that the d-spacing values are affected by the structural arrangement of the oleate anion within the LDH interlayer which varies with the synthesis method and conditions used.

2.9 Porous matrices

2.9.1 Spent coffee grounds, SCGs

Coffee is a popular hot beverage consumed globally. The annual global coffee consumption between 2020/21 was at 9.98 billion tonnes of which 734.52 million tonnes were consumed in Africa (International, 2022). The global coffee beverage market is predicted to reach $20.78 billion by 2030 (Research & Markets 2021). Coffee beverage is obtained from coffee beans which are processed from the coffee cherry fruit. **Figure 2.12** which shows that of the

42

coffee beans processed, 45-50 % end up as spent coffee ground (SCG) (Campos-Vega *et al*, 2015). For each kilogram of coffee processed, a double portion of wet SCG is generated (Karmee, 2018).
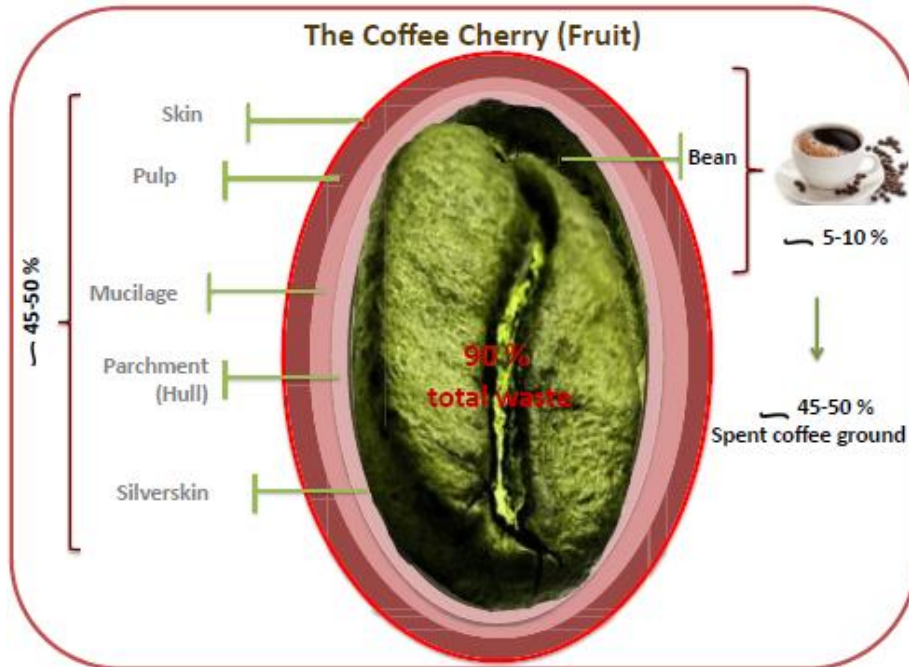
Figure 2.12: Coffee fruit composition reprinted from Campos-Vega *et al* (2015) with permission from Elsevier

SCGs are a non-edible insoluble residue by-product of coffee brewing. SCGs are a highly abundant renewable by-product which will remain if coffee consumption persists. SCGs are dumped at landfills (McNutt & He, 2019). However, the high organic content poses a combustion threat due to methane produced by anaerobic digestion process (Saberian *et al*, 2021). Furthermore, SCGs contain caffeine, polyphenols, tannins and other substances which may render them unsafe to be disposed to the natural environment (Mussatto *et al*, 2011). To mitigate the environmental challenges posed by SCGs, alternative measures must be explored to utilise this highly abundant by-product. It is therefore a requisite to fully understand the composition of the SCGs.

2.9.2 SCGs composition

The chemical composition of SCGs varies on the type or source of coffee beans, roasting temperature conditions and the extraction process (Kovalcik *et al*, 2018). SCGs mainly comprises of cellulose, hemicellulose, and lignin (Campos-Vega *et al*, 2015; Chan *et al*, 2022; Kovalcik *et al*, 2018; Massaya *et al*, 2019; Rajesh Banu *et al*, 2020; Saberian *et al*,

43

2021). Detailed compositional analysis of SCGs is covered in the reviews by Campos-Vega *et al* (2015), Kovalcik *et al* (2018), Massaya *et al* (2019), Rajesh Banu *et al* (2020) and Saberian *et al* (2021).

In a study by Ballesteros *et al* (2014), SCGs composition in g/100g dry material was constituted of 12.40 ± 0.79 cellulose, 9.10 ± 1.94 hemicellulose, and 23.90 ± 1.7 of lignin. According to Massaya *et al* (2019), SCGs comprises of 32–42 wt.% hemicellulose, 0–26 wt.% lignin, 7–13 wt.% cellulose, 10-18 wt.% protein and 2-24 wt.% lipids. Lipids and proteins also constitute a bigger portion of the SCGs. Minor components in SCGs comprises of ash, phenolic compounds, caffeine, and tannins (Ballesteros *et al*, 2014; Campos-Vega *et al*, 2015; McNutt & He, 2019). In addition, SCGs also contain different types of sugars, i.e., mannose, galactose, glucose, and arabinose (Karmee, 2018).

Lipids in the SCGs forms an oil fraction with a characteristic coffee odour. Oil extracted from SCGs contains, glycerides, fatty acids and unsaponifiable compounds (Massaya *et al*, 2019). The oil fraction in SCGs can be extracted by solvents (polar/non-polar). Non-polar solvents are preferred as they have better oil extraction yield compared to polar solvents (Kovalcik *et al*, 2018). Among non-polar solvents, hexane is the most utilised for the extraction of oil in SCGs (Campos-Vega *et al*, 2015; Kovalcik *et al*, 2018). Soxhlet extraction in hexane with increased liquid to solid ratio (Acevedo *et al*, 2013) and extraction time enhances the oil extraction yield. An experimental value of up to 30.4 % yield have been reported by Efthymiopoulos *et al* (2019).

2.9.3 Applications of SCGs

Due to their abundance as a low-cost, agricultural by-product, which is a renewable resource, SCGs attracts the attention of many researchers. The first review on SCGs by Campos-Vega *et al* (2015) shows that as early as 1985, SCGs had been explored for coffee oil recovery. In their review, Kovalcik *et al* (2018) categorised the SCGs to contain oil fraction (lipids and diterpenes), crude fibre and additional constituents (polyphenols, carbohydrates, solid residue) from whence all the alternative value added products are derived. SCGs have been investigated to produce biodiesel, biogas, biopolymers, antioxidants, biosorbents, construction materials, fillers for polymers, bio-oil, biochar and activated carbons among others (Hejna, 2021; Massaya *et al*, 2019; McNutt & He, 2019; Saberian *et al*, 2021).

SCGs have a microporous structure therefore possesses a high surface of 300 – 1000 m^2/g (Kovalcik *et al*, 2018). The surface area of the SCG can be enhanced through thermochemical

44

processing (pyrolysis) producing a more porous biochar (Massaya *et al*, 2019). Biochar can be further developed by initially removing the ash content to synthesize a highly porous activated carbon with a surface area of up to 2408 m^2/g (Chiang *et al*, 2020). The activated carbon produced from SCGs can be utilised as adsorbents for the removal of dyes in water and heavy metals (Boudrahem *et al*, 2011; Pagalan Jr *et al*, 2020).

Biochar have also been investigated to develop slow-release fertilisers for sustainable agriculture (Marcińczyk & Oleszczuk, 2022). Various synthesis methods have been proposed for the synthesis of slow-release fertilisers, i.e., in-situ pyrolysis, impregnation, co-pyrolysis, encapsulation, and granulation (Wang *et al*, 2022). Corn stover-derived biochar phosphate based slow-release fertiliser was successfully synthesised by impregnation by immersion in saturated potassium dihydrogen phosphate (Sepúlveda-Cadavid *et al*, 2021).

The pyrolyzed biochar at 500 °C was cooled and sieved (< 2 mm) followed by immersion for 48 h at solids: solution ratio of 1:40 and washing excess solution in distilled water. Slow release in 120 ml deionised water and stirring at 100 rpm showed a 20 % release of phosphate after 1 day doubling to 40 % after 5 days (Sepúlveda-Cadavid *et al*, 2021). The impregnation process of biochar by Sepúlveda-Cadavid *et al* (2021) with saturated solutions presents an intriguing concept which can be exploited for the slow release of mosquito larvicides in water bodies. To fully benefit from the impregnation process for slow release, it thus compels an understanding into the characteristics and synthesis of the biochar.

2.9.4 Biochar synthesis

Biochar is a carbon rich, solid material generated by pyrolysis. Pyrolysis is a physicochemical thermal transformation of biomass at elevated temperatures between 500-1000 °C in the absence of air or oxygen (Primaz *et al*, 2018). The products of pyrolysis comprise bio-oil, non-condensable gases and the residual biochar (Massaya *et al*, 2019). Porosity on the residual biochar emanates from the release of non-carbon elements as gaseous components. The minimum carbonizing temperature can be determined from the onset plateau temperature of the TGA plot of the SCGs (Laksaci *et al*, 2017).

The process parameters used to categorise pyrolysis as slow, intermediate, fast pyrolysis, and gasification are specified in a review by Ghodszad *et al* (2021). Residence times for these pyrolysis categories are, 7200-14 400s, 10-20s, 2s, and 10-20s respectively. According to Samoraj *et al* (2022), fast pyrolysis promotes formation of bio-oil whilst slow pyrolysis

45

promotes high biochar yield. The pyrolysis process is influenced by the pre-treatment process, process parameters (residence time, heating rate and the pyrolysis temperature) and the biomass waste type (Samoraj *et al*, 2022). Investigation on pyrolysis temperature between 450-500 °C established an increase in fixed carbon and ash contents with temperature (Tongcumpou *et al*, 2019). The authors therefore established that a good quality biochar can be obtained at 500 °C. This concurs with the earlier study by Jutakridsada *et al* (2016). Biochar produced by pyrolysis at low temperature results in a temporary hydrophobicity which can be displaced when exposed in water (Das & Sarmah, 2015).

2.10 Starch as an encapsulating matrix

2.10.1 The chemistry of starch

Starch is comprised of two homopolymers of glucopyranose, amylose and amylopectin which organize in granules of semi-crystalline structure (Nessi *et al*, 2019). Amylose is predominantly a linear macromolecule which constitutes of α-(1-4)-D-glucopyranosyl linkages. Amylopectin is highly branched macromolecule composed of α-(1-4)-D-glucopyranose units with branches resulting from α-(1-6) linkages. The ratio of amylose to amylopectin varies with the plant source, grain shape and size of starch granule, and differs even within different parts of the same plant (Belgacem & Gandini, 2008). Due to these variations of properties, starch is usually designated by its plant source i.e., cornstarch, rice starch, tapioca starch etc. (Hsieh *et al*, 2019; Qiao *et al*, 2011; Tiozon *et al*, 2021).

Table 2.4: Properties of starch granules from various sources (Belgacem & Gandini, 2008)

Source	Diameter (µm)	Amylose content (wt.%)	Shape
Maize	5-25	28	Polyhedral
Waxy maize	5-25	~0	Polyhedral
High amylose	5-35	55-85	Varied smooth spherical to elongated
Cassava	5-35	16	Semi-spherical
Potato	5-100	20	Ellipsoidal
Wheat	20-22	30	Lenticular, polyhedral
Rice normal	3-8	20-30	Polyhedral
Banana	26-35	9-13	Elongated oval with ridges

46

2.10.2 Starch crystallinity

Native starch is partially crystalline due to the structural arrangements of amylose and amylopectin (Mohammadi Nafchi *et al*, 2013). When observed by X-ray diffraction, native starch exhibits three different crystal forms, A-, B- and C- crystals. A- type is most linked with cereal starches whilst B- is an amylose-rich variant found in tuber starches (Lendvai *et al*, 2019). C-type starch is usually found in legume starches, cereals grown in specific conditions and some rhizomes. The C- polymorph is a combination of A- and B- allomorphs (i.e., B- surrounded by A- allomorphs). The A- and B- crystals differ in their packing density due to the structural arrangements of the sixfold double amylose helices within the crystal cell. Native starch crystallinity (A-, B- or C-) can be identified from the XRD by their characteristic peaks (He & Wei, 2017; van Soest *et al*, 1996)
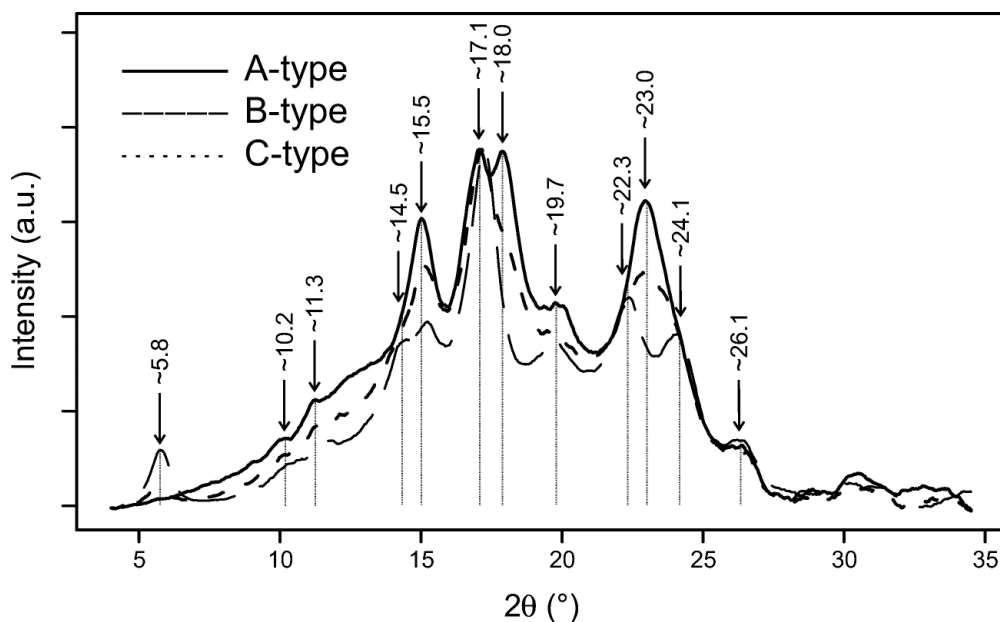
Figure 2.13: XRD characteristic peaks for the three native starches reprinted from Pozo *et al* (2018) with permission from Springer Nature

2.10.3 Extrusion processing of TPS

When heated in the presence of plasticizers under pressure and shear forces, starch granules swell and undergo a phase transition from an ordered crystalline structure to a highly disordered amorphous state (Šárka & Dvořáček, 2017). Amylose and amylopectin leach out as the granules are broken by the disruption of the hydrogen bonds within starch molecules (Ahmed *et al*, 2016). This process is known as gelatinization and is dependent on the botanical starch source, available plasticizer, and processing temperature among others. Gelatinization is a continuous process with the extent increasing with temperature over a

47

certain range which varies with the type of starches (Chang *et al*, 2021). The new mouldable material which is like synthetic polymers (Pushpadass *et al*, 2009) produced by gelatinization is known as thermoplastic starch (TPS).

2.10.4 Crystallinity of TPS

The crystallinity in TPS is attributed to residual native starch crystallinity and process-induced crystallinity which can be V_H, V_A or E_H type (van Soest *et al*, 1996). The V- type crystallinity is observed immediately after extrusion which is formed by inclusion complex of amylose and substances such as surfactants, lipids (Mondragón *et al*, 2008) and plasticizers (Janssen & Moscicki, 2009). A molecular modelling study by Immel & Lichtenthaler (2000) estimated that the V_H- type crystallinity is formed by the single helical structure of amylose which constitute a central hydrophobic cavity of up to 5.4 Å and an overall helix diameter reaching about 13.5 Å.
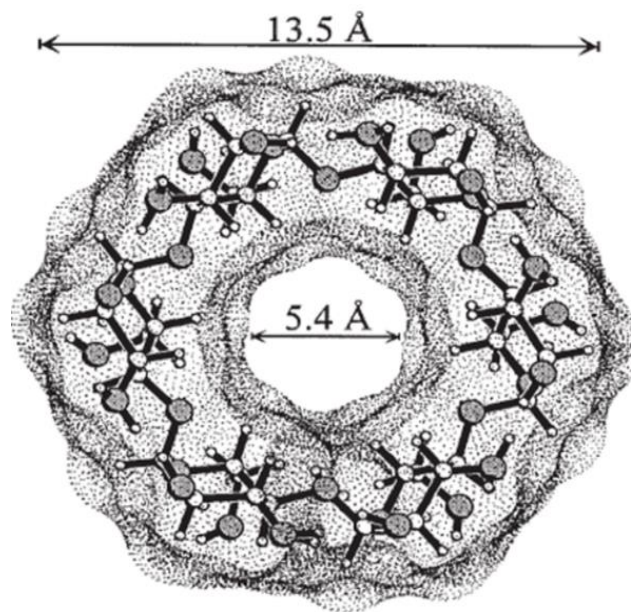
Figure 2.14: Molecular view along helix axis of V_H-amylose complex reprinted from Immel & Lichtenthaler (2000) with permission from John Wiley & Sons

The hydrated V_H type consists of a six-fold single helical structure of amylose that can be transformed by dehydration into the anhydrous V_A type (Rico *et al*, 2016). The E_H type is a seven-fold single helical structure of amylose which occurs at very low moisture content but is highly unstable and transforms to V_H-type in the presence of humidity (Montero *et al*, 2017). Process-induced crystallinity is a function of the type of plasticizer used, nature of starch matrix and the processing parameters.

48

2.10.5 Factors affecting extrusion of TPS

Extrusion of starch is a complex process due to multiphase transitions of starch during thermal processing (González-Seligra *et al*, 2017). Starch extrusion is affected by many parameters which need to be optimized to ensure the desired properties in the final TPS product. These parameters include type and amount of plasticizer used, processing aids, barrel temperature profile and extrusion speed among others. Generally, excluding factors emanating from the native starch, these factors can be broadly categorized as additives for the extrusion process and extrusion processing conditions. Though numerous additives can be added for TPS processing, the major additive which must be considered is the plasticizer.

a. Plasticizers

Plasticizers for starch are basically substances capable of forming hydrogen bonds with the starch. Starch plasticizer are low molecular weight substances which contain either hydroxyl or amine groups. Plasticizers help disrupt native starch hydrogen bonds, increase the free volume and movement of starch chains to behave like a thermoplastic (Mohammadi Nafchi *et al*, 2013). The starch-starch bonds are replaced by starch-plasticizer interactions. The effectiveness of starch plasticizers varies on their structure, size and the number hydroxyl groups present (Pushpadass *et al*, 2008). According to Ivanič *et al* (2017), hydrogen bond strength between starch-urea > starch-formamide > starch-acetamide > starch-polyols.

Water and glycerol are commonly used starch plasticizers (Mohammadi Nafchi *et al*, 2013). Glycerol is the most used polyol to plasticize starch as it is economic, biodegradable, non-toxic and has a high boiling point (Vieira *et al*, 2011). According to Lourdin *et al* (1997), glycerol content above a critical concentration of 12 wt.% averts the anti-plasticization effect. Curvelo *et al* (2001) suggests a glycerol content between 20-40 wt.% for best starch melt extrusion processing. Urea as a plasticizer in comparison to glycerol was proven to effect high tensile strength and modulus (Ivanič *et al*, 2019). However, urea crystallizes and separates from the plasticized starch which also results in rigid and brittle starches. Glycerol and urea mixture were used to plasticize starch and produced modest results but lower compared to each plasticizer (Ivanič *et al*, 2017).

Isosorbide a bicyclic non-toxic diol produced from catalytic dehydration of D-sorbitol (obtained from starch hydrolysis) can be utilized as a plasticizer to produce thermoplastic starch. At 40 wt.%, isosorbide proved to be a good biodegradable plasticizer for maize starch

49

and produced a thermoplastic starch which showed no signs of retrogradation after 9 months (Battegazzore *et al*, 2015). The use of isosorbide plasticizer at 35 wt.% for starch films resulted in low oxygen and water vapor permeability and higher strain at break compared to glycerol and 1,3 propane diol plasticized starch (González *et al*, 2017).

Area *et al* (2019) investigated microcrystalline cellulose reinforced starch composites using glycerol and isosorbide as the plasticizers. It was determined that isosorbide requires more time and shear force compared to glycerol (100 rpm vs 60 rpm). However, isosorbide can be processed at lower temperatures compared to glycerol (90°C vs 120°C). High shearing forces for isosorbide favours E_H crystals formation compared to V_H for glycerol (Battegazzore *et al*, 2015). It is noteworthy that isosorbide is biodegradable, non-toxic with high water solubility thus it can be considered green and can be used as a plasticizer for starch.

Citric acid, tartaric acid and malic acid are some of the non-toxic carboxylic acids which can be used as starch cross-linking agents as well as co-plasticizers for TPS (Zuraida *et al*, 2012). The addition of citric acid to starch aids to form stronger interaction with the plasticizers and helps prevent starch retrogradation (Shi *et al*, 2007). Lubricants can also be added to improve TPS extrusion, 1 wt.% magnesium stearate was used in glycerol plasticized starch (Lendvai *et al*, 2019) and 1 wt.% stearic acid for sorbitol plasticized starch (Hietala *et al*, 2013).

In a nutshell, plasticizers are the major additives for TPS processing hence they should be economical yet effective.

b. Extrusion processing conditions

I. Extruder processing speed

According to García *et al* (2015), specific mechanical energy (SME) is one of the key parameters which influence the starch reactions during the extrusion process. It is defined as the mechanical energy transformed into heat energy per unit mass of the extruded material.

$$\text{SME} = \frac{P \times \tau \times \frac{RPM_{act}}{RPM_{rated}}}{\dot{m}} \qquad [2.1]$$

Where, P is the motor electric power (*kW*), RPM is screw speed i.e., actual (act) and allowable (rated), $\dot{m}$ is mass flow rate (*kgs*$^{-1}$) and $\tau = \frac{torque\ difference\ (running\ vs\ empty)}{allowable\ torque}$.

The effect of screw speed on glycerol plasticized starch revealed that 80 rpm results in a homogeneous and completely gelatinised starch films whilst at 40 rpm and 120 rpm results in

50

grains of broken starch (González-Seligra *et al*, 2017). This is consistent with a study by Lee *et al* (2009) which also determined that a screw speed of 80 rpm had better properties of extruded starch compared to 100 rpm. Screw speed also affects the rate of fragmentation of starch granules and the final properties of TPS. Amylopectin fragmentation lessens with, reducing screw speed and increasing the temperature profile (121-177 ^{o}C) (Liu *et al*, 2009). Increasing the screw speed promotes the formation of single amylose helical structures (van Soest *et al*, 1996).

II.   Barrel temperature

The temperature profile inside the extruder should be properly set to ensure complete gelatinization of starch. Different temperature profiles can be used for TPS processing. A profile of 50-120 ^{o}C was used by Pushpadass *et al* (2008), 90-140 ^{o}C (González-Seligra *et al*, 2017), 50-110 ^{o}C (Nessi *et al*, 2019) and 85-120 ^{o}C by Lendvai *et al* (2019). The temperature profile is also determined by other the type of starch used, type and amount of plasticizer, extruder characteristics and the screw speed. Extrusion processing of starch with low moisture content using a high temperature profile promotes E_H crystallinity (van Soest *et al*, 1996). This is due to more amylose chains being liberated by the destruction of the granular structure.

2.10.6 Challenges of TPS

Thermoplastic starch exhibits many challenges to be fully utilised commercially. TPS is highly hydrophilic and absorbs water leading to poor mechanical properties overtime. The starch chains recrystallizes after processing and suffers from plasticizer leaching resulting in a brittle material thereby limiting its applications (Zhang *et al*, 2018). This process of amorphous TPS becoming crystalline and shrinking due to structural reassociation and reconstruction of starch chains is known as retrogradation depicted in **Figure 2.15**.

The overall process from starch granules I, through gelatinization II (by swelling IIa, granule disruption IIb) and the retrogradation of amylose IIIa and amylopectin IIIb. Amylose is mainly responsible for the early fast recrystallization in TPS (IIIa) which is observed under XRD as V- and E- polymorphs or the single helical complexes (van Soest *et al*, 1996). Overtime as the TPS loses more water, amylopectin eventually begins to rearrange and recrystallize (IIIb). The resulting stronger hydrogen bonds between the macromolecules leads

51

to pronounced shrinkage and an ultimately more brittle material (Lendvai *et al*, 2019). Starch chains also rearrange into double helices during retrogradation (Chang *et al*, 2021)
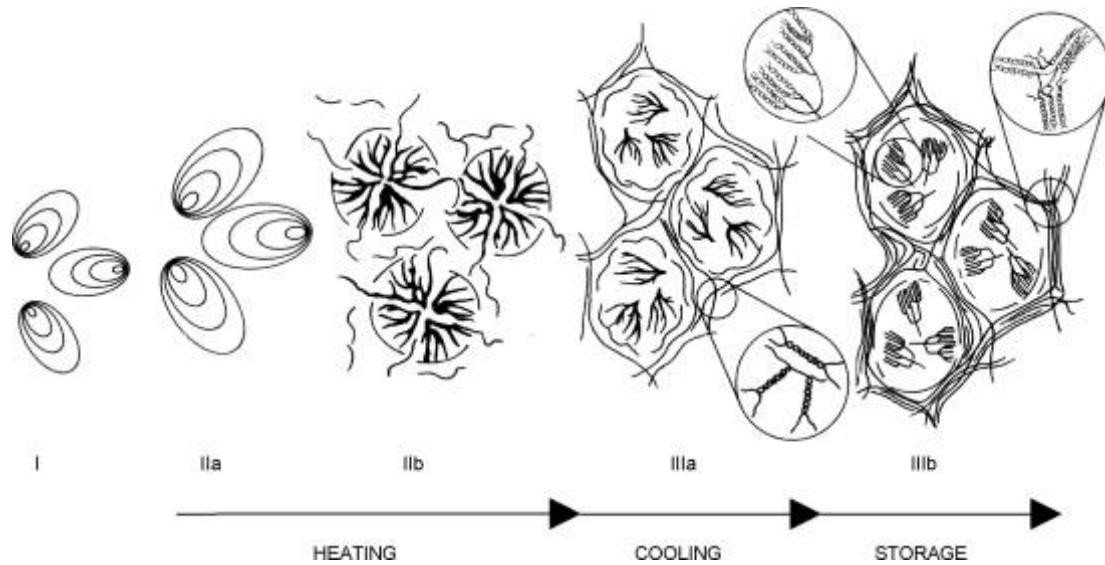
Figure 2.15: Structural changes in starch-water mixture reprinted from Wang *et al* (2015) with permission from John Wiley & Sons

A variety of methods have been suggested to restrict retrogradation. Chemical modification can also be utilized to reduce the rate of water absorption of TPS. This can be achieved through reactive extrusion process (Castaño *et al*, 2014). Additives can also be added to TPS processing to restrain retrogradation. According to Chang *et al* (2021), lipids can help to curb retrogradation by forming amylose-lipid complexes. Fatty acids such as lauric, linoleic, mystic, oleic, stearic, and palmitic forms amylose inclusion complexes with starch (Cervantes-Ramírez *et al*, 2020; Kawai *et al*, 2012; Marinopoulou *et al*, 2016a).

Nanofillers, nano-clays and cellulose nanofibers has also been shown to retard the rate of retrogradation of dextrin starch nanocomposites (Phillips *et al*, 2020). Addition of some plasticizers such as isosorbide (Area *et al*, 2019; Battegazzore *et al*, 2015) and co-plasticizers such as citric acid (Shi *et al*, 2007) helps to prevent retrogradation. Furthermore, emulsifiers addition also aids in reducing retrogradation (Fu *et al*, 2015). Emulsifiers or surfactants such as sorbitan monostearate (span 60), sorbitan monooleate (span 80) and sorbitan monopalmitate (span 40), also serve as processing agents to incorporate non-polar additives to the polar starch matrix (Ortega-Toro *et al*, 2014).

Retrogradation is a complicated phenomenon which is influenced by various factors therefore, no single method in isolation can be used to investigate this process. Of the many

52

options explored to investigate retrogradation, XRD and DSC are usually utilized as a combination to fully gain an insight of starch retrogradation (Karim *et al*, 2000; Phillips *et al*, 2020).

2.10.7 Conditioning of TPS

To investigate the retrogradation phenomena, conditioning of TPS is vital. Wang *et al* (2015) specifies storage under isothermal conditions (4, 25 or 30 $^{\circ}$C) and temperature cycling within the same temperatures as the commonly utilised methods for TPS conditioning. However, there are contrasting opinions regarding the effect of these conditioning methods. According to Zhou *et al* (2010b), temperature cycling results in more homogeneous crystallites and higher thermal stability. Xie *et al* (2014) insists that temperature cycling leads to numerous imperfect crystallite formation. Shamai *et al* (2004) also added that retrogradation at low temperature results in B- polymorphs whilst when the temperature is high, A- and V- polymorphs are prominent.

The A- and B- polymorphs differ in their potential water content. It is therefore necessary to monitor the humidity when conditioning thermoplastic starch samples. Saturated salt solutions can be utilised for this purpose. The appropriate salt should be determined to obtain the desired relative humidity for thermoplastic starch conditioning. Various saturated salts and their respective humidity at varying temperatures are presented in **Annexure 3**.

2.10.8 Thermoplastic starch/nanocellulose nanocomposites

Nanocellulose can be in form of nano-fibrillated cellulose (CNF), cellulose nanocrystals (CNC) and bacterial nanocellulose (BNC). Nanocellulose has a very high tensile strength of up to 10 GPa (Sharma *et al*, 2019a). As a result, nanocellulose has gained momentum as a reinforcement material. CNF dispersion in the starch matrix can be improved by dispersing it in the glycerol plasticiser before extrusion (Nessi *et al*, 2019; Phillips *et al*, 2020).

Incorporation of CNF and CNC in thermoplastic starch improves the tensile strength and Young's modulus whilst decreasing elongation at break (Dufresne & Castano, 2017). CNC reinforced starch nanocomposites were melt processed in twin screw extruder by Nessi *et al* (2019). The screw speed was set at 20 rpm with a temperature profile of 50-110 $^{\circ}$C and CNC composition varied from 1.5-10 wt.%. Their results in **Figure 2.16** shows that CNC reinforced TPS by benchmarking the nanocomposites to the neat TPS (REF). However, the trend shows storage modulus decreases as the CNC content increases beyond 2.5 wt.%. This

53

is due to poor CNC dispersion leading to agglomeration which weakens the material properties.
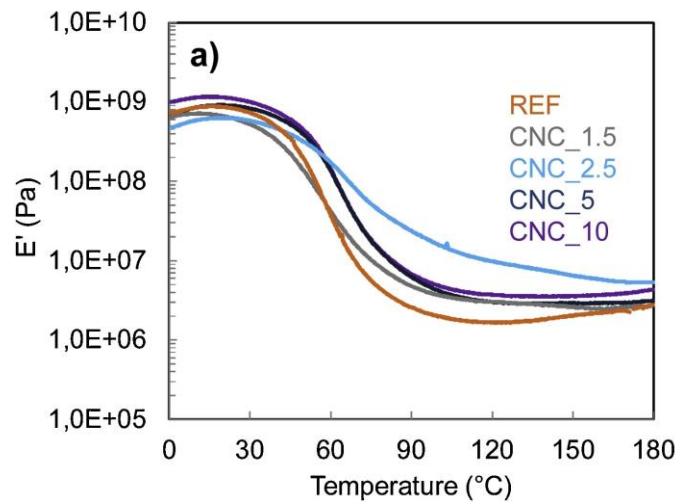
Figure 2.16: Storage modulus of TPS(REF) and the nanocomposites with different CNC loading (1.5, 2.5, 5 and 10 wt.%) reprinted from Nessi *et al* (2019) with permission from Elsevier

González-Seligra *et al* (2017) suggests that for glycerol plasticised cassava starch, increasing screw speed to 120 rpm produced an amorphous film with improved modulus and tensile strength. However, doubling the screw speed from 40 rpm resulted in reduced mechanical properties of glycerol plasticized potato starch reinforced CNF (Cobut *et al*, 2014). Hietala *et al* (2013), produced bio-nanocomposites from potato starch, sorbitol, and CNF with 1 wt.% stearic acid as a lubricant. Screw speed was set at 200 rpm and a temperature profile in the range 80-110 °C. The findings of the study concurred with those by Nessi *et al* (2019) with best properties obtained at 10 wt.% loading.

It was also suggested that the use of sorbitol compared to glycerol as plasticizer help lower moisture absorption of starch. Cellulose nanofibers (CNF) at 1.5 wt.% loading improved the thermal and water absorption properties of glycerol plasticized corn starch (Ghanbari *et al*, 2018). Twin screw co-rotating extruder can be used to process cellulose suspension to produce CNF (Rol *et al*, 2019). Cellulose nano whiskers (CNC) can be further broken down by the extrusion decreasing their size to form a monodisperse with new size distribution (Kargarzadeh *et al*, 2017). Generally, the screw speed must be properly set as it helps to uniformly disperse the nanocellulose. Caution must be exercised as screw speed also affects the melt temperature, melt viscosity and the residence time of material in the extruder.

54

2.11 Emulsion-based systems

Emulsions are colloidal dispersions formulated by high shear mixing two immiscible liquids where one is distributed as droplets in another which acts as the continuous phase by the aid of an emulsifier (surfactant) (Kapiamba, 2022). The emulsion phases can be water-in-oil (W/O), oil-in-water (O/W), water-in-oil-in-water (W/O/W), oil-in-water-in-water (O/W/W) and oil-in-water-in-oil (O/W/O) (Marhamati *et al*, 2021; Ye & Chi, 2018).

Emulsions can be categorised either according to the type of emulsifier or the structural arrangement of the system (Tadros, 2013). The former comprises for example the Pickering emulsion and the latter, macroemulsions (particle size range 0.1 - 5 µm), nano-emulsions (20 - 100 nm), microemulsions (5 - 50 nm), double and multiple emulsions and mixed emulsions (Tadros, 2013). Nano-emulsions and microemulsions are the common forms of O/W emulsions. Microemulsions are thermodynamically stable whilst nano-emulsions are unstable breaking down overtime (McClements, 2012; Tadros, 2013). Surfactant hydrophobic tails forms a hydrophobic core encapsulating oil molecules forming micelles. This aids to reduce the contact area of oil and water. Oil molecules are entrapped in the micelle of a microemulsion as either separate core oil droplets or in between surfactant tails as shown in **Figure 2.17**.
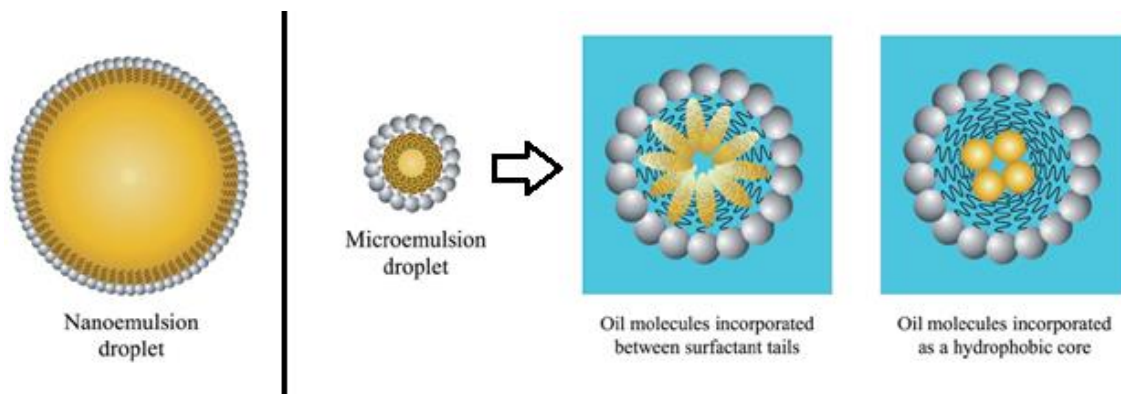
Figure 2.17: Nano-emulsion and microemulsion made from oil, water and surfactant reprinted from McClements (2012) with permission from Royal Society of Chemistry

2.11.1 Stability of emulsions

Stability of colloidal dispersions depends on the interparticle forces (repulsive or attractive) between droplet particles. The forces can be due to Van der Waals, electrostatic, solvent forces and steric forces (Washington, 1996). These forces are affected by gravitational forces and surfactants interactions with the emulsion phases (Yonguep *et al*, 2022). Kinetically

stable emulsions break down by a process of demulsification overtime. The mechanisms of emulsion breakdown are represented in **Figure 2.18**.
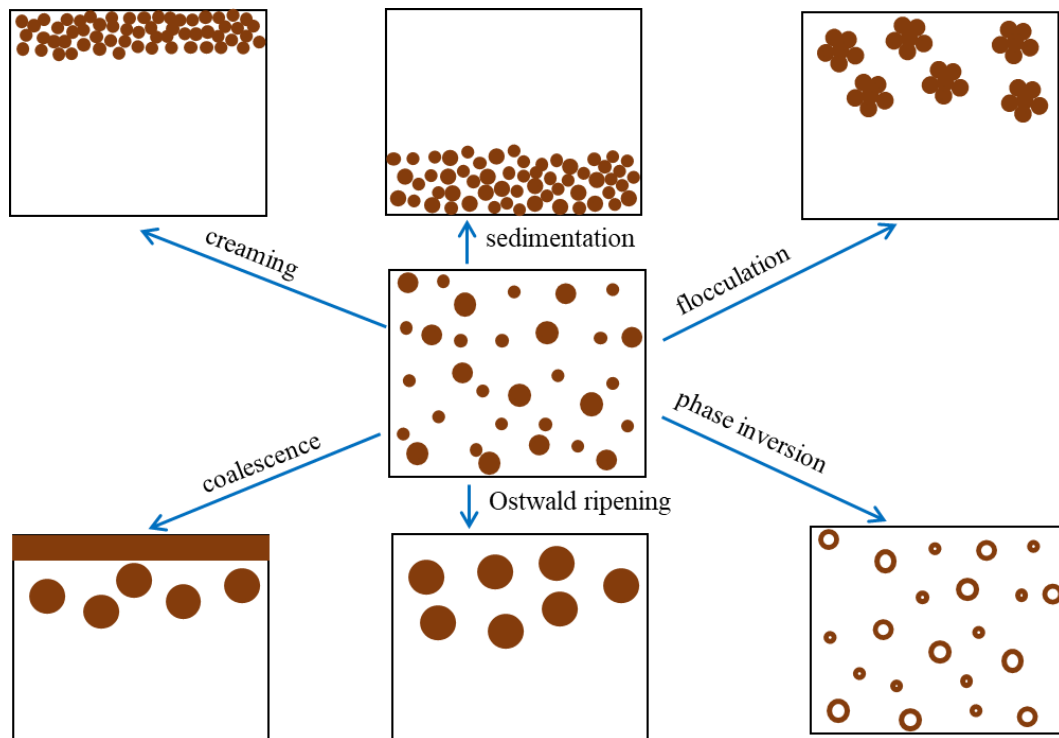
Figure 2.18: Breakdown mechanism of emulsion adapted from Tadros (2004)

Creaming and sedimentation are reversible processes caused by external gravitational forces and the tendency of particles to float or sink due to differences in densities (Yonguep *et al*, 2022). When density of distributed phase is smaller than that of the continuous phase, creaming occurs and vice versa for sedimentation. Flocculation is a process caused by weak van der Waals forces between droplet particles leading to clumping together forming a "floc". These are larger clumps formed without rupture of the individual oil droplets (Heidari *et al*, 2022).

Coalescence is the formation of much bigger particles from smaller particles aggregating to combine into a larger droplet. This process reduces the number of droplets present. It is caused by elimination or thinning of interfacial film separating the dispersed phase leading to ultimate demulsification into two separate distinct phases as shown in **Figure 2.18**. Coalescence can be due to high flocculation rate, low viscosity, high temperature and interfacial tension among other factors (Yonguep *et al*, 2022).

The solubility of the contents of an emulsion droplet varies with droplet size. During storage, the contents of the smaller droplets may migrate via the continuous phase to the larger

56

droplets. This means that smaller droplets tend to decrease in size over time whereas the larger droplets grow (Tadros, 2004). This phenomenon is known as Ostwald ripening. It is an irreversible process which shifts the emulsion particle size distribution to larger values. Phase inversion occurs when the continuous medium becomes the dispersed phase and vice versa. Measurement of the dispersed phase droplet size and size distribution is therefore vital to assess the kinetic stability of the emulsions (Kabong, 2020).

To improve the emulsion stability, emulsifiers, or surfactants sometimes with co-surfactants are also added. The review by Marhamati *et al* (2021) covers the different classes of emulsifiers and their physicochemical effects on O/W nano-emulsions. O/W emulsions stability can be is affected by droplet size, type and concentration of emulsifier, density and viscosity of emulsifier, temperature, and interfacial tension (Heidari *et al*, 2022; Marhamati *et al*, 2021).

2.11.2 Emulsions for mosquito larvicidal applications

Emulsions can be utilised as delivery systems to improve the activity and persistence of oil-based actives in aqueous media. In addition, Mishra & Pandit (1990) proved that emulsion systems can also be utilised as prolonged release dosage forms. Emulsions based systems can therefore be exploited for mosquito larvicidal applications. Preparation of emulsion formulations is less energy intensive hence reduce productiton costs. Osanloo *et al* (2017) formulated essential oil-based nano-emulsions as *An. stephensi* mosquito larvicide delivery system. Inactive nano-emulsion ingredients were established not to possess larvicidal activity on *An. stephensi* and the most stable emulsion to possess significant larvicidal potency.

Ferreira *et al* (2019) successfully used herbal oil extract-based nano-emulsion as a larvicide delivery system for *Ae. aegypti* and *culex* species. Lopes Martins *et al* (2021) formulated an essential oil nano-emulsion as a larvicide on *Ae. aegypti*. The nano-emulsion was potent on the tested mosquito larvae with low toxicity of non-target organisms. Essential oil based microemulsions were also formulated and tested on *Culex quinquefasciatus* larvae by Pavela *et al* (2019a). The microemulsions resulted in acute toxicity in mosquito larvae and reduction in adult emergence. The microemulsions were also determined to possess no negative impact on two important non target species. However, in all these studies, the emulsions were diluted to required doses in 100 mL of distilled water and did not test the residual efficacy of these methods. Emulsion based systems can therefore be formulated with oleic acid for larvicidal applications.

57

CHAPTER 3: EXPERIMENTAL

This section outlines, the raw materials that were used as well as the methods and procedures followed to develop the systems for the slow release of oleic acid as a mosquito larvicide. The raw materials and prepared samples were also characterized, and the techniques used are outlined. In addition, laboratory bioassays were conducted to ascertain the efficacy of the developed systems. The procedure followed to perform the bioassays are also specified.

3.1 Materials

A technical grade oleic acid (90 % purity) [CAS-No. 112-80-1] was used as the main larvicidal active in this study. Technical grade methyl oleate (70 % purity) [CAS-No. 112-62-9] was used as a proxy for oleic acid for oxidative stability experiments. These together with the singled out natural antioxidants, curcumin (90 % purity) [CAS-No. 458-37-7], and eugenol (≥ 99 % purity) [CAS-No. 97-53-0] were obtained from Sigma Aldrich. Acetone (99.99 % purity) obtained from Associated Chemicals Enterprises (ACE) South Africa was used as a solvent during larvicidal bioassays of oleic acid as a free-standing oil.

A commercial Mg-Al carbonate anion-based layered double hydroxide (Alcamizer 1) used for intercalation of oleic acid was obtained from Kisuma Chemicals, Netherlands. The sodium acetate trihydrate, (99 % purity) [CAS-No. 6131-90-4] and acetic acid, (≥ 99 % purity) [CAS-No. 64-19-7] used to make buffer solutions for investigating the effect of pH on LDH-oleate were obtained from Merck, South Africa. Spent coffee grounds used to produce carbon-based spent coffee biochar for trapping oleic acid were collected from TriBeCa coffee making shop from Centurion, Gauteng, South Africa. Activated charcoal granules were obtained from Associated Chemicals Enterprises (ACE) South Africa.

Dextrin starch powder (Stydex white dextrin 072012) with an estimated degree of polymerization of 53 ± 5 (Phillips *et al*, 2020) was obtained from Tongaat Hulett Starch, , Meyerton, South Africa. Prof Stephen Ochigbo supplied amora starch powder produced by NRCRI Umudike in collaboration with RMRDC, Abuja, Nigeria. A fibrillated cellulose nanofiber (CNF) suspension containing 8 wt.% solids (Valida-S191C) was donated by Sappi South Africa. Glycerol (99.5 % purity) for plasticising starch was also obtained from Associated Chemicals Enterprises (ACE). An additional starch plasticiser, isosorbide (≥ 98.5 % purity) was obtained from Henan Allgreen Chemical, China. Dellite 43B organoclay used as a processing aid was supplied by Laviosa Chimica Mineraria SpA, Italy. Sorbitan

monooleate-based emulsifier (Anfomul S4M) used to formulate oleic acid emulsions was obtained from Croda Chemicals, South Africa.

3.2 Methods and sample preparations

3.2.1 Antioxidant formulations for oxidative stability analysis

The eugenol- and curcumin-based antioxidants formulations are listed in **Table 3.1**. The lower range of 0.1 - 0.25 wt.% chosen for curcumin was informed by antioxidant stability results for biodiesel (de Sousa *et al*, 2014). Previous work by van der Westhuizen & Focke (2018) specifically proved effectiveness of synthetic antioxidants at 0.15 wt.%. For eugenol, previous studies reported dosage values of 1 wt.% and 1.5 wt.% (de Souza *et al*, 2018; Ramos *et al*, 2021). Hence, values were considered for the lower and upper limits to establish a trend.

Table 3.1: Curcumin and eugenol formulations evaluated

Eugenol, wt.%	Curcumin, wt.%
0.5	0.1
0.75	0.15
1.0	0.20
1.25	0.25
1.5	
2.0	

3.2.2 Synthesis of oleic acid intercalated LDH

The intercalation of the oleic acid into the LDH was performed via the hydrothermal reconstruction process described by Yang *et al* (2009) with some modifications. Typically, MgAl carbonate LDH precursor was calcined at 500 °C for 3 h (Celis *et al*, 2014). The calcined LDH was cooled to room temperature in a desiccator. Deionized water in a 1 L beaker was boiled for 30 minutes to remove dissolved carbon dioxide. The temperature was then lowered and maintained at 80 ± 2 °C. Subsequently, 29 g of calcined LDH, and 17 g of oleic acid were added to the beaker (at 1:1 molar ratio of LDH: oleic acid). The beaker was sealed with a plastic wrap. To improve the crystallinity of the final product, the reaction conditions were maintained at 80 ± 2 °C and 500 rpm for 20 h. After the reaction, the solid

59

product was recovered by centrifugation. It was redispersed in deionised water before recovering the solids again. This washing procedure was repeated three times to remove the soluble salt by-product. Finally, the solids were allowed to dry at ambient conditions. The procedure was repeated in triplicate to ensure reliability of the method. In both cases, near 100 % product yield was obtained as previously reported by Yang *et al* (2009).

3.2.3 Pyrolysis of spent coffee grounds to develop a porous carbon-based biochar

Raw spent coffee grounds collected from the local coffee shop were initially washed and filtered with hot water to remove residual water-soluble substances (Boudrahem *et al*, 2011). Subsequently, the samples were oven dried at 130 °C to remove the excess moisture. The dry spent coffee grounds were pyrolyzed in a laboratory fabricated rotary kiln furnace operated at a temperature of 500 °C. The pyrolysis process produced a carbon-rich spent coffee biochar (pyrolyzed spent coffee grounds) with a yield of 18 %. The spent coffee biochar charge was sieve classified by a vibrating sieve shaker for 45 minutes yielding 5 different particle sizes. The largest aperture size was > 1180 μm whilst the smallest aperture size was < 90 μm. **Table 3.2** shows a typical sieve analysis.

Table 3.2: Results of obtained in a typical sieve analysis

Sieve size range, (μm)	Sieve fractions		Nominal aperture size (μm)	Cumulative %	
	wt (g)	wt (%)		undersize	oversize
> 1180	13.6	58.4	1180	41.6	58.4
600 - 850	1.4	6.0	850	35.7	64.3
250 - 600	6.3	27.2	600	8.5	91.3
90 - 250	1.9	8.1	250	0.4	99.6
< 90	0.1	0.4			

3.2.4 Porous carbon matrices loaded with oleic acid

A known mass of the solids (AC and spent coffee biochar) sample M_1, was added to a beaker with excess oleic acid. The beaker was kept under a vacuum overnight. The samples were then sieved to separate remaining excess oleic acid. The residue was rinsed with a 70 wt.% ethanol solution under vacuum filtration to remove excess oleic acid present on the surface of the granules. The solvent was left to dry for 15 minutes after which the sample reached a constant mass M_2. The amount of loaded oleic acid was determined from the change in mass

from M_1 to M_2. On average, activated charcoal absorbed *ca.* 50 ± 2 wt.% of oleic acid whilst spent coffee biochar absorbed *ca.* 60 ± 2 wt.% of oleic acid.

3.2.5 Thermoplastic starch/nanocellulose nanocomposite extrusion

Glycerol and isosorbide were evaluated at different compositions as plasticizers for dextrin, amora starch as well a blend of dextrin and amora starch. Isosorbide resulted in poor dispersion of nanocellulose and poor material properties. On the other hand, amora starch and its blends produced products which disintegrated and dissolved very rapidly in water. This was undesirable as the aim of this study was to establish a sustainable slow-release system with residual efficacy exceeding four weeks. As a result, only dextrin starch plasticized with glycerol was considered going forward.

Prior to extrusion, nanocellulose was dispersed in a mixture of glycerol, curcumin, sorbitan monooleate emulsifier, and oleic acid in a milk shake maker for seven minutes. The dispersed nanocellulose paste was mixed with dextrin and Dellite 43B organoclay in a blender for two additional minutes. The overall blend had a composition of 52 wt.% dextrin, 30 wt.% plasticizer (62 wt.% glycerol, 38 wt.% water from nanocellulose), 10 wt.% OA, 5 wt.% organoclay, 2 wt.% emulsifier and 1 wt.% nanocellulose fibres. Curcumin powder was loaded at 0.02 wt.% of OA as a natural antioxidant as determined by the Rancimat analysis. The negative starch control had the same composition excluding OA which was replaced by more dextrin.

The resulting blended mixtures were melt-processed using a ThermoFischer TSE twin screw co-rotating extruder with an L/D ratio of 34 and seven temperature heating zones. The barrel temperature profile was 60/80/100/110/110/110/110 and the screw speed was set at 80 rpm. A circular single slit die with a diameter of 5.5 mm was used to extrude the stands. Addition of 5 wt.% Dellite 43B organoclay prevented oleic acid exudation as shown in **Figure 3.1.** The extruded samples were conditioned under an environment with a relative humidity of 75 % at 25 °C maintained by a supersaturated sodium chloride solution.

61

Figure 3.1: The white structure indicated by the arrow on the left is a fountain of liquid escaping from the vent due to the exudation of the oleic acid from the melt. This formulation did not contain any organoclay. On the right this effect was completely suppressed by the presence of 5 wt.% organoclay in the formulation

3.2.6 Oleic acid in water emulsion

Oleic acid in water emulsions were prepared using a laboratory Silverson L4RT high shear mixer. Anfomul S4M (sorbitan monooleate) was employed as an emulsifier used to disperse the oleic acid in deionised water. Three 200 g total mass emulsion samples were prepared. The oleic acid content was fixed at 35 wt.% whilst varying the emulsifier compositions (3 wt.%, 4 wt.% and 5 wt.%).

A typical formulation procedure was as follows. The required oil and surfactant were initially mixed for a minute using a magnetic stirrer at 100 rpm to form the oil phase. The oil phase was then added slowly to the deionised water whilst stirring at 3000 rpm using the high shear Silverson L4RT mixer for a minute. Subsequently, the stirring speed was increased to 3500 rpm. This speed was maintained for seven minutes until a homogeneous emulsion mixture was made.

The prepared emulsion sample was transferred and stored in closed glass containers. It was stored under ambient conditions. The stability was checked on a regular basis by visual inspection. All the emulsion formulations though initially homogeneous underwent creaming. However, the homogeneous state was easy to recover by simple shaking of the formulation. The formulation with 5 wt.% emulsifier had best stability with the largest oil rich fraction

after four weeks of ageing, **Figure 3.2**. Only the 5 wt.% emulsifier sample was characterised and later utilised in residual bioassay experiments.

Figure 3.2: Homogeneous emulsion containing 5 wt.% surfactant just after preparation, (left) and after four weeks showing creaming (right)

3.2.7 Laboratory Bioassays

a. Rearing of mosquito colony

An. arabienis KGB strain larvae used for this study were derived from the stock colony reared at the insectary at University of Pretoria Institute for sustainable malaria control (UPISMC), Pretoria, South Africa. The insectary is maintained at 25 ℃ ± 2 ℃, 75 % ± 5 % relative humidity and a 12:12 (light: dark) cycle photoperiod.

b. Larvicidal bioassays of pure oleic acid as a free-standing oil

The ethical clearance, to conduct the bioassays studies, was granted by the Faculty of Health Sciences ethics committee of the University of Pretoria under protocol number (EBIT/226/2020). Larvicidal activity was determined using an adaptation of the method described by World Health (2005a) and Mavundza *et al* (2013). A 1 % stock solution was made by dissolving 200 mg of pure oleic acid in 20 ml of acetone solvent. Serial dilutions were later prepared from the stock solution as required, see **Annexure 1**. Batches of 25 healthy 3rd and 4th instar larvae were added to cups each containing 100 mL distilled water and allowed to acclimatise. The desired dosage was carefully added using a micropipette. Each test concentration and its corresponding negative control (acetone solvent only)

63

constituted of four replicates. Moribund and dead larvae after 24 h and 48 h were recorded on bioassays data recordings forms, **Annexure 2**. The mosquito larvae were fed with dog biscuits and brewer's yeast at a 3:1 ratio during the test period. The bioassays were performed three times on three separate days using freshly prepared solutions and new batches of larvae as stipulated by WHO guidelines. To evaluate the LC_{50} and LC_{90} values, a robust statistical analysis was performed utilising the "drc" extension of the R statistical software (Ritz & Streibig, 2005).

c. Evaluation of residual efficacy of the developed slow-release mechanisms

The required mass of the delivery systems, corresponding to a maximum possible dosage of 500 ppm of oleic acid, was determined. The only exception was the LDH-oleate to which a double amount of 1000 ppm was used as it is the only mechanism where oleic acid is in oleate form. The weighed mass was added to 3 L of distilled water placed in large glass containers as shown in **Figure 3.3**. Neat, distilled water was used as the negative control. Additionally, a thermoplastic starch free from oleic acid was also considered. For each mechanism, the bioassays were replicated four times. The emulsion was vigorously shaken for a minute before addition to ensure homogeneous quantity was added.

Batches of 25 healthy 3rd and 4th instar larvae were added to cups containing 100 mL of water withdrawn from each glass container. The amount of water withdrawn was replaced to maintain the same volume of water. Moribund and dead larvae were recorded after 24 h and 48 h. The larvae were fed with dog biscuits and brewer's yeast at a 3:1 ratio during the test period. The tests were performed at the end of each week over a period of five weeks.

Figure 3.3: Experimental setup to evaluate residual efficacy

64

3.2.8 Effect of pH on the rate of LDH-oleate dissolution

The effect of pH on dissolution of LDH-oleate was investigated by determining the Mg^{2+} and Al^{3+} ions released in sodium acetate-acetic acid buffer solutions with time. **Table 3.3** presents volumetric portions of sodium acetate trihydrate (**NaOAc**) and acetic acid (**HOAc**) solutions required to make buffer solutions of different pH values.

Table 3.3: Volumes of NaOAc-HOAc buffer solutions used to set the pH

ml (0.2M NaOAc)	ml (0.2M HOAc)	pH
10	90	3.7
37	63	4.4
70	30	5.0
91	9	5.6

LDH-oleate to corresponding to a dosage of 1000 ppm of oleate anions when fully dissolved was loaded to each of the solution in 1 L beakers. After weekly time intervals, 60 ml aliquots were extracted and filtered to arrest the LDH-oleate dissolution reaction. The volume of solution withdrawn was replaced. The experiment was conducted for a period of five weeks. The dissolved Mg^{2+} and Al^{3+} cations in solution were determined by UIS Analytical services using inductively coupled plasma spectroscopy (ICP). A Perkin Elmer optima 5300 DV ICP-OES spectrometer was used.

3.3 Material characterization techniques

3.3.1 Rancimat oxidation stability test

The determination of oxidative stability of methyl oleate, as a proxy for oleic acid, was conducted on a Metrohm 895 Professional PVC Thermomat, Switzerland as shown in **Figure 3.4**. Three grams of the sample was weighed into the reaction vessel and placed within a heater block maintained at 110 ºC. Purified air flowing at a rate of 10 L.h^{-1} was bubbled through the liquid sample. The measuring vessel contained 60 mL of ultra-pure deionized water. The induction period (IP) was automatically evaluated by the Metrohm Stabnet software.

65
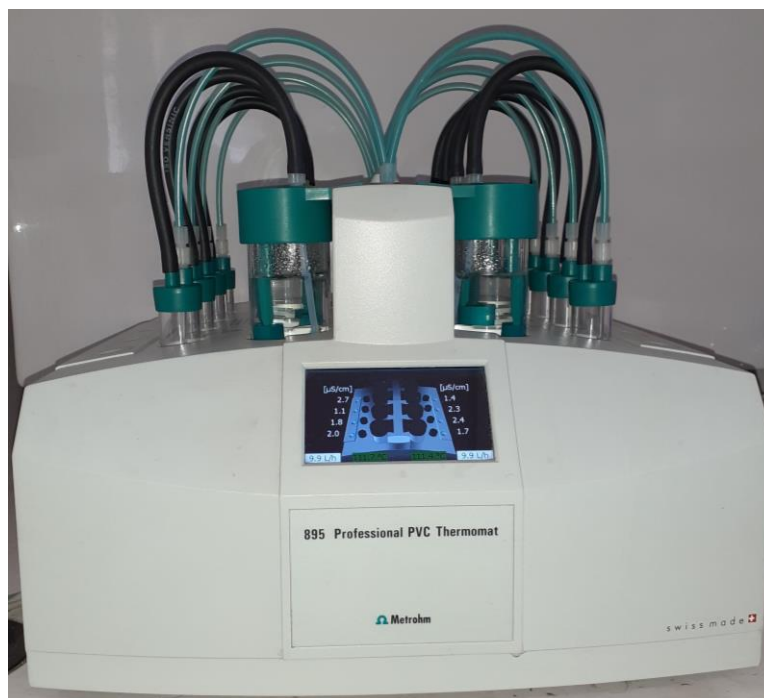
Figure 3.4: Metrohm 895 Professional PVC Thermomat

3.3.2 X-ray Diffraction (XRD)

The samples were analysed using Panalytical X'Pert Pro powder diffractometer in (θ-θ) configuration with an X'Celerator detector, variable divergence, and fixed receiving slits with filtered Cu-Kα radiation (λ = 1.54184Å) at 40 kV and 40 mA. The samples were analysed in the scan range of 2-70° (2θ) at a rate of $0.02°$ s^{-1}. The standard Panalytical backloading technique was utilised to prepare powdered samples to provide a random particle distribution.

3.3.3 Scanning Electron Microscopy (SEM) analysis

The sample morphologies were analyzed using a Zeiss Supra 55 VP FEG SEM (Zeiss, Germany). Samples were placed on adhesive carbon tape placed on SEM aluminium stubs and rendered conductive by sputter coating with about 5 nm tungsten (Quorum 150 TES; Quorum, UK) before imaging. The activated charcoal pellets were dipped in liquid nitrogen and fractured before coating. The SEM images depict the fractured cross sections.

3.3.4 Fourier transform infrared spectroscopy (FTIR) analysis

FTIR spectra were recorded on a Perkin-Elmer Spectrum 100 instrument fitted with a universal attenuated total reflection (ATR) attachment. FTIR spectra were recorded in the absorbance range of 400 to 4000 cm^{-1} at a resolution of 4 cm^{-1}. The results represent an average of 16 scans.

66

3.3.5 Raman analysis

The spectra were recorded on a WITec confocal Raman microscope (WITec Alpha 300R, Germany). The excitation laser was set at 532 nm and power was set at 10 mW with an acquisition time of $2 \times 30s$. Raman spectra were used to characterize the carbon phases of the pyrolyzed spent coffee grounds and the activated charcoal.

3.3.6 Thermogravimetric analysis (TGA)

The thermal properties of the samples were analysed using TA instruments SQT-Q600 instrument. The samples weighing between 15-20 mg were heated in 40 µL alumina pans at using a heating ramp of 10 $^{\circ}$C/min. An inert furnace atmosphere was maintained with nitrogen flowing at 50 mL.min^{-1}.

3.3.7 Droplet size distribution and zeta potential

The most stable emulsion sample was analysed using a Malvern Zetasizer Nano ZS instrument to determine the droplet size distribution and the zeta potential. The mixed oleic acid emulsion samples by gentle shaking were initially diluted with deionised water to attain emulsion: deionised water ratios of 1:10. The refractive index of the continuous dispersant medium of 1.33 was used. Refractive index of oleic acid was taken as 1.46. Experiments were run in triplicate and the reported results shows the average.

3.3.8 Optical microscopy

Optical light images of the emulsions were captured by a Zeiss Axio Imager 2 fitted with a digital camera. The mixed oleic acid emulsion samples by gentle shaking were initially diluted with deionised water to attain emulsion: deionised water ratios of 1:10 and 1:20. Diluted emulsion samples were dropped on a microscope slide and subsequently a cover slip was carefully placed before analysis. The samples were viewed under bright field (BF) contrast.

67

CHAPTER 4: RESULTS AND DISCUSSION

4.1 Rancimat oxidative stability analysis

Induction period (IP) as a function of concentration for the two antioxidants is shown on **Figure 4.1**. The IP value of neat methyl oleate was very low (0.08 ± 0.01 h). Both antioxidants significantly improved the thermal oxidative stability. Considering eugenol as the antioxidant it seems that similar IP values were obtained for methyl oleate and neat oleic acid. However, in the case of curcumin, the conductivity curves generated by the instrument did not show the required inflection point even after 12 h of testing. IP values could not be determined for oleic acid. Therefore, the results for methyl oleate are taken as conservative estimates for the stability of the neat oleic acid. This means that both eugenol and curcumin improved the thermal oxidative stability of the methyl oleate. Curcumin proved a better antioxidant compared to eugenol with an IP > 15 h at a dosage of 0.25 wt.% compared to IP ≈ 8 h at 1.0 wt.% for eugenol. These values compared favourably with the specifications for biodiesel (> 6 h) (EN14112, 2016; Focke *et al*, 2012).
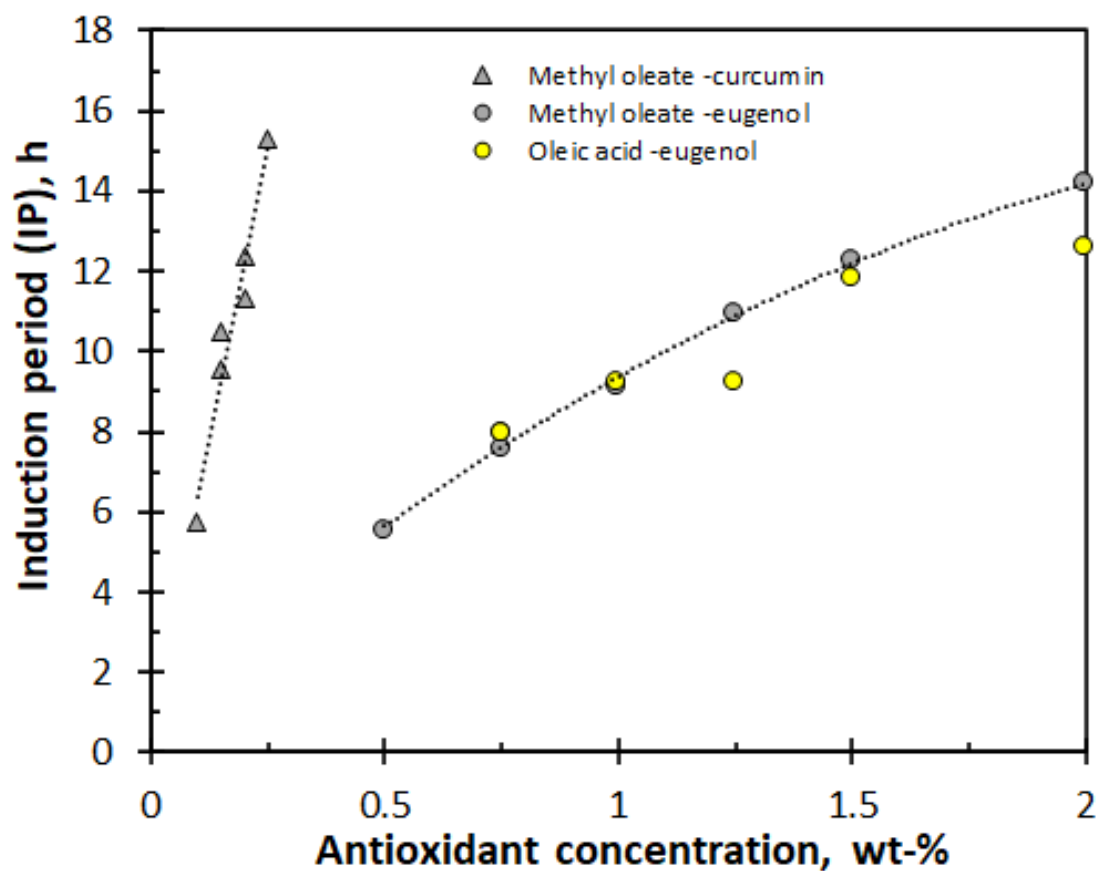
Figure 4.1: Antioxidant properties of eugenol and curcumin as a function of composition

The effectiveness of curcumin compared to eugenol as an antioxidant can be ascribed to the lower bond dissociation energies for the two phenolic hydroxyl groups and its higher molecular weight (Varatharajan & Pushparani, 2018). Reportedly the presence of the alkoxy group at the ortho position to the phenolic groups also plays a role (Romola *et al*, 2021). Depending on the environment, curcumin also exhibits additional antioxidant mechanisms beyond the hydrogen atom donation mechanism (Galano *et al*, 2009).

4.2 Scanning Electron Microscopy (SEM)

The SEM images of the pure LDH, calcined LDH and the LDH-oleate are shown in **Figure 4.2**. The pure LDH (a) exhibits hexagonal structure which is typical of brucite-like sheets (Cavani *et al*, 1991). The hexagonal structure of calcined LDH (b) at 500 °C morphology is identical to that of the pristine LDH but thinner compared to the precursor (refer **Annexure 4a** for clearer view). This is consistent with the findings of Kang *et al* (2015). The LDH-oleate (c) also presents a layered structure which possess a platy hexagonal structure. It is evident that the oleate anions where successfully intercalated into the LDH interlayer galleries by the hydrothermal reconstruction process. The morphology also shows an improved particle size which justifies an expanded structure by intercalation as determined by the XRD d-spacing values.
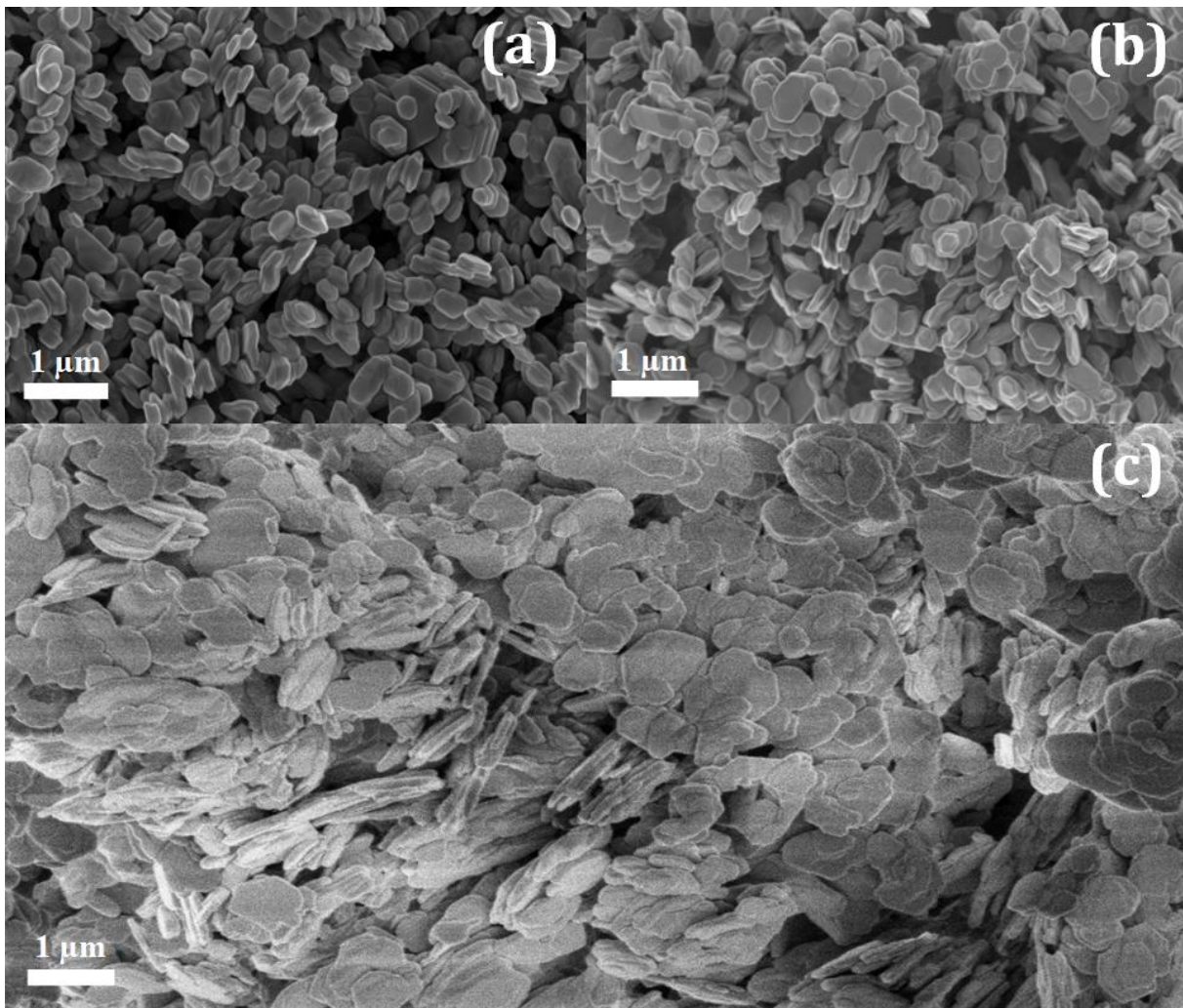
Figure 4.2: SEM images of (a) as received pristine LDH, (b) calcined LDH and (c) LDH-oleate. Scale bar: 1 µm

Figure 4.3 shows that the morphology of the washed and dried spent coffee grounds (a, a') was transformed by pyrolysis at 500 °C. The surface of the pyrolyzed spent coffee grounds displays a highly heterogeneous porous morphology with thinner walls as shown in (b, b'). This is similar to the structures reported by Benyekkou et al (2020). Both spent coffee biochar and its precursor shows honeycomb-shaped structures which agrees with the findings of Jang *et al* (2015). As expected, the fracture surfaces of the activated charcoal (c, c') also show a porous morphology.
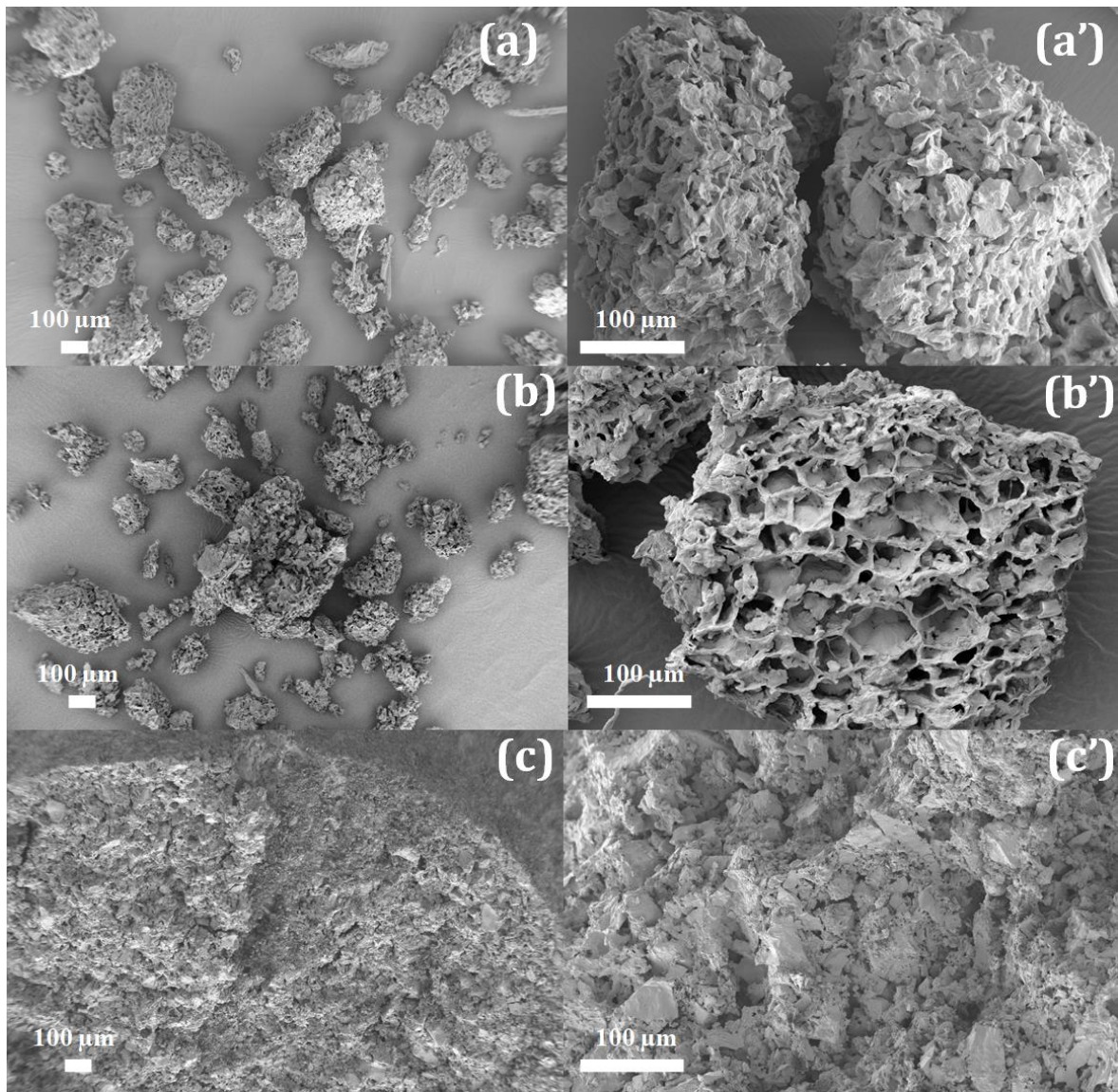
Figure 4.3: SEM images at 50× (left) and 200× magnification (right) of SCG (a, a'), PSCG (b, b'), as received AC (c, c'). Scale bar: 100 µm

The morphology of pure dextrin and the fractured surface of the extruded nanocomposite are shown in **Figure 4.4**. The dextrin powder (left) comprised of a combination of polyhedral and spherical shaped granules. The spherical granules (red arrow) are from the floury centre of corn kernel and the indents (yellow arrow) are due to protein from the horny endosperm (BeMiller, 2019). Upon extrusion (right), the starch granules are disrupted as the matrix is plasticised. The fractured cross sections of the extruded samples shows that organoclay is well dispersed within the matric structure. This explains the mechanism whereby the exudation of oleic acid was prevented. Additional images of same materials are provided in **Annexure 5.**

71
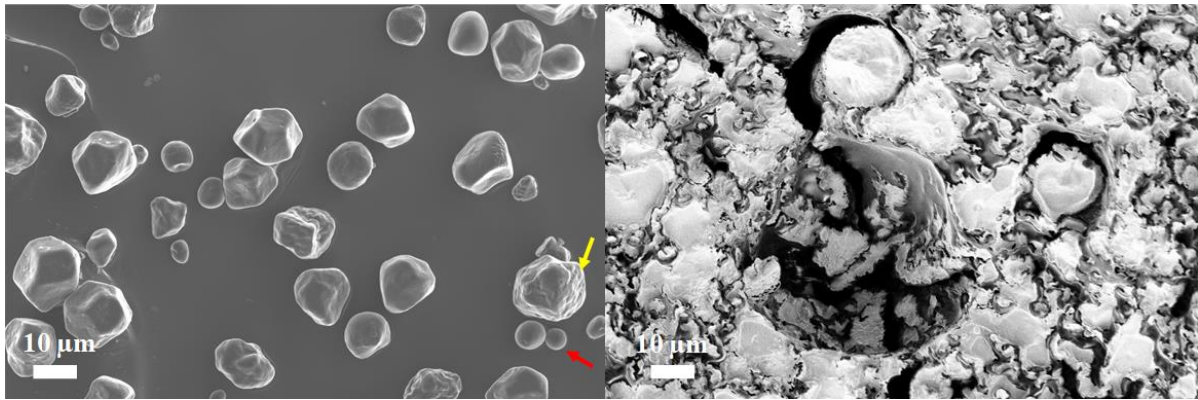
Figure 4.4: SEM images of dextrin powder (left) and the fractured surface of the extruded nanocomposite strand (right). Scale bar: 10 µm

4.2 XRD Analysis

Figure 4.5 illustrates the XRD diffractogram of pristine as received LDH (LDH-Neat), LDH calcined at 500 °C (LDH-Calcined), and LDH intercalated with oleate ions (LDH-Oleate). The sharp and narrow reflections for MgAl-LDH is consistent with highly crystalline hydrotalcite-like phase (Li *et al*, 2013; Mondal *et al*, 2016).

Calcination at 500 °C of the neat LDH converted it to a layered double oxide. This is proven by the d-spacing reflection shift to a much higher 2θ value. The LDH-oleate diffraction pattern shows the appearance of new reflections. The d-spacing corresponding to 2θ = 2.42° is 3.65 nm as expected for intercalated oleate anions. However, the sample also contains some reformed LDH-carbonate (Nhlapo *et al*, 2008). This means that during the intercalation process some CO_2 must have been available.

72
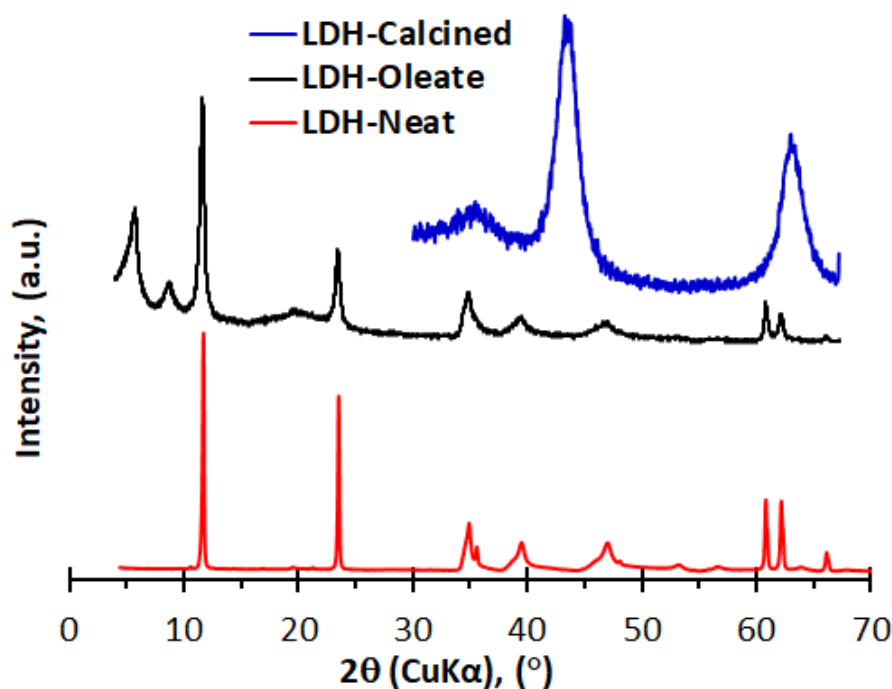
Figure 4.5: X-ray diffractogram of the LDH-neat, LDH-calcined at 500 °C and LDH-oleate

4.4 FTIR analysis

Figure 4.6 portrays the obtained FTIR spectra of the pure oleic acid, pristine LDH, calcined LDH and LDH-oleate processed via hydrothermal reconstruction at 80 °C. The range for the wavenumber was considered from 700 to 3700 cm^{-1}. Oleic acid in its pure form as received, has three major characteristic absorption bands with two around 2800-2900 cm^{-1} and one prominent absorption band at 1708 cm^{-1}. The former double peaks are ascribed to asymmetric stretching and symmetric stretching vibrations of aliphatic C-H in the methylene (-CH$_2$) and methyl (-CH$_3$) groups (Niu *et al*, 2017) whilst the latter and most pronounced peak is attributed to the carbonyl group (C=O) asymmetric stretching vibrations. The minor OA peaks are olefinic C-H stretching peak at 3000 cm^{-1}; between 1200 -1500 cm^{-1} aliphatic CH$_3$ and CH$_2$ bend scissoring, C-O stretch, O-H out of plane stretch at 925 cm^{-1} and lastly CH$_2$ rocking vibration at 717 cm^{-1} (Niu & Li, 2012; Premaratne *et al*, 2014).
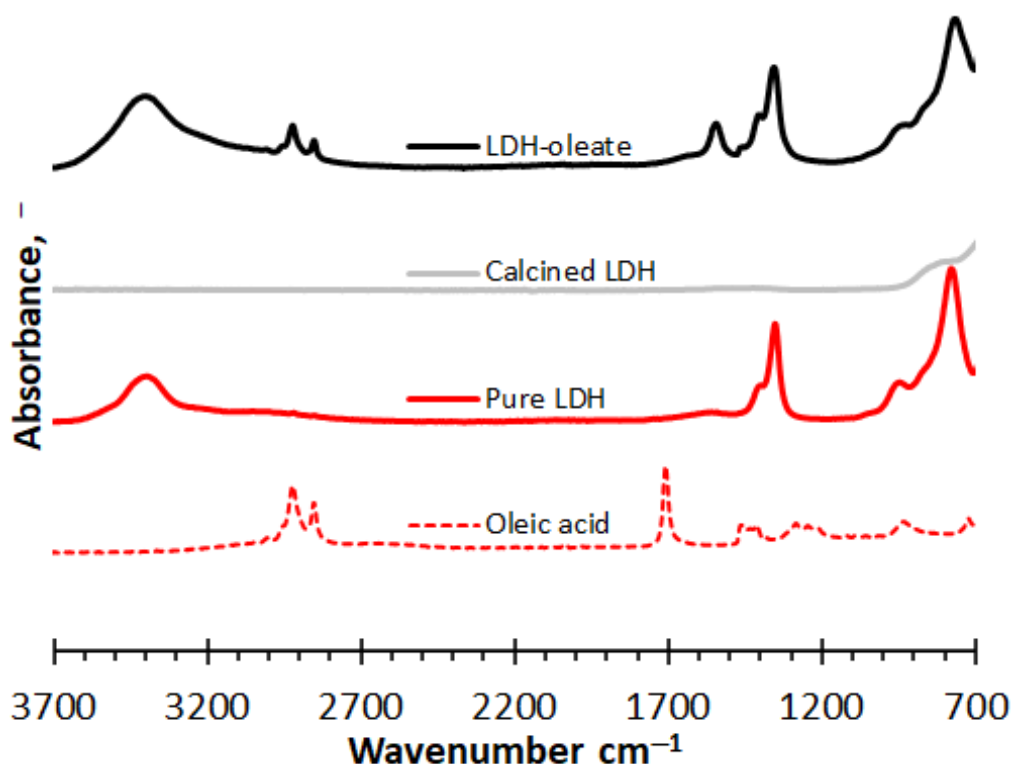
Figure 4.6: The FTIR spectra of OA, pristine LDH, calcined LDH at 500 °C and LDH-oleate

Pure LDH shows an O-H stretching vibration between 3300-3400 cm^{-1} ascribed to water molecules and hydroxyl groups (Zhou *et al*, 2010a), carbonate (CO_3^{2-}) associated bands at 1352 cm^{-1} and at 774 cm^{-1}. The first carbonate peak is attributed to hydrogen bonding with associated water molecules (Li *et al*, 2013; Yang *et al*, 2009) whilst the latter is associated with the interaction of the carbonate ions and the hydroxyl groups of the brucite-like layers (Li *et al*, 2013). All major LDH bands are absent in the dehydroxylated and decarbonated LDH calcined at 500 °C. This resulted in the formation of layered mixed oxides with a different morphology as also shown in SEM image in **Figure 4.2**.

LDH-oleate shows the two bands at 2800-2900 cm^{-1} characteristic for the asymmetric- and symmetric stretching vibrations of aliphatic C-H in the methylene (-CH$_2$) and methyl (-CH$_3$) groups which are contributed by the oleic acid. The carbonyl vibration peak at 1708 cm^{-1} corresponding to the free -COOH oleic acid (Yang *et al*, 2016) is missing in the LDH-oleate. Instead, a new absorption band is found at 1541 cm^{-1}. This is characteristic for the asymmetric stretching vibration of the carboxylate ion (COO^-) (Celis *et al*, 2014; Nhlapo *et al*, 2008). This new band proves the interaction between oleate anions with the LDH inner layers (Zhou *et al*, 2010a) and confirms that oleic acid is intercalated as oleate anions. The

74

LDH-oleate formed is impure. The presence of carbonate is indicated by the bands located at 1352 cm^{-1} and 774 cm^{-1}. This supports the findings from the XRD analysis.

The FTIR spectra of the carbon matrices, neat and loaded with oleic acid are shown in **Figure 4.7.** As is clear from the Figure, the absorptions of the neat matrices are featureless. The exception is the PSCGs where hints for the presence of residual aliphatic components indicated by bands around 2800-3000 cm^{-1}. These are attributed to residual lipids and caffeine from the roasted coffee (Maree *et al*, 2020).
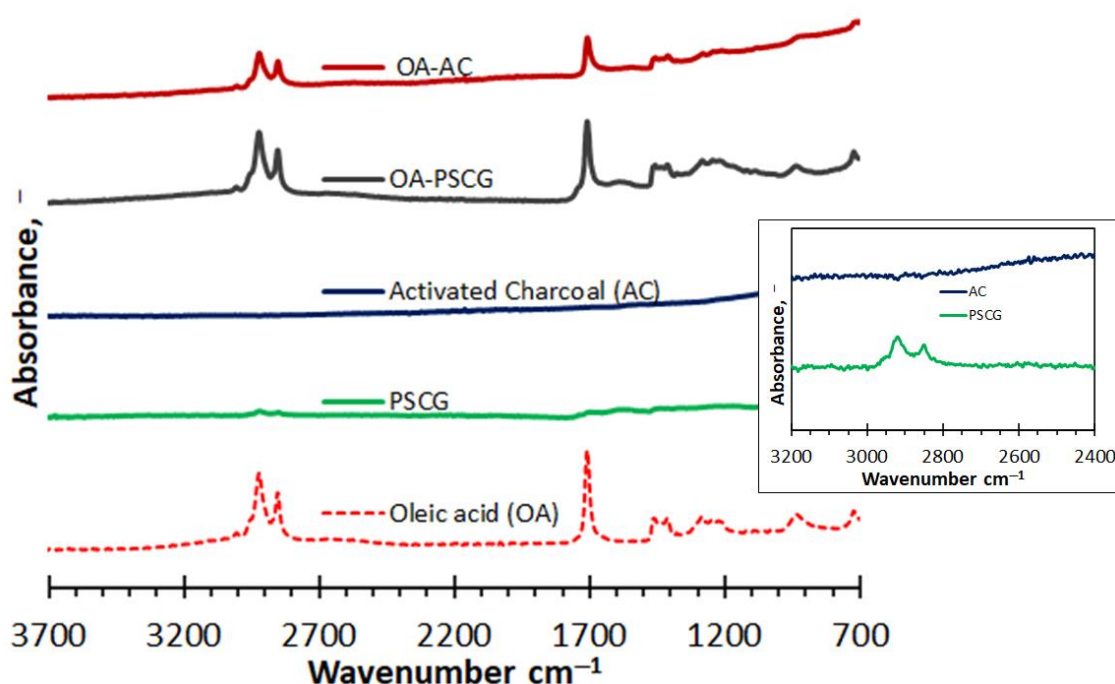
Figure 4.7: The FTIR spectra of oleic acid (OA), pyrolyzed spent coffee grounds (PSCG), activated charcoal (AC), oleic acid loaded pyrolyzed spent coffee grounds (OA-PSCG), oleic acid loaded activated charcoal (OA-AC) and **insert**, zoomed in spectrum of PSCG and AC

The FTIR spectra of neat thermoplastic starch and thermoplastic starch with 10 wt.% OA in the range 1500 -3600 cm^{-1} are shown in **Figure 4.8**. Neat thermoplastic starch shows vibration bands at 3280 cm^{-1} (O-H symmetrical stretching), between 2800-2900 cm^{-1} (aliphatic C-H stretching) and at 1635 cm^{-1} (due to glycosidic C-O-C bond vibration) (Cervantes-Ramírez *et al*, 2020; Intan & Rachmawati, 2019). Thermoplastic starch with 10 wt.% OA features new vibration bands at 3000 cm^{-1} (olefinic C-H stretching) and at 1715 cm^{-1} (asymmetric stretching of carbonyl group C=O).

75
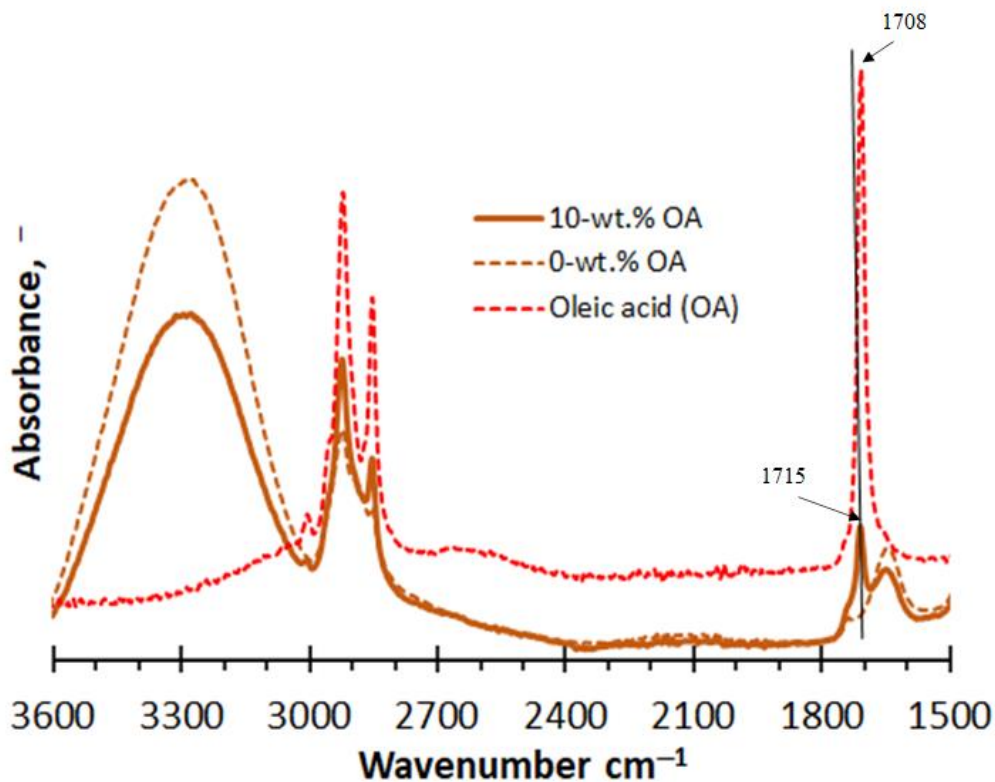
Figure 4.8: FTIR spectra of OA, neat thermoplastic starch and thermoplastic starch with 10 wt.% OA

The oleic acid carbonyl band, in the thermoplastic starch compound, shifted from 1708 to a higher wavenumber (1715 cm^{-1}). According to Marinopoulou *et al* (2016b), this carbonyl shift shows interaction of OA with starch. The OA molecules form inclusion complexes with the amylose starch helix. Absorption intensities for the bands between 2800-2900 cm^{-1} (aliphatic C-H stretching) in thermoplastic starch increased when 10 wt.% OA was present. This was just an additional contribution from the aliphatic part of the OA. However, the other bands in the neat thermoplastic starch (3280 cm^{-1} O-H symmetrical stretching, 1635 cm^{-1} glycosidic C-O-C bond vibration) decreased in intensity with 10 wt.% OA. The former is due to new weakened hydrogen bonding between OA, starch, nanocellulose and glycerol (Sun *et al*, 2019) whilst the latter is a consequence of reduced starch content by oleic acid inclusion.

4.5 Raman analysis

The Raman spectra for the as-received activated charcoal and the pyrolyzed spent coffee grounds is shown in **Figure 4.9**. Two distinctive carbon bands are indicated between 1200-1400 cm^{-1} and 1500-1700 cm^{-1}. The former is known as the D-band, and it is attributed to disordered (amorphous) or defect-rich sp^{3}-hybridized carbon vibrations. The latter G-band

76

correspond to graphitic sp^2-hybridised carbon vibrations (Hsieh *et al*, 2021; Thirumal *et al*, 2022). In activated charcoal the D-band peaked at 1341 cm^{-1} and G-band at 1595 cm^{-1} with I_D/I_G of 1.12. In the pyrolyzed spent coffee spectrum, the corresponding values were 1361 cm^{-1} and 1575 cm^{-1} with $I_D/I_G = 0.93$. The implication is that the pyrolyzed spent coffee grounds are slightly more graphitic in nature than the activated charcoal (Lazzarini *et al*, 2016).
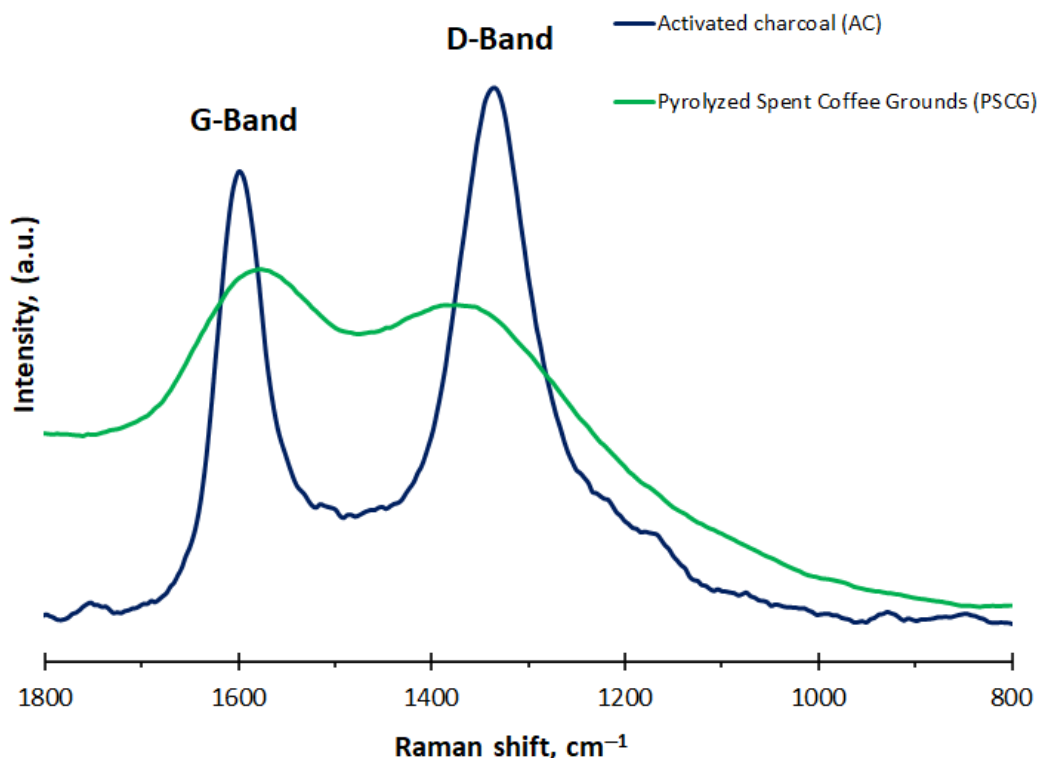
Figure 4.9: Raman spectra of the activated charcoal as received and the pyrolyzed spent coffee grounds

4.6 Thermogravimetric analysis (TGA)

The thermal decomposition behaviour of the LDH samples and oleic acid are presented in **Figure 4.10.** Oleic acid, as a free-standing oil undergoes a rapid single step mass loss with the rate peaking at *ca*. 300 °C. This is attributed primarily to evaporation rather than thermal degradation. Pure LDH and LDH-oleate exhibit a similar thermal decomposition behaviour. The derivative curves (DTG) of both, in **Figure 4.10** displays a three-step overlapping mass loss progression. The first occurs between 150 - 250 °C, the second around 250 - 350 °C, and the third and final occurs in the range 350 - 450 °C. Thereafter the mass loss plateaus leaving a final residue. The first event corresponds to the dehydration, i.e., the loss of interlayer

77

water. The second is attributed to dehydroxylation, while the third corresponds to a combination of dehydroxylation and decarbonation (Forano *et al*, 2013; Mondal *et al*, 2016; Nhlapo *et al*, 2008).
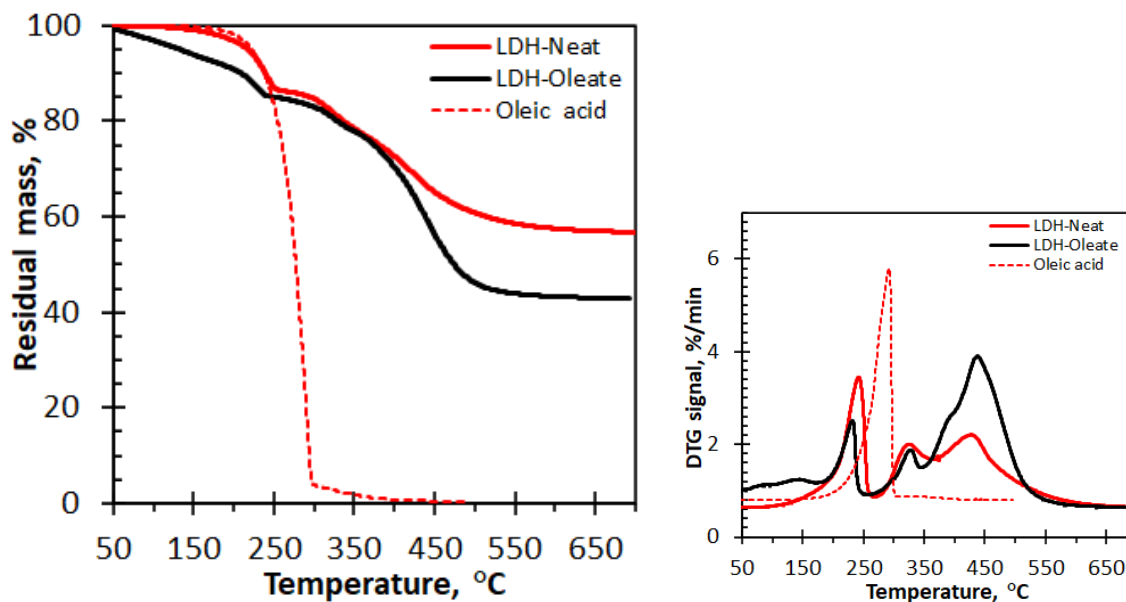
Figure 4.10: TGA and DTG curves of neat LDH as received (LDH-Neat), LDH intercalated with oleate ions from the oleic acid (LDH-oleate) and neat oleic acid

The oleic acid mass loss from the LDH-oleate occurs at much higher temperatures because the oleate anions are intercalated into the LDH interlayer galleries. Their volatility is suppressed because of the ionic bonding. The final release is probably associated with the decomposition of the fatty acid molecules (Yang *et al*, 2009). The decomposition of the LDH-oleate is occurs in the temperature range of 350 - 450 °C. These observations are in agreement with the findings by Blasi *et al* (2021) who proved that intercalation of oleate anions into LDH improves not only thermal stability but also the oxidative stability. The difference in the residue between pure LDH and LDH-oleate indicates that *ca.* 25 % of oleate ions were successfully intercalated into LDH.

Figure 4.11 represents the thermal behaviour, of neat thermoplastic starch, thermoplastic starch with 10 wt.% OA and their respective pure components. Oleic acid and glycerol undergo single step evaporation process with peak temperatures recorded at *ca.* 293 °C and 237 °C respectively. Dextrin undergoes a 2-step mass loss with initial *ca.* 9 wt.% water loss by evaporation up to 150 °C followed by major degradation step at *ca.* 300 °C leaving a partial carbonized residue of 14 wt.% at 600 °C. Organoclay loses water and volatile components leaving a residue of 70 wt.%. Cellulose nanofibers (CNF) show a major mass

78

loss from 50 - 150 °C with peak at *ca.* 101 °C due to water evaporation leaving a residue of 7 wt.%.
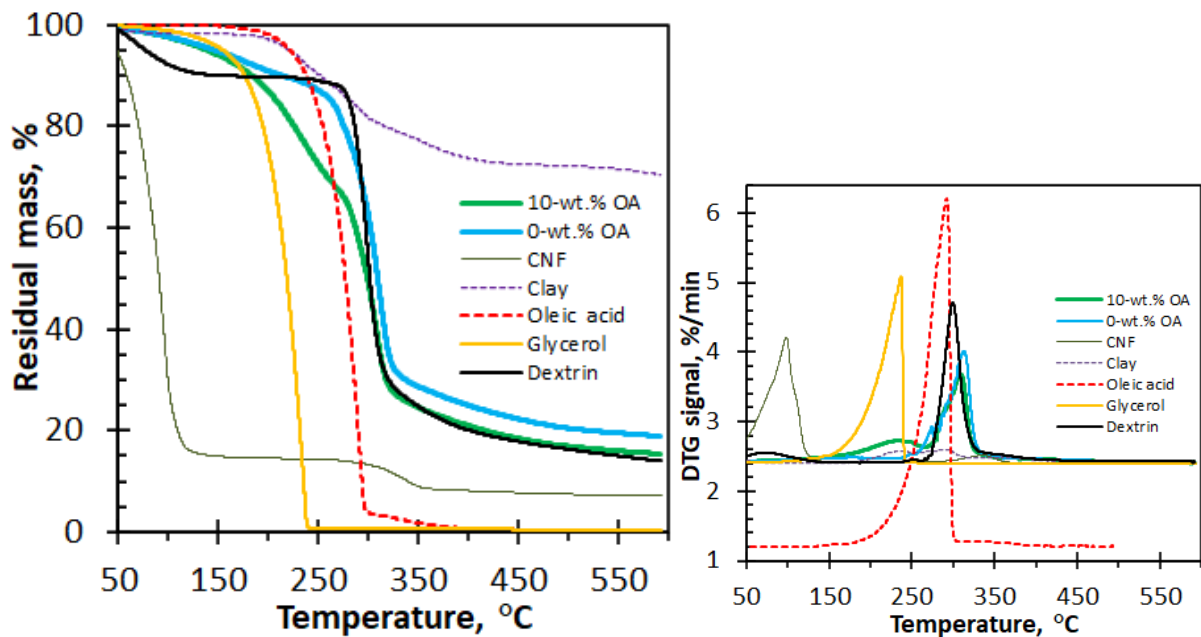
Figure 4.11: TGA and DTG curves neat thermoplastic starch 0 wt.% OA and thermoplastic starch with 10 wt.% OA and the corresponding pure components

Neat thermoplastic starch nanocomposite undergoes a single continuous degradation step from 300 - 350 °C with a peak at 314 °C higher than all single components. This is contributed by strong interactions between glycerol, starch and nanocellulose via hydrogen bonding in the plasticized matrix and enhanced tendency to form non-volatile char. Thermoplastic starch with 10 wt.% oleic acid shows distinct two-step overlapping mass loss between 150 - 280 °C and 280 - 350°C. The former step has a peak at *ca* 237 °C whilst the latter has a peak at *ca.* 310 °C which is lower compared to neat thermoplastic starch. The former peak loss is associated to plasticizer (glycerol) rich phase loss whilst the latter is due to dextrin and nanocellulose rich phase (Area *et al*, 2019; Rico *et al*, 2016). OA forms inclusion complexes with the amylose starch improving its oxidative stability (Marinopoulou *et al*, 2016b).

No distinct OA single peak loss is observed therefore it can be postulated that this proves OA interacts with starch and nanocellulose freeing some glycerol molecules. The free glycerol molecules form the rich plasticizer phase which is lost in the first step missing in neat thermoplastic starch. Oleic acid results in weak hydrogen bonding and less intensity of O-H stretching vibrations as proved by FTIR.

79

4.7 Droplet size distribution and zeta potential

The emulsion droplet size distributions of the triplicate runs, and their average are presented in **Figure 4.12**. A fixed step was added to allow visualisation of the differences in the distributions. The droplet size displays a bimodal distribution with a broader peak in the size range 40 - 400 nm and a narrower peak from 1.1 - 6.0 µm. The average particle size was 211 $\pm$ 80 nm and zeta potential of -56 ± 10 mV after 4 weeks of ageing. The mean particle size values and a negative zeta potential concurs with previous studies of oleic acid and olive oil-based emulsions (Jaworska *et al*, 2013; Li *et al*, 2019b; Yukuyama *et al*, 2019). A high value of -56 mV for the zeta potential indicated a good emulsion stability compared to a value of -30 mV obtained by Kamogawa *et al* (2001) for a surfactant-free OA-in-water emulsion.
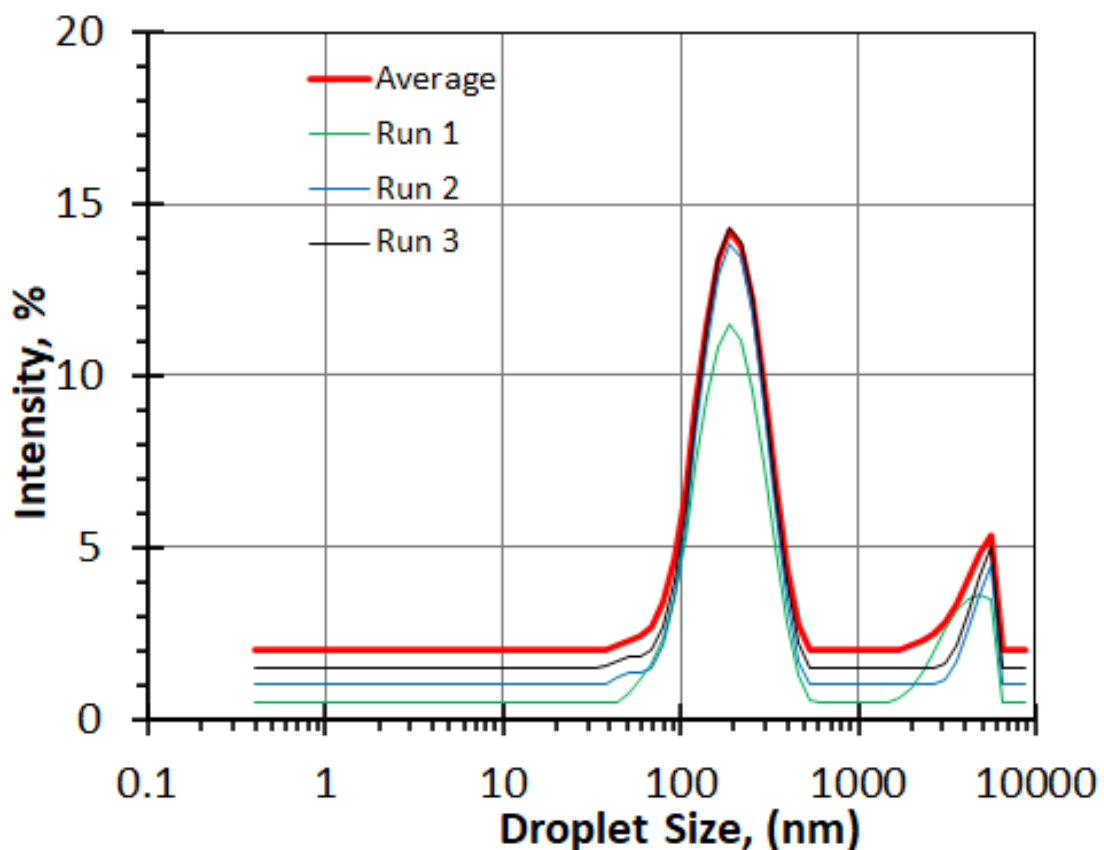
Figure 4.12: Droplet size distribution of O/W emulsion containing 35 wt.% OA and 5 wt.% SMO-based emulsifier after 4 weeks of storage at ×10 dilution

80

4.8 Optical Microscopy

Figure 4.13 shows the optical micrographs of the diluted emulsion sample. The images further confirm the bimodal particle size distribution of the emulsion droplets.
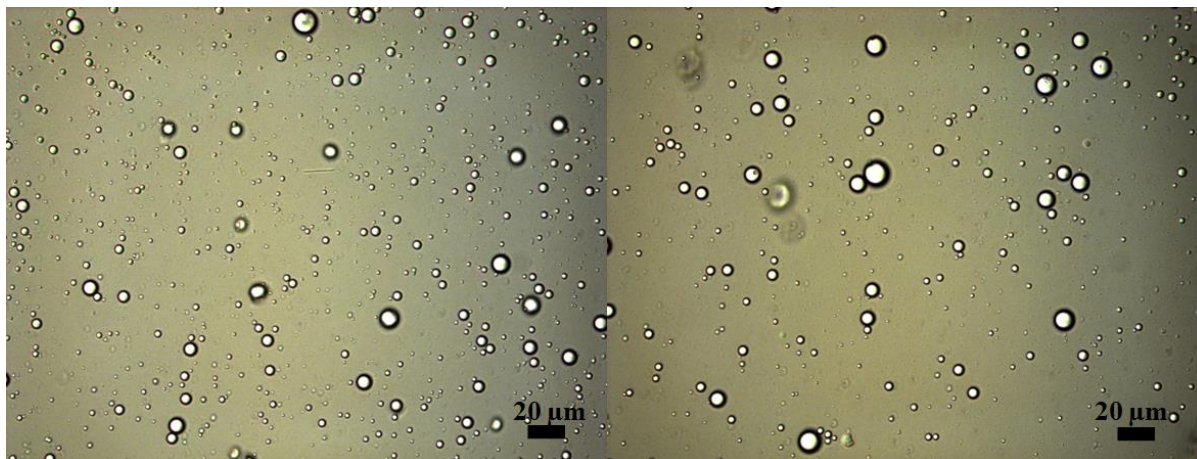
Figure 4.13: Optical images of O/W emulsion containing 35 wt.% OA and 5 wt.% SMO-based emulsifier after 4 weeks of storage. Left: ×10 dilution, right: ×20 dilution. Scale bar: 20 μm

4.9 Larvicidal bioassays

4.9.1 Pure oleic acid as a free-standing oil

A robust statistical analysis, to estimate the LC_{50} and LC_{90} values, was performed utilizing the "drc" extension of the R software package (Christian *et al*, 2015). Results obtained from laboratory bioassays was transformed to be utilised as binomial data. Subsequently, this data was used to generate dose response curves for 24 h and 48 h. Six models i.e., four-parameter logistic, Weibull Type I, Weibull Type II, log-normal, log-logistic and Gompertz models were utilised to analyse the dose response curves (Christian *et al*, 2015; Ritz & Streibig, 2005). The overall statistical analysis (average of all models) is shown in **Table 4.1**. The statistical analysis results suggests that oleic acid, as a free-standing oil, has an LC_{50} of 13 ppm and LC_{90} of 31 ppm against 3rd and 4th *An. arabiensis* instar after 48h. A more detailed statistical analysis report is included as supplementary material, **Annexure 7.**

81

Table 4.1: Lethal concentrations (LC) estimates of the 6 averaged models

Time, LC_n	Estimate	Std Error	Lower	Upper
24 h, LC_{10}	2.6	2.2	−1.7	6.9
24 h, LC_{50}	12.7	29	−44	70
24 h, LC_{90}	28.6	1020	−1975	2030
48 h, LC_{10}	2.1	1.4	−0.64	4.9
48 h, LC_{50}	13	21	−27	54
48 h, LC_{90}	31	666	−1270	1335

4.9.2 Residual efficacy of the developed slow-release mechanisms

Figure 4.14 shows the mortality results obtained for the different delivery systems during the bioassay tests. The first striking observation is the low mortality achieved during the early phases of the bioassay testing. The second point is that over the period of five weeks only the emulsion-based system achieved the requisite mortality levels. Even so, 50 % mortality was only exceeded after two weeks of ageing.

Note that the results obtained with the thermoplastic starch samples are not reported since the negative control (the 3rd and 4th *An. arabiensis* instar) showed unacceptably high mortality. This invalidated the test results. This applies even to the neat TPS being used as the negative control. The implication that valid test results would not be possible since the test larvae themselves appeared to be sensitive to the neat matrix. Therefore, starch-based oleic acid release mechanism was not evaluated further and was therefore not reported.
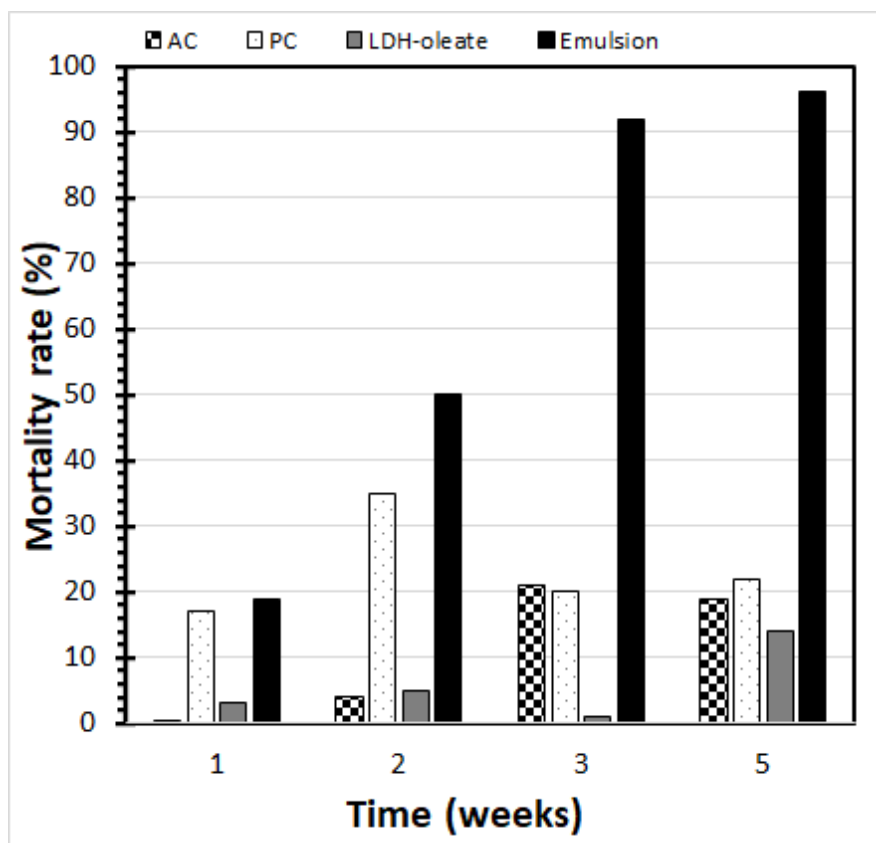
Figure 4.14: Residual bioassays of the formulated products, oleic acid impregnated activated charcoal (OA-AC), oleic acid impregnated pyrolyzed spent coffee grounds (OA-PSCG), LDH intercalated with oleate ions from oleic acid (LDH-oleate) and oleic acid in water emulsion (Emulsion)

Oleic acid/water emulsion had the best results with 20 % mortality at one week of ageing. The mortality increased rapidly thereafter reaching values exceeding 90 % at week three and beyond. The mortalities achieved using oleic acid loaded spent coffee biochar (OA-PSCG) at the release matrix averaged about 20 % mortality throughout the test period. The results of the oleic acid loaded activated charcoal (OA-AC) were slightly more erratic. They increased from 0 % mortality on the first week to *ca.* 20 % on week three which remained constant till week five. LDH-oleate delivered the worst results only achieving mortality of 14 % at week five.

These disappointing results were quite unexpected. Potential reasons for this failure to release toxic levels of the oleic acid into the water reservoir are discussed below. It is speculated that the oleic acid was too tightly held by the two solid dosage forms and that the emulsion droplets creamed to the top of the water too quickly. That is why it took very long before

83

toxic levels were established at the bottom of the water since the diffusion path was very long.

4.10 Effect of pH on the rate of LDH-oleate dissolution

LDH-oleate results were very poor than anticipated. It was therefore necessary to try and explain possible reasons for it. To investigate this, LDH-oleate was further investigated by performing dissolution experiments to establish the effect of pH on the dissolution rate in sodium acetate-acetic acid buffer solutions.

The effect of pH on dissolution of LDH-oleate was investigated by determining the Mg^{2+} and Al^{3+} ions released in sodium acetate-acetic acid buffer solutions with time. **Figure 4.15** presents the dissolved cations in solution for a tested period of five weeks. The released Mg^{2+} and Al^{3+} data trends fit the Korsmeyer *et al* (1983) model perfectly. The results of the release profile shows that LDH-oleate release is pH dependent, increasing with decreasing pH which is quite low at pH of 5.6. The water used for the residual bioassays had a pH of 6.5 ± 0.3.
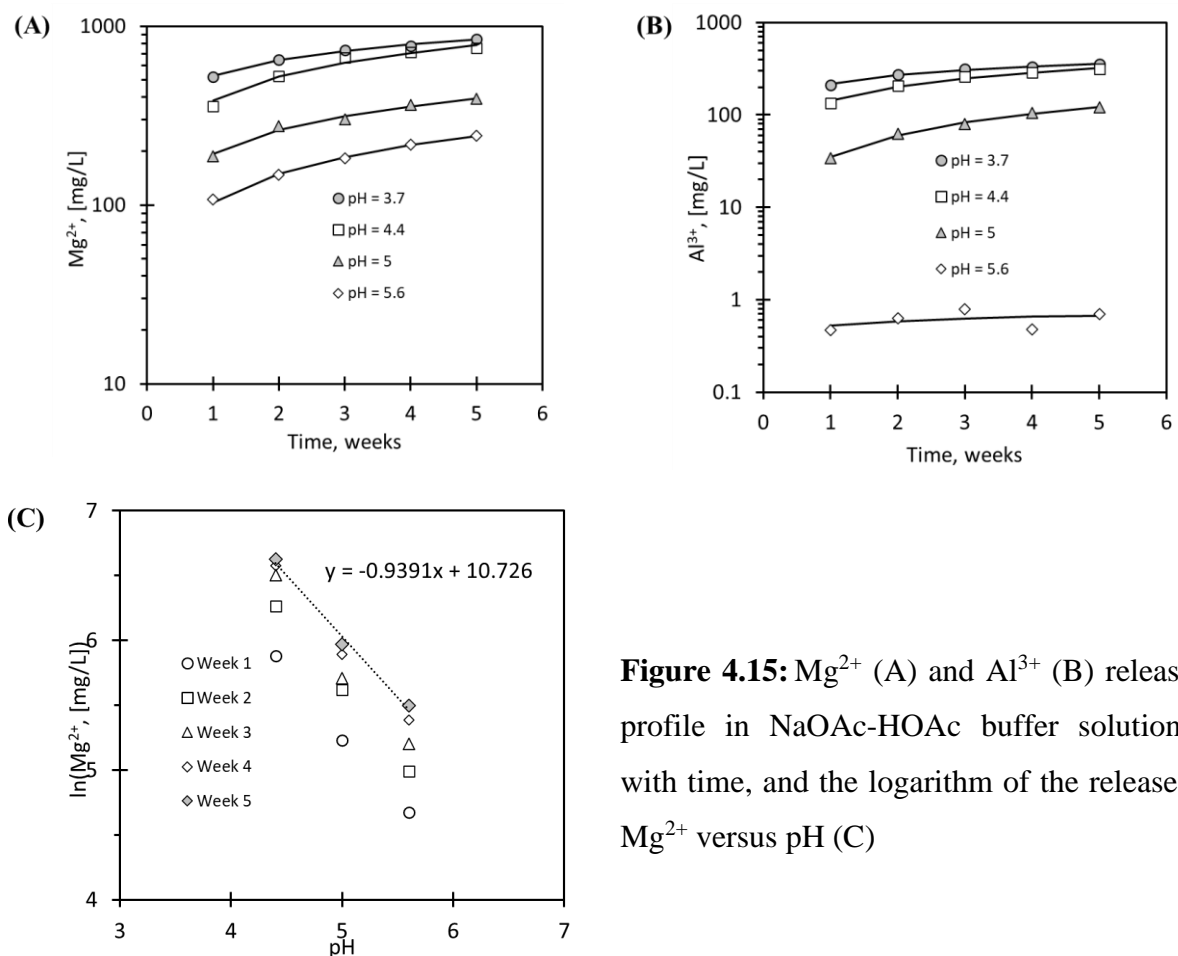
Figure 4.15: Mg^{2+} (A) and Al^{3+} (B) release profile in NaOAc-HOAc buffer solutions with time, and the logarithm of the released Mg^{2+} versus pH (C)

84

The observed mortality after 5 weeks in the water which had a pH of 6.5 was only 14 %. The plot of the logarithm of the Mg^{2+} concentration varied linearly with pH as shown in **Figure 4.15 (C)**. Extrapolation to a pH of 6.5 indicated a Mg^{2+} concentration of 102 mg/L. The maximum Mg^{2+} concentration, if all the LDH had dissolved was 1185 mg/L. This means that about 8.6 % of the LDH had disintegrated. It is assumed that the oleic acid release would be proportional to this value. Therefore, the oleic acid concentration should have reached 86 ppm if it had been released. This is not reflected in the observed mortality after five weeks. Therefore, there must have been another factor that reduced the toxicity. A possibility is that the released oleic acid formed salts with the magnesium of aluminium. Tattersfield & Gimingham (1927) did indeed find that the toxicity of alkanoic acid salts, to insects, is generally much lower than the free acid. It is also noticeable that the aluminium concentration was not in a proper proportion to the amount of magnesium ions released into the water. This might indicate that the oleic acid could have formed insoluble aluminium salts which were inactive as larvicides. This explains the poor performance of LDH-oleate which was observed in the bioassay experiments.

4.11 Dissolution of an emulsion droplet

The fastest dissolution of the active ingredient in the emulsion droplet can be determined by the assumption that the active ingredient is homogeneous in the continuous phase. Therefore, we can consider the spherical emulsion droplet in isolation with the portion of the continuous phase corresponding to the initial dose applied. The situation is shown schematically in **Figure 4.16**.
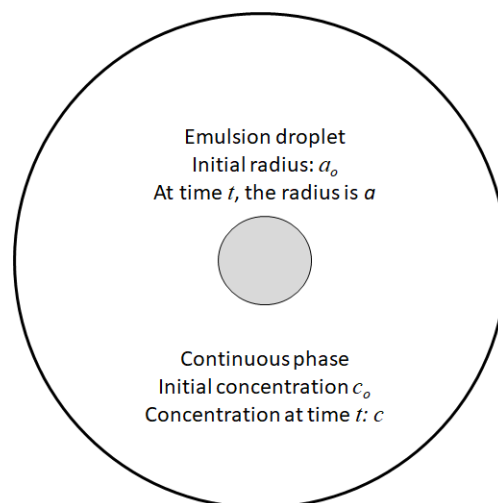
Figure 4.16: Schematic for an isolated emulsion droplet suspended in a liquid in which it is soluble

85

In the residual bioassay experiments, the water was dosed with 500 ppm oleic acid in the form of an emulsion. Let us assume that the emulsion droplets are uniformly and homogeneously dispersed in the water phase. This means that each droplet only needs to release oleic acid to the water in its immediate vicinity. Consider a droplet with an initial radius of a_o μm. We assume that it is acceptable to treat a spherical shell of water with this droplet. This means that the ratio of the cubes of the two radii multiplied by the densities of the two phases must equal the dosage rate of 500 ppm. Therefore, the following equation holds:

$$\frac{\rho_{OA}}{\rho_w}\left(\frac{a_o}{R}\right)^3 \approx 0.0005$$

$$R \approx \left(2000\frac{\rho_{OA}}{\rho_w}\right)^{\frac{1}{3}} a_o = \left(2000\frac{895}{1000}\right)^{\frac{1}{3}} a_o = 12.14\, a_o$$

The Cable & Frade (1987) analysis of diffusion limited dissolution behaviour of an isolated spherical particle was considered.

This specifies, a as radius of sphere and c_s as the pure solute concentration in sphere. The temperature and pressure are non-variable, the liquid is uniform and hence it is logically assumed that spherical symmetry is maintained. Material transfer across the sphere is controlled by Fickian diffusion, diffusivity (D) and concentration of solute, c_a in the liquid remains constant. Effects of viscosity, inertia, surface tension and gravity are excluded. Considering partial molar volumes of solute (v) and solvent as constant but not essentially equal, under these circumstances the solute diffusion in solution is described by:

$$\frac{\partial c}{\partial t} = D\left[\frac{\partial^2 c}{\partial r^2} + \frac{2}{r}\frac{\partial c}{\partial r}\right] - \varepsilon\left(\frac{a}{r}\right)^2 \frac{\partial a}{\partial t}\frac{\partial c}{\partial r} \qquad [4.1]$$

where $\varepsilon = (1 - c_s v)$ is Scriven's volume change parameter

      c = concentration

      r = radius

      t = time

The rate of change of the sphere size is then determined from:

$$\frac{da}{dt} = \frac{D}{c_s\left(1-c_a v\right)}\left(\frac{\partial c}{\partial r}\right)_{r=a} = \frac{D}{c_s - \left(1-\varepsilon\right)c_a}\left(\frac{\partial c}{\partial r}\right)_{r=a} \qquad [4.2]$$

86

The volumetric ratio of mole of solute in solution to that in the sphere is represented as $(1 - \varepsilon)$. Where for many solids, $\varepsilon = 0$ is considered a valid approximation.

The following initial and boundary conditions are specified:

$$c(a) = c_s; \qquad t \geq 0$$
$$c(\infty) = c_\infty; \qquad t \geq 0 \qquad\qquad [4.3]$$
$$c(r) = c_\infty; \qquad t = 0, \, r > a$$

Dimensionless variables are considered as:

$$F(z,e) = \frac{c - c_\infty}{c_s - c_a(1 - \varepsilon)}; \quad e = \frac{r}{a_o}; \quad R = \frac{a}{a_o}; \quad z = \frac{Dt}{a_o^2} \qquad [4.4]$$

The dimensionless variables transform equations 4.1 and 4.2 into:

$$\frac{\partial F}{\partial z} = \frac{\partial^2 F}{\partial e^2} + \frac{2}{e}\frac{\partial F}{\partial z} - \varepsilon\left(\frac{R}{e}\right)^2 \frac{dR}{dz}\frac{dF}{de} \qquad [4.5]$$

The initial boundary conditions are also transformed:

$$F(z, e \to \infty) = 0; \qquad\qquad\qquad z \geq 0$$
$$F\left(z, e = R = \frac{a}{a_o}\right) = F_a = \frac{c_a - c_\infty}{c_s - c_a(1 - \varepsilon)}; \quad z \geq 0 \qquad [4.6]$$
$$F(z = 0, e) = 0; \qquad\qquad\qquad z = 0, \, e > R = a/a_o$$

When these partial differential equations were solved by numerical methods, it was observed that when the solubility is very low, the effect of ε becomes negligible. The solutions approach the quasi-steady state approximation of Duda & Vrentas (1969) which incorporates convection and this simplifies to:

$$R^2 = 1 - 2\left[\frac{\ln(2 - \varepsilon)}{1 - \varepsilon}\right] F_a z \qquad [4.7]$$

Time to full dissolution, is obtained by setting $R = 0$.

4.11.1 Application to the dissolution of oleic acid emulsion droplet in water

The solubility of oleic acid in water is very low. Furthermore, we can assume that $\varepsilon = 0$, therefore equation [4.7] becomes:

$$R^2 = 1 - 2\ln(2) F_a z \qquad [4.8]$$

87

$$\left(\frac{a}{a_o}\right)^2 = 1 - 2\ln(2)\left(\frac{c_a - c_\infty}{c_s - c_a}\right)\frac{Dt}{a_o^2} \qquad [4.9]$$

But $c_\infty = 0$:

$$\left(\frac{a}{a_o}\right)^2 = 1 - 2\ln(2)\left(\frac{c_a}{c_s - c_a}\right)\frac{Dt}{a_o^2} \qquad [4.10]$$

Let X represent the fraction of the oil remaining at time t. Note that

$$X = \left(\frac{a}{a_o}\right)^3 \qquad [4.11]$$

$$X = \left[1 - 2\ln(2)\left(\frac{c_a}{c_s - c_a}\right)\frac{Dt}{a_o^2}\right]^{\frac{3}{2}} \qquad [4.12]$$

Complete dissolution (disappearance) of the droplet corresponds to $X = 0$. Therefore,

$$2\ln(2)\left(\frac{c_a}{c_s - c_a}\right)\frac{Dt_d}{a_o^2} = 1 \qquad [4.13]$$

This can be rearranged to:

$$t_d = \frac{c_s - c_a}{2\ln(2)c_a}\frac{a_o^2}{D} \qquad [4.14]$$

Equation 4.12 can be expressed to incorporate t_d as:

$$X = \left[1 - 2\ln(2)\left(\frac{c_a}{c_s - c_a}\right)\frac{Dt_d}{a_o^2}\frac{t}{t_d}\right]^{\frac{3}{2}} \qquad [4.15]$$

Substituting equation [4.14] into equation [4.15] and simplifying becomes:

$$X = \left[1 - \frac{t}{t_d}\right]^{\frac{3}{2}} \qquad [4.16]$$

Which can be rewritten:

$$t = t_d\left(1 - X^{2/3}\right) \qquad [4.17]$$

Substituting for X using equation [4.11] and simplifying gives:

$$t = t_d\left[1 - (a/a_o)^2\right] \qquad [4.18]$$

Substituting equation [4.14] for t_d in [4.17] results in:

88

$$t = \frac{(c_s - c_a)a_o^2}{2\ln(2)Dc_a}\left(1 - X^{2/3}\right) \qquad [4.19]$$

The fraction of the active remaining after time t when the radius of the droplet is equal to a is:

$$X = \left(1 - 2\ln(2)\frac{Dt}{a_o^2}\frac{c_a}{c_s - c_a}\right)^{\frac{3}{2}} \qquad [4.20]$$

The diffusion coefficient for oleic acid in water was estimated using the Scheibel (1954) correlation;

$$D = 8.2 \times 10^{-8}\frac{T}{\mu}\frac{1 + \left(\frac{3V_w}{V_s}\right)^{\frac{2}{3}}}{V_s^{\frac{1}{3}}} \qquad [4.21]$$

Where, D is the diffusion coefficient (cm^2/s); T is the absolute temperature (K); μ is the viscosity of the liquid medium (cP), and V_s and V_w are the molar volumes of oleic acid and water respectively (cm^3/gmol). Application of equation [4.21] estimated the diffusion coefficient of oleic acid in water to be 4.7×10^{-6} cm^{2}s^{-1} = 4.7×10^{-10} m^{2}s^{-1}.

Therefore, if a single emulsion droplet, corresponding to a dose amount equivalent to 500 ppm (if it were to dissolve completely), and if the toxic level amounted to 25 ppm, it means that the required level of release that must be reached is $X = 0.95$. Let's assume that $a_o = 6$ μm; $c_a = 888$ ppm (oleic acid solubility); $c_s = 895\,000$ ppm (oleic acid density); $D = 4.7 \times 10^{-10}$ m^{2}s^{-1}. Substitution into equation [4.14], gives the time required to full dissolution, t_d as 55.6 s. Substitution into equation [4.17] gives the time to release the toxic amount as just 1.48 s.

However, the residual bioassay results are clearly not in agreement with the predictions of Cable & Frade (1987) model. The emulsion sample only achieved 20 % mortality at one week of ageing. The mortality increased rapidly thereafter reaching values exceeding 90 % at week three and beyond. Possible reasons for the failure of the model are as follows. First, the actual solubility of the oleic acid in water is likely much lower than the estimated value of 888 ppm. It means that the much lower value indicated by Vorum *et al* (1992) might be more correct. Secondly, the model did not take into account the surfactant surrounding the emulsion droplets. It is possible that it presented a barrier for the migration of the oleic acid into the water. Lastly, it was observed that the emulsion rapidly creamed, i.e., it accumulated at the top of the water in the container. Water samples for bioassays

89

were collected via a tap located at the bottom of the container, setup in **Figure 3.3**. This means that the oleic acid might not have reached toxic levels at the bottom of the container due to the much longer diffusion path.

CHAPTER 5: CONCLUSIONS AND RECOMMENDATIONS

Oleic acid was evaluated for its larvicidal potency against *An. arabiensis,* the principal malaria vector in South Africa. Oleic acid, as a free-standing oil, on 3rd and 4th *An. arabiensis* instar had an LC_{50} of 13 ppm and LC_{90} of 31 ppm after 48h at the 95% confidence interval. This was the first attempt to evaluate the larvicidal potency of oleic acid against *An. arabiensis* at the time this work was done.

Oleic acid was emulsified using 5 wt.% sorbitan mono oleate as the surfactant. The average particle size of the emulsion droplets was 211 ± 80 nm and the zeta potential was -56 ± 10 mV measured after 4 weeks of ageing. The emulsion was tested in the residual bioassays. This was done in glass containers containing 3 L of water. The oleic acid emulsion was dosed to a level of 500 ppm. The toxicity was measured using samples removed from the bottom of the container. The bioassays showed that mortality developed slowly over time, but mortality reached 90 % after 3 weeks and was maintained thereafter. Emulsion release modelling indicated that mortality should have developed much faster. There are several potential reasons why this was not the case. In particular, the emulsion creamed rapidly forming a layer of oil rich phase at the top of the container. This means that the diffusion path for the oil to reach the bottom was very long. Other potential reasons for the slow development of the expected mortality levels might be found in the low solubility of the oleic acid in water or perhaps even be due to the surfactant inhibiting migration of the oil into the water.

Layered double hydroxide, (LDH) intercalated with oleate anions were also explored as a dosage form. The idea was that the oleic acid would be released as the LDH decompose in the water. Unfortunately, the bioassay results were even more disappointing. After five weeks, the larvae mortality only reached 14 %. Studies on the effect of pH on the dissolution of the LDH indicated that the problem was not related to the amount of oleic acid potentially released. It is likely that the toxicity of the acid was ameliorated due to insoluble aluminium salt formation. This idea is supported by ICP results which showed higher than expected ratios of magnesium to aluminium present in the water.

The two porous carbon matrices also proved ineffective as controlled release reservoirs for oleic acid. The bioassay results showed very low mortalities. The likely explanation is that the oleic acid was strongly absorbed by the high surface area matrices.

© University of Pretoria

Oleic acid is a safe food-based additive which can be obtained at an economical price. It is environmentally benign and non-toxic to higher life forms. However, the present bioassay results indicate that it is highly toxic to the larvae of the main malaria vector in Southern Africa. In this regard, it is effective at very low concentration comparable to the much mor expensive essential oils considered for this application. Therefore, it is recommended that investigations continue to find effective ways of utilising it as a larvicide.

This work also showed that activated charcoal and pyrolyzed coffee grounds were able to absorb large amounts of liquid. Unfortunately, oleic acid was tenaciously held by these vehicles to the extent that they were ineffective for the targeted larviciding application. However, they may prove to be effective controlled-release devices for other liquid actives that might be more easily released into the environment. It is therefore recommended that they be considered for such potential applications.

REFERENCES

Acevedo, Rubilar, Scheuermann, Cancino, Uquiche, Garcés, Inostroza, and Shene (2013), "Spent Coffee Grounds as a Renewable Source of Bioactive Compounds" *Journal of Biobased Materials and Bioenergy*, 7(3), 420-428.

Ahmed, J, Tiwari, BK, Imam, SH, and Rao, MA (2016), *Starch-based polymeric materials and nanocomposites : chemistry, processing, and applications*, CRC Press, Boca Raton, United States, ISBN: 978-1-4398-5117-3, 1-396

Andemo, A, Yewhalaw, D, Alemayehu, B, and Ambelu, A (2014), "Evaluation of the mosquitocidal effect of Birbira (Mellitia ferruginea) seed extract against Anopheles arabiensis (Diptera: Culicidae) from Ethiopia" *Acta Tropica*, 136, 68-73.

Area, MR, Rico, M, Montero, Bn, Barral, L, Bouza, R, López, Jn, and Ramírez, C (2019), "Corn starch plasticized with isosorbide and filled with microcrystalline cellulose: Processing and characterization" *Carbohydrate Polymers*, 206, 726-733.

Ballesteros, LF, Teixeira, JA, and Mussatto, SI (2014), "Chemical, Functional, and Structural Properties of Spent Coffee Grounds and Coffee Silverskin" *Food and Bioprocess Technology : An International Journal*, 7(12), 3493-3503.

Bär, F, Knorr, M, Schröder, O, Hopf, H, Garbe, T, and Krahl, J (2021), "Rancimat vs. rapid small scale oxidation test (RSSOT) correlation analysis, based on a comprehensive study of literature" *Fuel*, 291, 120160.

Barahuie, F, Hussein, MZ, Hussein-Al-Ali, SH, Arulselvan, P, Fakurazi, S, and Zainal, Z (2013), "Preparation and controlled-release studies of a protocatechuic acid-magnesium/aluminum-layered double hydroxide nanocomposite" *International journal of nanomedicine*, 8, 1975-1987.

Barbosa, JD, Silva, VB, Alves, PB, Gumina, G, Santos, RL, Sousa, DP, and Cavalcanti, SC (2012), "Structure-activity relationships of eugenol derivatives against Aedes aegypti (Diptera: Culicidae) larvae" *Pest management science*, 68(11), 1478-1483.

Battegazzore, D, Bocchini, S, Nicola, G, Martini, E, and Frache, A (2015), "Isosorbide, a green plasticizer for thermoplastic starch that does not retrogradate" *Carbohydrate Polymers*, 119, 78-84.

Becker, N, Petric, D, Zgomba, M, Boase, C, Madon, M, Dahl, C, and Kaiser, A (2010), *Mosquitoes and their control*, Second Edition, Springer, Berlin, Germany, eISBN: 978-3-540-92874-4, 1-575

Belgacem, MN, and Gandini, A (2008), *Monomers, Polymers and Composites from Renewable Resources*, Elsevier, Oxford, UK, ISBN: 978-0-08-045316-3, 321-342

BeMiller, JN (2019), *Carbohydrate Chemistry for Food Scientists (3rd Edition),* Elsevier, Oxford, UK, ISBN 978-0-12-812069-9, 161-171.

Benelli, G, and Mehlhorn, H (2018), *Mosquito-borne diseases : implications for public health*, Volume 10, Springer, Cham, Switzerland, eISBN: 978-3-31994075-5, 69-129.

Benelli, G, Pavela, R, Canale, A, Cianfaglione, K, Ciaschetti, G, Conti, F, Nicoletti, M, Senthil-Nathan, S, Mehlhorn, H, and Maggi, F (2017), "Acute larvicidal toxicity of five essential oils (Pinus nigra, Hyssopus officinalis, Satureja montana, Aloysia citrodora and Pelargonium graveolens) against the filariasis vector Culex quinquefasciatus: Synergistic and antagonistic effects" *Parasitology International*, 66(2), 166-171.

Benício, LPF, Silva, RA, Lopes, JA, Eulálio, D, dos Santos, RMM, De Aquino, LA, Vergütz, L, Novais, RF, Da Costa, LM, Pinto, FG, and Tronto, J (2015), "Layered double hydroxides: Nanomaterials for applications in agriculture" *Revista Brasileira de Ciencia do Solo*, 39(1), 1-13.

Benyekkou, N, Ghezzar, MR, Abdelmalek, F, and Addou, A (2020), "Elimination of paracetamol from water by a spent coffee grounds biomaterial" *Environmental Nanotechnology, Monitoring & Management*, 14, 100396.

Berber, MR, Hafez, IH, Minagawa, K, and Mori, T (2014), "A sustained controlled release formulation of soil nitrogen based on nitrate-layered double hydroxide nanoparticle material" *Journal of Soils and Sediments*, 14(1), 60-66.

Bini, M, and Monteforte, F (2018), "Layered Double Hydroxides (LDHs): Versatile and Powerful Hosts for Different Applications" *Journal of Analytical & Pharmaceutical Research*, 7(1), 11-12.

Blasi, F, Chiesi, C, Spogli, R, Cossignani, L, and Nocchetti, M (2021), "Oxidative Stability of Long-Chain Fatty Acids with Different Unsaturation Degrees into Layered Double Hydroxides" *Applied Sciences*, 11(15), 7035.

Boudrahem, F, Soualah, A, and Aissani-Benissad, F (2011), "Pb(II) and Cd(II) Removal from Aqueous Solutions Using Activated Carbon Developed from Coffee Residue Activated with Phosphoric Acid and Zinc Chloride" *Journal of Chemical & Engineering Data*, 56(5), 1946-1955.

Boumeriame, H, Da Silva, ES, Cherevan, AS, Chafik, T, Faria, JL, and Eder, D (2022), "Layered double hydroxide (LDH)-based materials: A mini-review on strategies to improve the performance for photocatalytic water splitting" *Journal of Energy Chemistry*, 64, 406-431.

Brooke, B, Koekemoer, L, Kruger, P, Urbach, J, Misiani, E, and Coetzee, M (2013), "Malaria vector control in South Africa" *South African Medical Journal*, 103(10), 784-788.

Bukhtiyarova, MV (2019), "A review on effect of synthesis conditions on the formation of layered double hydroxides" *Journal of Solid State Chemistry*, 269, 494-506.

Burke, A, Dahan-Moss, Y, Duncan, F, Qwabe, B, Coetzee, M, Koekemoer, L, and Brooke, B (2019a), "Anopheles parensis contributes to residual malaria transmission in South Africa" *Malaria Journal*, 18(1), 257.

Burke, A, Dandalo, L, Munhenga, G, Dahan-Moss, Y, Mbokazi, F, Ngxongo, S, Coetzee, M, Koekemoer, L, and Brooke, B (2017), "A new malaria vector mosquito in South Africa" *Scientific Reports (Nature Publisher Group)*, 7, 43779.

Burke, AM, Brooke, BD, and Duncan, FD (2019b), "Metabolic rate does not vary with seasonal change in Anopheles arabiensis adults in South Africa" *Journal of Insect Physiology*, 118, 103942.

Cable, M, and Frade, JR (1987), "The diffusion-controlled dissolution of spheres" *Journal of Materials Science*, 22(5), 1894-1900.

Campos-Vega, R, Loarca-Piña, G, Vergara-Castañeda, HA, and Oomah, BD (2015), "Spent coffee grounds: A review on current research and future prospects" *Trends in Food Science & Technology*, 45(1), 24-36.

Carlino, S, Hudson, MJ, Husain, SW, and Knowles, JA (1996), "The reaction of molten phenylphosphonic acid with a layered double hydroxide and its calcined oxide" *Solid State Ionics*, 84(1), 117-129.

Casida, JE, and Durkin, KA (2013), "Anticholinesterase insecticide retrospective" *Chemico-Biological Interactions*, 203(1), 221-225.

Castaño, J, Rodríguez-Llamazares, S, Contreras, K, Carrasco, C, Pozo, C, Bouza, R, Franco, CML, and Giraldo, D (2014), "Horse chestnut (Aesculus hippocastanum L.) starch: Basic physico-chemical characteristics and use as thermoplastic material" *Carbohydrate Polymers*, 112, 677-685.

Cavani, F, Trifirò, F, and Vaccari, A (1991), "Hydrotalcite-type anionic clays: Preparation, properties and applications" *Catalysis Today*, 11(2), 173-301.

Celis, R, Adelino, MÁ, Gámiz, B, Hermosín, MC, Koskinen, WC, and Cornejo, J (2014), "Nanohybrids of Mg/Al layered double hydroxide and long-chain (C18) unsaturated fatty acid anions: Structure and sorptive properties" *Applied Clay Science*, 96, 81-90.

Cervantes-Ramírez, JE, Cabrera-Ramirez, AH, Morales-Sánchez, E, Rodriguez-García, ME, Reyes-Vega, MdlL, Ramírez-Jiménez, AK, Contreras-Jiménez, BL, and Gaytán-Martínez, M (2020), "Amylose-lipid complex formation from extruded maize starch mixed with fatty acids" *Carbohydrate Polymers*, 246, 116555.

Chaillot, D, Bennici, S, and Brendlé, J (2021), "Layered double hydroxides and LDH-derived materials in chosen environmental applications: a review" *Environmental science and pollution research international*, 28(19), 24375-24405.

Chan, H, Shi, C, Wu, Z, Sun, S, Zhang, S, Yu, Z, He, M, Chen, G, Wan, X, and Tian, J (2022), "Superhydrophilic three-dimensional porous spent coffee ground reduced palladium nanoparticles for efficient catalytic reduction" *Journal of Colloid and Interface Science*, 608, 1414-1421.

Chang, Q, Zheng, B, Zhang, Y, and Zeng, H (2021), "A comprehensive review of the factors influencing the formation of retrograded starch" *International Journal of Biological Macromolecules*, 186, 163-173.

Chellappandian, M, Senthil-Nathan, S, Karthi, S, Vasantha-Srinivasan, P, Kalaivani, K, Hunter, WB, Ali, AM, Veerabahu, C, Elshikh, MS, and Al Farraj, DA (2022), "Larvicidal and repellent activity of N-methyl-1-adamantylamine and oleic acid a major derivative of bael tree ethanol leaf extracts against dengue mosquito vector and their biosafety on natural predator" *Environmental science and pollution research international*, 29(11), 15654-15663.

Cheng, SS, Liu, JY, Tsai, KH, Chen, WJ, and Chang, ST (2004), "Chemical composition and mosquito larvicidal activity of essential oils from leaves of different Cinnamomum osmophloeum provenances" *Journal of agricultural and food chemistry*, 52(14), 4395-4400.

Chiang, C-H, Chen, J, and Lin, J-H (2020), "Preparation of pore-size tunable activated carbon derived from waste coffee grounds for high adsorption capacities of organic dyes" *Journal of Environmental Chemical Engineering*, 8(4), 103929.

Christian, R, Florent, B, Jens, CS, and Daniel, G (2015), "Dose-Response Analysis Using R" *PLOS ONE*, 10(12), 0146021.

Chuaycharoensuk, T, Manguin, S, Duvallet, G, and Chareonviriyaphap, T (2012), Assessment of geraniol-incorporated polymers to control Aedes albopictus (Diptera: culicidae). *Parasite*, 19(4), 427-432.

Cobut, A, Sehaqui, H, and Berglund, LA (2014), "Cellulose Nanocomposites by Melt Compounding of TEMPO-Treated Wood Fibers in Thermoplastic Starch Matrix" *BioResources*, 9(2), 3276-3289.

Conterosito, E, Gianotti, V, Palin, L, Boccaleri, E, Viterbo, D, and Milanesio, M (2018), "Facile preparation methods of hydrotalcite layered materials and their structural characterization by combined techniques" *Inorganica Chimica Acta*, 470, 36-50.

Corbet, SA, Danahar, GW, King, V, Chalmers, CL, and Tiley, CF (1995), "Surfactant-enhanced essential oils as mosquito larvicides" *Entomologia Experimentalis et Applicata*, 75(3), 229-236.

Curvelo, AAS, de Carvalho, AJF, and Agnelli, JAM (2001), "Thermoplastic starch–cellulosic fibers composites: preliminary results" *Carbohydrate Polymers*, 45(2), 183-188.

Dahalan FA, Churcher TS, Windbichler N, Lawniczak MKN (2019) "The male mosquito contribution towards malaria transmission: Mating influences the *Anopheles* female midgut transcriptome and increases female susceptibility to human malaria parasites" *PLoS Pathogens*, 15(11), 1008063

Damtie, D, and Mekonnen, Y (2021), "Toxicity and Oviposition Deterrent Activities of Thyme Essential Oils against *Anopheles arabiensis*" *Psyche: A Journal of Entomology*, 2021, 6684156.

Das, O, and Sarmah, AK (2015), "The love-hate relationship of pyrolysis biochar and water: A perspective" *Science of The Total Environment*, 512-513, 682-685.

Daud, M, Hai, A, Banat, F, Wazir, MB, Habib, M, Bharath, G, and Al-Harthi, MA (2019), "A review on the recent advances, challenges and future aspect of layered double hydroxides (LDH) – Containing hybrids as promising adsorbents for dyes removal" *Journal of Molecular Liquids*, 288, 110989.

de Melo, AR, Pereira Garcia, IJ, Serrão, JE, Santos, HL, Rodrigues dos Santos Lima, LA, and Alves, SN (2018), "Toxicity of different fatty acids and methyl esters on Culex quinquefasciatus larvae" *Ecotoxicology and Environmental Safety*, 154, 1-5.

de Sousa, ALMD, dos Santos, WM, de Souza, ML, Silva, LCPBB, Yun, AEHK, Aguilera, CSB, Chagas, BdF, Rolim, LA, da Silva, RMF, and Neto, PJR (2021), "Layered Double Hydroxides as Promising Excipients for Drug Delivery Purposes" *European Journal of Pharmaceutical Sciences*, 165, 105922.

de Sousa, LS, de Moura, CVR, de Oliveira, JE, and de Moura, EM (2014), "Use of natural antioxidants in soybean biodiesel" *Fuel*, 134, 420-428.

de Souza, E. F., Ramos, T. C. P. M., Simionatto, E., Cavalheiro, A. A., Fiorucci, A. R., da Silva, M. S. (2018), "Evaluating Antioxidant Eugenol on Oxidation Stability of Biodiesel Synthesized from Used Frying Oil", *Orbital: The Electronic Journal of Chemistry*, *10*, 37-41.

de Souza, LM, Venturini, FP, Inada, NM, Iermak, I, Garbuio, M, Mezzacappo, NF, de Oliveira, KT, and Bagnato, VS (2020), "Curcumin in formulations against Aedes aegypti: Mode of action, photolarvicidal and ovicidal activity" *Photodiagnosis and Photodynamic Therapy*, 31, 101840.

Dey, P, Goyary, D, Chattopadhyay, P, Kishor, S, Karmakar, S, and Verma, A (2020), "Evaluation of larvicidal activity of Piper longum leaf against the dengue vector, Aedes aegypti, malarial vector, Anopheles stephensi and filariasis vector, Culex quinquefasciatus" *South African Journal of Botany*, 132, 482-490.

Dias, CN, and Moraes, DF (2014), "Essential oils and their compounds as Aedes aegypti L. (Diptera: Culicidae) larvicides: review" *Parasitology research*, 113(2), 565-592.

Donato, RK, Luza, L, da Silva, RF, Moro CC, Guzatto, R, Samios, D, Matějka L, Dimzoski, B, Amico, SC, and Schrekker, HS (2012), "The role of oleate-functionalized layered double hydroxide in the melt compounding of polypropylene nanocomposites" *Materials Science and Engineering: C*, 32(8), 2396-2403.

Duda, JL, and Vrentas, JS (1969), "Mathematical analysis of bubble dissolution" *AIChE Journal*, 15(3), 351-356.

Dufresne, A, and Castano, J (2017), "Polysaccharide nanomaterial reinforced starch nanocomposites: A review" *Starch/Staerke*, 69(1-2), 1500307.

Edriss, AE, Satti, AA, and Alabjar, ZA (2013), "Larvicidal properties of two asclepiadaceous plant species against the mosquito Anopheles arabiensis Patton (Diptera: Culicidae)" *Journal of the Saudi Society of Agricultural Sciences*, 12(1), 59-66.

Efthymiopoulos, I, Hellier, P, Ladommatos, N, Kay, A, and Mills-Lamptey, B (2019), "Effect of Solvent Extraction Parameters on the Recovery of Oil From Spent Coffee Grounds for Biofuel Production" *Waste and Biomass Valorization*, 10(2), 253-264.

Elimam, AM, Elmalik, KH, and Ali, FS (2009), "Efficacy of leaves extract of Calotropis procera Ait. (Asclepiadaceae) in controlling Anopheles arabiensis and Culex quinquefasciatus mosquitoes" *Saudi Journal of Biological Sciences*, 16(2), 95-100.

Embuscado, ME (2015), "Spices and herbs: Natural sources of antioxidants – a mini review" *Journal of Functional Foods*, 18, 811-819.

EN14112 (2016), Fat and oil derivatives - fatty acid methyl esters (FAME) - determination of oxidation stability (accelerated oxidation test).

Fan, GGG (2014), "Catalytic applications of layered double hydroxides: Recent advances and perspectives" *Chemical Society Reviews*, 43(20), 7040-7066.

Farag, SM, Essa, EE, Alharbi, SA, Alfarraj, S, and Abu El-Hassan, GMM (2021), "Agro-waste derived compounds (flax and black seed peels): Toxicological effect against the West Nile virus vector, Culex pipiens L. with special reference to GC–MS analysis" *Saudi Journal of Biological Sciences*, 28(9), 5261-5267.

Ferreira, RMA, Duarte, JL, Cruz, RAS, Oliveira, AEMFM, Araújo, RS, Carvalho, JCT, Mourão, RHV, Souto, RNP, and Fernandes, CP (2019), "A herbal oil in water nano-emulsion prepared through an ecofriendly approach affects two tropical disease vectors" *Revista Brasileira de Farmacognosia*, 29(6), 778-784.

Fillinger, U, and Lindsay, SW (2011), "Larval source management for malaria control in Africa: myths and reality" *Malaria Journal*, 10(1), 353.

Focke, WW, Westhuizen, IH, Grobler, ABL, Nshoane, KT, Reddy, JK, and Luyt, AS (2012), "The effect of synthetic antioxidants on the oxidative stability of biodiesel" *Fuel*, 94, 227-233.

Forano, C, Costantino, U, Prévot, V, and Gueho, CT (2013), Layered Double Hydroxides (LDH). *In:* Bergaya, F, and Lagaly, G (eds.) *Developments in Clay Science.* Elsevier, 745-782.

Foster, WA, and Walker, ED (2002), 12 - MOSQUITOES (Culicidae). *In:* Mullen, G, and Durden, L (eds.) *Medical and Veterinary Entomology.* San Diego: Academic Press, 203-263.

Fu, Z, Chen, J, Luo, S-J, Liu, C-M, and Liu, W (2015), "Effect of food additives on starch retrogradation: A review" *Starch - Stärke*, 67(1-2), 69-78.

Galano, A, Álvarez-Diduk, R, Ramírez-Silva, MT, Alarcón-Ángeles, G, and Rojas-Hernández, A (2009), "Role of the reacting free radicals on the antioxidant mechanism of curcumin" *Chemical Physics*, 363(1), 13-23.

García N.L, FL, D'Accorso N.B, Goyanes S. (2015), "Biodegradable Starch Nanocomposites" In: Thakur, VK, and M.K., T (Eds), *Eco-friendly Polymer Nanocomposites : Processing and properties*, Springer, 17-77.

Ghanbari, A, Tabarsa, T, Ashori, A, Shakeri, A, and Mashkour, M (2018), "Preparation and characterization of thermoplastic starch and cellulose nanofibers as green nanocomposites: Extrusion processing" *International Journal of Biological Macromolecules*, 112, 442-447.

Ghodszad, L, Reyhanitabar, A, Maghsoodi, MR, Asgari Lajayer, B, and Chang, SX (2021), "Biochar affects the fate of phosphorus in soil and water: A critical review" *Chemosphere*, 283, 131176.

Ghosh, A, Chowdhury, N, and Chandra, G (2012), "Plant extracts as potential mosquito larvicides" *The Indian journal of medical research*, 135(5), 581-598.

González-Seligra, P, Guz, L, Ochoa-Yepes, O, Goyanes, S, and Famá, L (2017), "Influence of extrusion process conditions on starch film morphology" *LWT*, 84, 520-528.

González, K, Martin, L, González, A, Retegi, A, Eceiza, A, and Gabilondo, N (2017), "D-isosorbide and 1,3-propanediol as plasticizers for starch-based films: Characterization and aging study" *Journal of Applied Polymer Science*, 134(20), 44793.

Govindarajan, M, Rajeswary, M, and Benelli, G (2016a), "Chemical composition, toxicity and non-target effects of Pinus kesiya essential oil: An eco-friendly and novel larvicide against malaria, dengue and lymphatic filariasis mosquito vectors" *Ecotoxicology and Environmental Safety*, 129, 85-90.

Govindarajan, M, Rajeswary, M, Hoti, SL, Bhattacharyya, A, and Benelli, G (2016b), "Eugenol, α-pinene and β-caryophyllene from <i>Plectranthus barbatus</i> essential oil

as eco-friendly larvicides against malaria, dengue and Japanese encephalitis mosquito vectors" *Parasitology Research : Founded as Zeitschrift für Parasitenkunde*, 115(2), 807-815.

Hargreaves, K, Koekemoer, LL, Brooke, BD, Hunt, RH, Mthembu, J, and Coetzee, M (2000), "Anopheles funestus resistant to pyrethroid insecticides in South Africa" *Medical and Veterinary Entomology*, 14(2), 181-189.

He, W, and Wei, C (2017), "Progress in C-type starches from different plant sources" *Food Hydrocolloids*, 73, 162-175.

Heidari, F, Jafari, SM, Ziaiifar, AM, and Malekjani, N (2022), "Stability and release mechanisms of double emulsions loaded with bioactive compounds; a critical review" *Advances in Colloid and Interface Science*, 299, 102567.

Hejna, A (2021), "Potential applications of by-products from the coffee industry in polymer technology – Current state and perspectives" *Waste Management*, 121, 296-330.

Hietala, M, Mathew, AP, and Oksman, K (2013), "Bionanocomposites of thermoplastic starch and cellulose nanofibers manufactured using twin-screw extrusion" *European Polymer Journal*, 49(4), 950-956.

Hsieh, C-F, Liu, W, Whaley, JK, and Shi, Y-C (2019), "Structure, properties, and potential applications of waxy tapioca starches – A review" *Trends in Food Science & Technology*, 83, 225-234.

Hsieh, T-H, Wang, H-L, Yu, G-T, Huang, G-M, and Lin, J-H (2021), "Meso-pore dominant activated carbon from spent coffee grounds for high-performance electrochemical capacitors in organic electrolyte" *Journal of Environmental Chemical Engineering*, 9(6), 106418.

Huang, G, Jiang, L, Wang, D, Chen, J, Li, Z, and Ma, S (2016), "Intercalation of thiacalix[4]arene anion via calcined/restored reaction into LDH and efficient heavy metal capture" *Journal of Molecular Liquids*, 220, 346-353.

Huang, J, Sun, Q, Song, G, Qi, S, Chen, J, Zhang, P, Geng, T, Lin, Q, and Duan, Y (2020), "Antioxidant and anti-isomerization effects of sesamol and resveratrol on high oleic acid peanut oil" *LWT*, 123, 109077.

Hwang, YS, Schultz, GW, and Mulla, MS (1984), "Structure-activity relationship of unsaturated fatty acids as mosquito ovipositional repellents" *Journal of Chemical Ecology*, 10(1), 145-151.

Immel, S, and Lichtenthaler, FW (2000), "The Hydrophobic Topographies of Amylose and its Blue Iodine Complex" *Starch - Stärke*, 52(1), 1-8.

Inomata, K, and Ogawa, M (2006), "Preparation and Properties of Mg/Al Layered Double Hydroxide–Oleate and –Stearate Intercalation Compounds" *Bulletin of the Chemical Society of Japan*, 79(2), 336-342.

Intan, SN, and Rachmawati, R, (2019), "Inclusion Complexes between Starch and Oleic Acid as Hydrogel Materials" *Key Engineering Materials*, 811, 8-13.

International, CO (2022), "Trade Statistics Tables, Consumption: World coffee consumption", International Coffee Organization, London, United Kingdom, https://www.ico.org/prices/new-consumption-table.pdf [Accessed: 2022-02-01].

Ivanič, F, Jochec-Mošková, D, Janigová, I, and Chodák, I (2017), "Physical properties of starch plasticized by a mixture of plasticizers" *European Polymer Journal*, 93, 843-849.

Ivanič, F, Kováčová, M, and Chodák, I (2019), "The effect of plasticizer selectionon properties of blends poly(butylene adipate-co-terephthalate) with thermoplastic starch" *European Polymer Journal*, 116, 99-105.

Jang, H, Ocon, JD, Lee, S, Lee, JK, and Lee, J (2015), "Direct power generation from waste coffee grounds in a biomass fuel cell" *Journal of Power Sources*, 296, 433-439.

Janssen, LPBM, and Moscicki, L (2009), *Thermoplastic starch : a green material for various industries*, Wiley-VCH, Weinheim, Germany, ISBN: 978-3-527-32528-3, 78-102

Jaworska, M, Sikora, E, Zielina, M, and Ogonowski, J (2013), "Studies on the formation of O/W nano-emulsions, by low-energy emulsification method, suitable for cosmeceutical applications" *Acta Biochimica Polonica*, 60(4), 779-782.

103

Jayasundara, V, and Pathiratne, A (2008), "Effect of Repeated Application of Fenthion as a Mosquito Larvicide on Nile Tilapia (Oreochromis niloticus) Inhabiting Selected Water Canals in Sri Lanka" *Bulletin of Environmental Contamination and Toxicology*, 80(4), 374-377.

Romola, JCV, Meganaharshini, M, Rigby, SP, Ganesh Moorthy, I, Shyam Kumar, R, and Karthikumar, S (2021), "A comprehensive review of the selection of natural and synthetic antioxidants to enhance the oxidative stability of biodiesel" *Renewable and Sustainable Energy Reviews*, 145, 111109.

Jiang, T, Ghosh, R, and Charcosset, C (2021), "Extraction, purification and applications of curcumin from plant materials-A comprehensive review" *Trends in Food Science & Technology*, 112, 419-430.

Johnson, M, Maharaja, P, Murugesan, S, Janakiraman, N, Menezes, IRA, da Costa, JGM, Barbosa, CRS, and Coutinho, HDM (2018), "Larvicidal activity of some medicinal plant extracts against filariasis fever mosquito, Culex quinquefasciatus (Say.) (Diptera: Culicidae)" *Comparative Immunology, Microbiology and Infectious Diseases*, 61, 1-4.

Jutakridsada, P, Prajaksud, C, Kuboonya-Aruk, L, Theerakulpisut, S, and Kamwilaisak, K (2016), "Adsorption characteristics of activated carbon prepared from spent ground coffee" *Clean Technologies and Environmental Policy : Focusing on Technology Research, Innovation, Demonstration, Insights and Policy Issues for Sustainable Technologies*, 18(3), 639-645.

Kabong, MA (2020), *Stability of block copolymer surfactant-based emulsions in the presence of a salt*, Master's Dissertation, University of Pretoria, Pretoria.

Kameda, T, Takeuchi, H, and Yoshioka, T (2009), "Hybrid inorganic/organic composites of Mg-Al layered double hydroxides intercalated with citrate, malate, and tartrate prepared by co-precipitation" *Materials Research Bulletin*, 44(4), 840-845.

Kameshima, Y, Yoshizaki, H, Nakajima, A, and Okada, K (2006), "Preparation of sodium oleate/layered double hydroxide composites with acid-resistant properties" *Journal of Colloid and Interface Science*, 298(2), 624-628.

Kamogawa, K, Akatsuka, H, Matsumoto, M, Yokoyama, S, Sakai, T, Sakai, H, and Abe, M (2001), "Surfactant-free O/W emulsion formation of oleic acid and its esters with ultrasonic dispersion" *Colloids and Surfaces A: Physicochemical and Engineering Aspects*, 180(1), 41-53.

Kang, G-H, and Park, I-K (2022), "Reconstruction and intercalating anion exchange of ZnAl-layered double hydroxide" *Ceramics International*, 48(3), 3030-3036.

Kang, H, Kim, H-J, Yang, J-H, Kim, T-H, Choi, G, Paek, S-M, Choi, A-J, Choy, J-H, and Oh, J-M (2015), "Intracrystalline structure and release pattern of ferulic acid intercalated into layered double hydroxide through various synthesis routes" *Applied Clay Science*, 112-113, 32-39.

Kapiamba, KF (2022), "Mini-review of the microscale phenomena during emulsification of highly concentrated emulsions" *Colloid and Interface Science Communications*, 47, 100597.

Kargarzadeh, H, Mariano, M, Huang, J, Lin, N, Ahmad, I, Dufresne, A, and Thomas, S (2017), "Recent developments on nanocellulose reinforced polymer nanocomposites: A review" *Polymer*, 132, 368-393.

Karim, AA, Norziah, MH, and Seow, CC (2000), "Methods for the study of starch retrogradation" *Food Chemistry*, 71(1), 9-36.

Karmee, SK (2018), "A spent coffee grounds based biorefinery for the production of biofuels, biopolymers, antioxidants and biocomposites" *Waste Management*, 72, 240-254.

Karthi, S, Vinothkumar, M, Karthic, U, Manigandan, V, Saravanan, R, Vasantha-Srinivasan, P, Kamaraj, C, Shivakumar, MS, De Mandal, S, Velusamy, A, Krutmuang, P, and Senthil-Nathan, S (2020), "Biological effects of Avicennia marina (Forssk.) vierh. extracts on physiological, biochemical, and antimicrobial activities against three challenging mosquito vectors and microbial pathogens" *Environmental Science and Pollution Research*, 27(13), 15174-15187.

Karunamoorthi, K (2011), "Vector control: a cornerstone in the malaria elimination campaign" *Clinical Microbiology and Infection*, 17(11), 1608-1616.

105

Karunamoorthi, K, Girmay, A, and Fekadu, S (2014), "Larvicidal efficacy of Ethiopian ethnomedicinal plant Juniperus procera essential oil against Afrotropical malaria vector Anopheles arabiensis (Diptera: Culicidae)" *Asian Pacific Journal of Tropical Biomedicine*, 4, S99-S106.

Karunamoorthi, K, and Ilango, K (2010), "Larvicidal activity of Cymbopogon citratus (DC) Stapf. and Croton macrostachyus Del. against Anopheles arabiensis Patton, a potent malaria vector" *European review for medical and pharmacological sciences*, 14(1), 57-62.

Kassir, JTD, Mohsen, ZHM, and Mehdi, NS (1989), "Toxic effects of limonene against *Culex quinquefasciatus* Say larvae and its interference with oviposition" *Anzeiger für Schädlingskunde, Pflanzenschutz, Umweltschutz*, 62(1), 19-21.

Kawai, K, Takato, S, Sasaki, T, and Kajiwara, K (2012), "Complex formation, thermal properties, and in-vitro digestibility of gelatinized potato starch–fatty acid mixtures" *Food Hydrocolloids*, 27(1), 228-234.

Kesavan Pillai, S, Kleyi, P, de Beer, M, and Mudaly, P (2020), "Layered double hydroxides: An advanced encapsulation and delivery system for cosmetic ingredients-an overview" *Applied Clay Science*, 199, 105868.

Khorshidi, M, Asadpour, S, Sarmast, N, and Dinari, M (2022), "A review of the synthesis methods, properties, and applications of layered double hydroxides/carbon nanocomposites" *Journal of Molecular Liquids*, 348, 118399.

Kibret, S, and Wilson, GG (2016), "Increased outdoor biting tendency of Anopheles arabiensis and its challenge for malaria control in Central Ethiopia" *Public Health*, 141, 143-145.

Kirschweng, B, Tátraaljai, D, Földes, E, and Pukánszky, B (2017), "Natural antioxidants as stabilizers for polymers" *Polymer Degradation and Stability*, 145, 25-40.

Kleyi, PE, Mudaly, P, Kesavan Pillai, S, and de Beer, M (2021), "Zn/Al Layered double hydroxides nanostructure as effective controlled release vehicle of nicotinic acid for topical applications" *Applied Clay Science*, 215, 106304.

Korsmeyer, RW, Gurny, R, Doelker, E, Buri, P, and Peppas, NA (1983), "Mechanisms of solute release from porous hydrophilic polymers" *International Journal of Pharmaceutics*, 15(1), 25-35.

Kovalcik, A, Obruca, S, and Marova, I (2018), "Valorization of spent coffee grounds: A review" *Food and Bioproducts Processing*, 110, 104-119.

Kumar, N (2017), "Oxidative stability of biodiesel: Causes, effects and prevention" *Fuel*, 190, 328-350.

Kweka, EJ, Lima, TC, Marciale, CM, and de Sousa, DP (2016), "Larvicidal efficacy of monoterpenes against the larvae of Anopheles gambiae" *Asian Pacific Journal of Tropical Biomedicine*, 6(4), 290-294.

Laksaci, H, Khelifi, A, Trari, M, and Addoun, A (2017), "Synthesis and characterization of microporous activated carbon from coffee grounds using potassium hydroxides" *Journal of Cleaner Production*, 147, 254-262.

Lazzarini, A, Piovano, A, Pellegrini, R, Agostini, G, Rudić, S, Lamberti, C, and Groppo, E (2016), "Graphitization of Activated Carbons: A Molecular-level Investigation by INS, DRIFT, XRD and Raman Techniques" *Physics Procedia*, 85, 20-26.

Ledesma, EB, Hoang, JN, Nguyen, Q, Hernandez, V, Nguyen, MP, Batamo, S, and Fortune, CK (2013), "Unimolecular Decomposition Pathway for the Vapor-Phase Cracking of Eugenol, A Biomass Tar Compound" *Energy & Fuels*, 27(11), 6839-6846.

Lee, SY, Eskridge, KM, Koh, WY, and Hanna, MA (2009), "Evaluation of ingredient effects on extruded starch-based foams using a supersaturated split-plot design" *Industrial Crops and Products*, 29(2), 427-436.

Lendvai, L, Sajó, I, and Karger-Kocsis, J (2019), "Effect of Storage Time on the Structure and Mechanical Properties of Starch/Bentonite Nanocomposites" *Starch - Sträke*, 71(1-2), 1800123.

Li, J, Zhou, M, Cheng, G, Cheng, F, Lin, Y, and Zhu, P-X (2019a), "Fabrication and characterization of starch-based nanocomposites reinforced with montmorillonite and cellulose nanofibers" *Carbohydrate Polymers*, 210, 429-436.

107

Li, R, He, Q, Rong, L, Lin, Y, Jia, N, Shao, J, and Liu, D (2019b), "High homogenization speeds for preparing unstable myofibrillar protein–olive oil emulsions" *Journal of Food Science*, 84(5), 1113-1121.

Li, S, Bai, Z, and Zhao, D (2013), "Characterization and friction performance of Zn/Mg/Al-CO3 layered double hydroxides" *Applied Surface Science*, 284, 7-12.

Li, S, Ren, L, and Bai, Z (2019c), "Friction performance and mechanisms of calcined products of Mg/Al layered double hydroxides as lubricant additives" *Applied Surface Science*, 470, 979-990.

Liu, H, Xie, F, Yu, L, Chen, L, and Li, L (2009), "Thermal processing of starch-based polymers" *Progress in Polymer Science*, 34(12), 1348-1368.

Liu, XC, Dong, HW, Zhou, L, Du, SS, and Liu, ZL (2013), "Essential oil composition and larvicidal activity of Toddalia asiatica roots against the mosquito Aedes albopictus (Diptera: Culicidae)" *Parasitology research*, 112(3), 1197-1203.

Liu, Z-Q (2022), "Why natural antioxidants are readily recognized by biological systems? 3D architecture plays a role!" *Food Chemistry*, 380, 132143.

Liu, Z, Ma, R, Osada, M, Iyi, N, Ebina, Y, Takada, K, and Sasaki, T (2006), "Synthesis, anion exchange, and delamination of Co-Al layered double hydroxide: assembly of the exfoliated nanosheet/polyanion composite films and magneto-optical studies" *Journal of the American Chemical Society*, 128(14), 4872-4880.

Lopes Martins, R, Bruno Lobato Rodrigues, A, de Menezes Rabelo, É, Lima Santos, L, Barreto Brandão, L, Gomes Faustino, C, Luzia Ferreira Farias, A, Maria da Cunha Sá, D, de Castro Cantuária, P, Kardec Ribeiro Galardo, A, and Susan Moreira da Silva de Almeida, S (2021), "Development of larvicide nanoemulsion from the essential oil of Aeollanthus suaveolens Mart. ex Spreng against Aedes aegypti, and its toxicity in non-target organism" *Arabian Journal of Chemistry*, 14(6), 103148.

Lourdin, D, Bizot, H, and Colonna, P (1997), ""Antiplasticization" in starch-glycerol films?" *Journal of Applied Polymer Science*, 63(8), 1047-1053.

Maharaj, R, Maharaj, V, Crouch, NR, Bhagwandin, N, Folb, PI, Pillay, P, and Gayaram, R (2012), "Screening of selected ethnomedicinal plants from South Africa for larvicidal activity against the mosquito Anopheles arabiensis" *Malaria Journal*, 11, 320.

Maia, JD, La Corte, R, Martinez, J, Ubbink, J, and Prata, AS (2019), "Improved activity of thyme essential oil (Thymus vulgaris) against Aedes aegypti larvae using a biodegradable controlled release system" *Industrial Crops and Products*, 136, 110-120.

Mallakpour, S, Hatami, M, and Hussain, CM (2020), "Recent innovations in functionalized layered double hydroxides: Fabrication, characterization, and industrial applications" *Advances in Colloid and Interface Science*, 283, 102216.

Manzi-Nshuti, C, Songtipya, P, Manias, E, Jimenez-Gasco, MM, Hossenlopp, JM, and Wilkie, CA (2009), "Polymer nanocomposites using zinc aluminum and magnesium aluminum oleate layered double hydroxides: Effects of LDH divalent metals on dispersion, thermal, mechanical and fire performance in various polymers" *Polymer*, 50(15), 3564-3574.

Marcińczyk, M, and Oleszczuk, P (2022), "Biochar and engineered biochar as slow- and controlled-release fertilizers" *Journal of Cleaner Production*, 339, 130685.

Maree, Z, Strydom, CA, and Bunt, JR (2020), "Chemical and physical characterization of spent coffee ground biochar treated by a wet oxidation method for the production of a coke substitute" *Waste Management*, 113, 422-429.

Marhamati, M, Ranjbar, G, and Rezaie, M (2021), "Effects of emulsifiers on the physicochemical stability of Oil-in-water Nanoemulsions: A critical review" *Journal of Molecular Liquids*, 340, 117218.

Marinopoulou, A, Papastergiadis, E, and Raphaelides, SN (2016a), "An investigation into the structure, morphology and thermal properties of amylomaize starch-fatty acid complexes prepared at different temperatures" *Food Research International*, 90, 111-120.

Marinopoulou, A, Papastergiadis, E, Raphaelides, SN, and Kontominas, MG (2016b), "Morphological characteristics, oxidative stability and enzymic hydrolysis of amylose-fatty acid complexes" *Carbohydrate Polymers*, 141, 106-115.

Massaya, J, Prates Pereira, A, Mills-Lamptey, B, Benjamin, J, and Chuck, CJ (2019), "Conceptualization of a spent coffee grounds biorefinery: A review of existing valorisation approaches" *Food and Bioproducts Processing*, 118, 149-166.

Massebo, F, Tadesse, M, Bekele, T, Balkew, M, and Gebre-Michael, T (2009), "Evaluation on larvicidal effects of essential oils of some local plants against Anopheles arabiensis Patton and Aedes aegypti Linnaeus (Diptera, Culicidae) in Ethiopia" *African Journal of Biotechnology*, 8(17), 4183-4188.

Mavundza, EJ, Chukwujekwu, JC, Maharaj, R, Finnie, JF, Van Heerden, FR, and Van Staden, J (2016), "Identification of compounds in Olax dissitiflora with larvacidal effect against Anopheles arabiensis" *South African Journal of Botany*, 102, 1-3.

Mavundza, EJ, Maharaj, R, Chukwujekwu, JC, Finnie, JF, and Van Staden, J (2013), "Larvicidal activity against Anopheles arabiensis of 10 South African plants that are traditionally used as mosquito repellents" *South African Journal of Botany*, 88, 86-89.

Mburu, MM, Mzilahowa, T, Amoah, B, Chifundo, D, Phiri, KS, van den Berg, H, Takken, W, and McCann, RS (2019), "Biting patterns of malaria vectors of the lower Shire valley, southern Malawi" *Acta Tropica*, 197, 105059.

McClements, DJ (2012), "Nanoemulsions versus microemulsions: terminology, differences, and similarities" *Soft Matter*, 8(6), 1719-1729.

McNutt, J, and He, Q (2019), "Spent coffee grounds: A review on current utilization" *Journal of Industrial and Engineering Chemistry*, 71, 78-88.

Mdoe, FP, Cheng, S-S, Msangi, S, Nkwengulila, G, Chang, S-T, and Kweka, EJ (2014), "Activity of Cinnamomum osmophloeum leaf essential oil against Anopheles gambiae s.s" *Parasites & vectors*, 7, 209.

Meng, Q, and Yan, H (2017), "Theoretical study on the topotactic transformation and memory effect of M (II) M (III)-layered double hydroxides" *Molecular Simulation*, 43(13-16), 1338-1347.

Mharakurwa, S, Thuma, PE, Norris, DE, Mulenga, M, Chalwe, V, Chipeta, J, Munyati, S, Mutambu, S, and Mason, PR (2012), "Malaria epidemiology and control in Southern Africa" *Acta Tropica*, 121(3), 202-206.

Michaelakis, A, Vidali, VP, Papachristos, DP, Pitsinos, EN, Koliopoulos, G, Couladouros, EA, Polissiou, MG, and Kimbaris, AC (2014), "Bioefficacy of acyclic monoterpenes and their saturated derivatives against the West Nile vector Culex pipiens" *Chemosphere*, 96, 74-80.

Mishra, B, and Pandit, JK (1990), "Multiple water-oil-water emulsions as prolonged release formulations of pentazocine" *Journal of Controlled Release*, 14(1), 53-60.

Mishra, G, Dash, B, and Pandey, S (2018), "Layered double hydroxides: A brief review from fundamentals to application as evolving biomaterials" *Applied Clay Science*, 153, 172-186.

Mittal, J (2021), "Recent progress in the synthesis of Layered Double Hydroxides and their application for the adsorptive removal of dyes: A review" *Journal of Environmental Management*, 295, 113017.

Miyata, S (1983), "Anion-exchange properties of hydrotalcite-like compounds" *Clays and Clay minerals*, 31(4), 305-311.

Mohammadi Nafchi, A, Moradpour, M, Saeidi, M, and Alias, AK (2013), "Thermoplastic starches: Properties, challenges, and prospects" *Starch - Stärke*, 65(1-2), 61-72.

Mondal, S, Dasgupta, S, and Maji, K (2016), "MgAl- Layered Double Hydroxide Nanoparticles for controlled release of Salicylate" *Materials Science and Engineering: C*, 68, 557-564.

Mondragón, M, Arroyo, K, and Romero-García, J (2008), "Biocomposites of thermoplastic starch with surfactant" *Carbohydrate Polymers*, 74(2), 201-208.

Montero, B, Rico, M, Rodríguez-Llamazares, S, Barral, L, and Bouza, R (2017), "Effect of nanocellulose as a filler on biodegradable thermoplastic starch films from tuber, cereal and legume" *Carbohydrate Polymers*, 157, 1094-1104.

Mouatcho, J, Cornel, AJ, Dahan-Moss, Y, Koekemoer, LL, Coetzee, M, and Braack, L (2018), "Detection of Anopheles rivulorum-like, a member of the Anopheles funestus group, in South Africa" *Malaria Journal*, 17, 195.

Muema, JM, Njeru, SN, Colombier, C, and Marubu, RM (2016), "Methanolic extract of Agerantum conyzoides exhibited toxicity and growth disruption activities against Anopheles gambiae sensu stricto and Anopheles arabiensis larvae" *BMC complementary and alternative medicine*, 16(1), 475.

Mussatto, SI, Machado, EiMS, and Teixeira, JeA (2011), "Production, Composition, and Application of Coffee and Its Industrial Residues" *Food and Bioprocess Technology*, 4(5), 661-672.

Nanyonga, SK, Opoku, A, Lewu, FB, and Oyedeji, AO (2012), "Chemical Composition and Larvicidal Activity of the Essential Oil of Tarchonanthus camphoratus Against Anopheles arabiensis Mosquito Larvae" *Journal of Essential Oil Bearing Plants*, 15(2), 288-295.

Nessi, V, Falourd, X, Maigret, J-E, Cahier, K, D'Orlando, A, Descamps, N, Gaucher, V, Chevigny, C, and Lourdin, D (2019), "Cellulose nanocrystals-starch nanocomposites produced by extrusion: Structure and behavior in physiological conditions" *Carbohydrate Polymers*, 225, 115123.

Ng'etich, WK, and Martincigh, BS (2021), "A critical review on layered double hydroxides: Their synthesis and application in sunscreen formulations" *Applied Clay Science*, 208, 106095.

Nhlapo, N, Motumi, T, Landman, E, Verryn, SMC, and Focke, WW (2008), "Surfactant-assisted fatty acid intercalation of layered double hydroxides" *Journal of Materials Science : Full Set - Includes `Journal of Materials Science Letters'*, 43(3), 1033-1043.

NICD (2019), "Malaria Elimination Strategic Plan for South Africa 2019-2023", National Institute for Communicable Diseases (NICD), National Department of Health, Johannesburg, South Africa, https://www.nicd.ac.za/diseases-a-z-index/malaria/, [Accessed: 2021-11-12].

Niu, S, Zhou, Y, Yu, H, Lu, C, and Han, K (2017), "Investigation on thermal degradation properties of oleic acid and its methyl and ethyl esters through TG-FTIR" *Energy Conversion and Management*, 149, 495-504.

Niu, Y, and Li, H (2012), "Controlled Release of Urea Encapsulated by Starch-g-poly(vinyl acetate)" *Industrial & Engineering Chemistry Research*, 51(38), 12173-12177.

Nkya, TE, Fillinger, U, Sangoro, OP, Rose, M, Chanda, E, and Clifford Maina, M (2022), "Six decades of malaria vector control in southern Africa: a review of the entomological evidence-base" *Malaria Journal*, 21, 1-16

Ortega-Toro, R, Jiménez, A, Talens, P, and Chiralt, A (2014), "Effect of the incorporation of surfactants on the physical properties of corn starch films" *Food Hydrocolloids*, 38, 66-75.

Osanloo, M, Amani, A, Sereshti, H, Abai, MR, Esmaeili, F, and Sedaghat, MM (2017), "Preparation and optimization nanoemulsion of Tarragon (Artemisia dracunculus) essential oil as effective herbal larvicide against Anopheles stephensi" *Industrial Crops and Products*, 109, 214-219.

Pagalan Jr, E, Sebron, M, Gomez, S, Salva, SJ, Ampusta, R, Macarayo, AJ, Joyno, C, Ido, A, and Arazo, R (2020), "Activated carbon from spent coffee grounds as an adsorbent for treatment of water contaminated by aniline yellow dye" *Industrial Crops and Products*, 145, 111953.

Pantoja, SS, da Conceição, LRV, da Costa, CEF, Zamian, JR, and da Rocha Filho, GN (2013), "Oxidative stability of biodiesels produced from vegetable oils having different degrees of unsaturation" *Energy Conversion and Management*, 74, 293-298.

Pavela, R (2015), "Essential oils for the development of eco-friendly mosquito larvicides: A review" *Industrial Crops and Products*, 76, 174-187.

Pavela, R, Benelli, G, Pavoni, L, Bonacucina, G, Cespi, M, Cianfaglione, K, Bajalan, I, Morshedloo, MR, Lupidi, G, Romano, D, Canale, A, and Maggi, F (2019a), "Microemulsions for delivery of Apiaceae essential oils—Towards highly effective and eco-friendly mosquito larvicides?" *Industrial Crops and Products*, 129, 631-640.

Pavela, R, Maggi, F, Iannarelli, R, and Benelli, G (2019b), "Plant extracts for developing mosquito larvicides: From laboratory to the field, with insights on the modes of action" *Acta Tropica*, 193, 236-271.

Perumalsamy, H, Jang, MJ, Kim, J-R, Kadarkarai, M, and Ahn, Y-J (2015), "Larvicidal activity and possible mode of action of four flavonoids and two fatty acids identified in Millettia pinnata seed toward three mosquito species" *Parasites & vectors*, 8(1), 237.

Phillips, J, Venter, J-L, Atanasova, M, Wesley-Smith, J, Oosthuizen, H, Emmambux, MN, Du Toit, EL, and Focke, WW (2020), "Dextrin Nanocomposites as Matrices for Solid Dosage Forms" *ACS Applied Materials & Interfaces*, 12(14), 16969-16977.

Piplani, M, Bhagwat, DP, Singhvi, G, Sankaranarayanan, M, Balana-Fouce, R, Vats, T, and Chander, S (2019), "Plant-based larvicidal agents: An overview from 2000 to 2018" *Experimental Parasitology*, 199, 92-103.

Pisoschi, AM, Pop, A, Iordache, F, Stanca, L, Predoi, G, and Serban, AI (2021), "Oxidative stress mitigation by antioxidants - An overview on their chemistry and influences on health status" *European Journal of Medicinal Chemistry*, 209, 112891.

Poonoosamy, J, Brandt, F, Stekiel, M, Kegler, P, Klinkenberg, M, Winkler, B, Vinograd, V, Bosbach, D, and Deissmann, G (2018), "Zr-containing layered double hydroxides: Synthesis, characterization, and evaluation of thermodynamic properties" *Applied Clay Science*, 151, 54-65.

Pozo, C, Rodríguez-Llamazares, S, Bouza, R, Barral, L, Castaño, J, Müller, N, and Restrepo, I (2018), "Study of the structural order of native starch granules using combined FTIR and XRD analysis" *Journal of Polymer Research*, 25(12), 266.

Premaratne, WAPJ, Priyadarshana, WMGI, Gunawardena, SHP, and De Alwis, AAP (2014), "Synthesis of Nanosilica from Paddy Husk Ash and Their Surface Functionalization" *Journal of Science of the University of Kelaniya Sri Lanka*, 8, 33.

Primaz, CT, Schena, T, Lazzari, E, Caramão, EB, and Jacques, RnA (2018), "Influence of the temperature in the yield and composition of the bio-oil from the pyrolysis of spent coffee grounds: Characterization by comprehensive two dimensional gas chromatography" *Fuel*, 232, 572-580.

114

Pullen, J, and Saeed, K (2012), "An overview of biodiesel oxidation stability" *Renewable and Sustainable Energy Reviews*, 16(8), 5924-5950.

Pushpadass, HA, Kumar, A, Jackson, DS, Wehling, RL, Dumais, JJ, and Hanna, MA (2009), "Macromolecular Changes in Extruded Starch-Films Plasticized with Glycerol, Water and Stearic Acid" *Starch - Stärke*, 61(5), 256-266.

Pushpadass, HA, Marx, DB, and Hanna, MA (2008), "Effects of Extrusion Temperature and Plasticizers on the Physical and Functional Properties of Starch Films" *Starch - Stärke*, 60(10), 527-538.

Qiao, X, Tang, Z, and Sun, K (2011), "Plasticization of corn starch by polyol mixtures" *Carbohydrate Polymers*, 83(2), 659-664.

Rahman, MS, Rahman, MA, and Nabi, MN (2003), "Ternary liquid equilibria of ethanol - water - oleyl alcohol and ethanol - water - oleic acid systems" *Pakistan journal of scientific and industrial research.*, 46(Part 6), 409-413.

Rahuman, AA, Venkatesan, P, and Gopalakrishnan, G (2008), "Mosquito larvicidal activity of oleic and linoleic acids isolated from Citrullus colocynthis (Linn.) Schrad" *Parasitology research*, 103(6), 1383-1390.

Rajesh Banu, J, Kavitha, S, Yukesh Kannah, R, Dinesh Kumar, M, Preethi, Atabani, AE, and Kumar, G (2020), "Biorefinery of spent coffee grounds waste: Viable pathway towards circular bioeconomy" *Bioresource Technology*, 302, 122821.

Raman, J, Morris, N, Frean, J, Brooke, B, Blumberg, L, Kruger, P, Mabusa, A, Raswiswi, E, Shandukani, B, Misani, E, Groepe, MA, and Moonasar, D (2016), "Reviewing South Africa's malaria elimination strategy (2012-2018): Progress, challenges and priorities" *Malaria Journal*, 15, 438.

Ramos, TCPM, Santos, EPS, Ventura, M, Pina, JC, Cavalheiro, AA, Fiorucci, AR, and Silva, MS (2021), "Eugenol and TBHQ antioxidant actions in commercial biodiesel obtained by soybean oil and animal fat" *Fuel,* 286(1), 119374.

Ranson, H, and Lissenden, N (2016), "Insecticide Resistance in African Anopheles Mosquitoes: A Worsening Situation that Needs Urgent Action to Maintain Malaria Control" *Trends in Parasitology*, 32(3), 187-196.

Rathore, S, Mukim, M, Sharma, P, Devi, S, Nagar, JC, and Khalid, M (2020), "Curcumin: A review for health benefits" *Int. J. Res. Rev*, 7(1), 273-290.

Rattan, RS (2010), "Mechanism of action of insecticidal secondary metabolites of plant origin" *Crop Protection*, 29(9), 913-920.

Reis, DR, Ambrosi, A, and Luccio, MD (2022), "Encapsulated essential oils: A perspective in food preservation" *Future Foods*, 5, 100126.

Research & Markets (2021), "Global Organic Coffee Market", Report, Research and Markets, Dublin, Ireland, https://www.researchandmarkets.com/reports/5310305/global-organic-coffee-market-2020-2030-by#:~:text=Global%20organic%20coffee%20market%20will,for%20confectionery%20and%20bakery%20products., 1-163, [Accessed: 2021-11-12]

Rico, M, Rodríguez-Llamazares, S, Barral, L, Bouza, R, and Montero, B (2016), "Processing and characterization of polyols plasticized-starch reinforced with microcrystalline cellulose" *Carbohydrate Polymers*, 149, 83-93.

Ritz, C, and Streibig, JC (2005), "Bioassay Analysis using R" *Journal of Statistical Software*, 12(5), 1-22.

Rives, V, del Arco, M, and Martín, C (2014), "Intercalation of drugs in layered double hydroxides and their controlled release: A review" *Applied Clay Science*, 88-89, 239-269.

Rocha, J, del Arco, M, Rives, V, and Ulibarri, MA (1999), "Reconstruction of layered double hydroxides from calcined precursors: a powder XRD and ^{27}Al MAS NMR study" *Journal of Materials Chemistry*, 9(10), 2499.

Rol, F, Belgacem, MN, Gandini, A, and Bras, J (2019), "Recent advances in surface-modified cellulose nanofibrils" *Progress in Polymer Science*, 88, 241-264.

Roy, Ad, Forano, C, Malki, KE, and Besse, J-P (1992), Anionic clays: trends in pillaring chemistry. In: Ocelli, Robson M.L., H.E (eds) *Expanded Clays and Other Microporous*

116

Solids. Springer, Boston, MA, 108-169, DOI: https://doi.org/10.1007/978-1-4684-8866-1_7

Rozendaal, JA (1997), *Vector Control : Methods for Use by Individuals and Communities*, World Health Organization, Geneva, Switzerland, ISBN 92 4 154494 5, 10-17.

Saberian, M, Li, J, Donnoli, A, Bonderenko, E, Oliva, P, Gill, B, Lockrey, S, and Siddique, R (2021), "Recycling of spent coffee grounds in construction materials: A review" *Journal of Cleaner Production*, 289, 125837.

Sagnou, M, Mitsopoulou, KP, Koliopoulos, G, Pelecanou, M, Couladouros, EA, and Michaelakis, A (2012), "Evaluation of naturally occurring curcuminoids and related compounds against mosquito larvae" *Acta Tropica*, 123(3), 190-195.

Saliba, D, and Al-Ghoul, M (2016), "Stability and particle size control of self-assembled cadmium–aluminum layered double hydroxide" *CrystEngComm*, 18(43), 8445-8453.

Samoraj, M, Mironiuk, M, Witek-Krowiak, A, Izydorczyk, G, Skrzypczak, D, Mikula K, Baśladyńska, S, Moustakas, K, and Chojnacka, K (2022), "Biochar in environmental friendly fertilizers - Prospects of development products and technologies" *Chemosphere*, 296, 133975.

Santos, JS, Craig, APL, Santana, JMO, Santos, AF, Heredia, MF, Franceschi, E, Dariva, C, and Corazza, ML (2015), "Liquid-Liquid Equilibrium for Ternary Systems Containing Water, Oleic Acid, and Alcohols at 313.15 K. Effect of Alcohol Chain Length" *Journal of Chemical and Engineering Data*, 60(7), 2050-2056.

Santos, SR, Silva, VB, Melo, MA, Barbosa, JD, Santos, RL, de Sousa, DP, and Cavalcanti, SC (2010), "Toxic effects on and structure-toxicity relationships of phenylpropanoids, terpenes, and related compounds in Aedes aegypti larvae" *Vector-Borne and Zoonotic Diseases*, 10(10), 1049-1054.

Santos, SRL, Melo, MA, Cardoso, AV, Santos, RLC, de Sousa, DP, and Cavalcanti, SCH (2011), "Structure–activity relationships of larvicidal monoterpenes and derivatives against Aedes aegypti Linn" *Chemosphere*, 84(1), 150-153.

Šárka, E, and Dvořáček, V (2017), "New processing and applications of waxy starch (a review)" *Journal of Food Engineering*, 206, 77-87.

Sasai, R, Sato, H, Sugata, M, Fujimura, T, Ishihara, S, Deguchi, K, Ohki, S, Tansho, M, Shimizu, T, Oita, N, Numoto, M, Fujii, Y, Kawaguchi, S, Matsuoka, Y, Hagura, K, Abe, T, and Moriyoshi, C (2019), "Why Do Carbonate Anions Have Extremely High Stability in the Interlayer Space of Layered Double Hydroxides? Case Study of Layered Double Hydroxide Consisting of Mg and Al (Mg/Al = 2)" *Inorganic chemistry*, 58(16), 10928-10935.

Scheibel, EG (1954), "Correspondence. Liquid Diffusivities. Viscosity of Gases" *Industrial & Engineering Chemistry*, 46(9), 2007-2008.

Senthil-Nathan, S (2020), "A Review of Resistance Mechanisms of Synthetic Insecticides and Botanicals, Phytochemicals, and Essential Oils as Alternative Larvicidal Agents Against Mosquitoes" *Frontiers in Physiology*, 10, 1591.

Sepúlveda-Cadavid, C, Romero, JH, Torres, M, Becerra-Agudelo, E, and López, JE (2021), "Evaluation of a Biochar-Based Slow-Release P Fertilizer to Improve Spinacia oleracea P Use, Yield, and Nutritional Quality" *Journal of Soil Science and Plant Nutrition*, 21(4), 2980-2992.

Serqueira, DS, Dornellas, RM, Silva, LG, de Melo, PG, Castellan, A, Ruggiero, R, Richter, EM, and Munoz, RAA (2015), "Tetrahydrocurcuminoids as potential antioxidants for biodiesels" *Fuel*, 160, 490-494.

Service, MW (1980), *A guide to medical entomology*, Macmillan International College Editions, London, UK, ISBN 978-0-333-23382-5, 44-52.

Shaalan, EA-S, Canyon, D, Younes, MWF, Abdel-Wahab, H, and Mansour, A-H (2005), "A review of botanical phytochemicals with mosquitocidal potential" *Environment International*, 31(8), 1149-1166.

Shamai, K, Shimoni, E, and Bianco-Peled, H (2004), "Small angle X-ray scattering of resistant starch type III" *Biomacromolecules*, 5(1), 219-223.

Sharma, A, Thakur, M, Bhattacharya, M, Mandal, T, and Goswami, S (2019a), "Commercial application of cellulose nano-composites – A review" *Biotechnology Reports*, 21, e00316.

Sharma, UC, Chandra, AK, and Sachan, S (2019b), "Investigation on thermo-oxidative stability of karanja oil derived biolubricant base oil" *Asian Journal of Chemistry*, 31(4), 839-844.

Shi, R, Zhang, Z, Liu, Q, Han, Y, Zhang, L, Chen, D, and Tian, W (2007), "Characterization of citric acid/glycerol co-plasticized thermoplastic starch prepared by melt blending" *Carbohydrate Polymers*, 69(4), 748-755.

Sigamani, S, Chinnasamy, R, Dharmaraj, RK, Ramamurthy, D, Devarajan, N, Narayanasamy, M, and Natarajan, H (2020), "Larvicidal potency of the extracts from Chlorella sp. against Aedes aegypti" *Biocatalysis and Agricultural Biotechnology*, 27, 101663.

Silva, LLdS, Fernandes, KM, Miranda, FR, Silva, SCC, Coelho, LCBB, Navarro, DMdAF, Napoleão, TH, Martins, GF, and Paiva, PMG (2019), "Exposure of mosquito (Aedes aegypti) larvae to the water extract and lectin-rich fraction of Moringa oleifera seeds impairs their development and future fecundity" *Ecotoxicology and Environmental Safety*, 183, 109583.

Singh, M, Suryanshu, Kanika, Singh, G, Dubey, A, and Chaitanya, RK (2021), "Plasmodium's journey through the Anopheles mosquito: A comprehensive review" *Biochimie*, 181, 176-190.

Stolp, LJ, and Kodali, DR (2022), Chapter 2 - Naturally occurring high-oleic oils: Avocado, macadamia, and olive oils. *In:* Flider, FJ (ed.) *High Oleic Oils.* AOCS Press, 7-52.

Sun, S, Hong, Y, Gu, Z, Cheng, L, Li, Z, and Li, C (2019), "An investigation into the structure and digestibility of starch-oleic acid complexes prepared under various complexing temperatures" *International Journal of Biological Macromolecules*, 138, 966-974.

119

Tadros, T (2004), "Application of rheology for assessment and prediction of the long-term physical stability of emulsions" *Advances in Colloid and Interface Science*, 108-109, 227-258.

Tadros, TF (2013), *Emulsion Formation and Stability,* John Wiley & Sons, United Kingdom, ePDF ISBN: 978-3-527-64797-2, 1-76.

Tattersfield, F, and Gimingham, CT (1927), "STUDIES ON CONTACT INSECTICIDES : PART VI. THE INSECTICIDAL ACTION OF THE FATTY ACIDS, THEIR METHYL ESTERS AND SODIUM AND AMMONIUM SALTS" *Annals of Applied Biology*, 14(3), 331-358.

Theiss, FL, Ayoko, GA, and Frost, RL (2016), "Synthesis of layered double hydroxides containing Mg2+, Zn2+, Ca2+ and Al3+ layer cations by co-precipitation methods—A review" *Applied Surface Science*, 383, 200-213.

Thirumal, V, Yuvakkumar, R, Ravi, G, Dineshkumar, G, Ganesan, M, Alotaibi, SH, and Velauthapillai, D (2022), "Characterization of activated biomass carbon from tea leaf for supercapacitor applications" *Chemosphere*, 291, 132931.

Thomas, A, Mazigo, HD, Manjurano, A, Morona, D, and Kweka, EJ (2017), "Evaluation of active ingredients and larvicidal activity of clove and cinnamon essential oils against Anopheles gambiae (sensu lato)" *Parasites & vectors*, 10(1), 411.

Tiozon, RJN, Bonto, AP, and Sreenivasulu, N (2021), "Enhancing the functional properties of rice starch through biopolymer blending for industrial applications: A review" *International Journal of Biological Macromolecules*, 192, 100-117.

Tongcumpou, C, Usapein, P, and Tuntiwiwattanapun, N (2019), "Complete utilization of wet spent coffee grounds waste as a novel feedstock for antioxidant, biodiesel, and bio-char production" *Industrial Crops and Products*, 138, 111484.

van der Westhuizen, IH, and Focke, WW (2018), "Stabilizing sunflower biodiesel with synthetic antioxidant blends" *Fuel*, 219, 126-131.

van Soest, JJG, Hulleman, SHD, de Wit, D, and Vliegenthart, JFG (1996), "Crystallinity in starch bioplastics" *Industrial Crops and Products*, 5(1), 11-22.

120

Varatharajan, K, and Pushparani, DS (2018), "Screening of antioxidant additives for biodiesel fuels" *Renewable and Sustainable Energy Reviews*, 82, 2017-2028.

Vieira, MGA, da Silva, MA, dos Santos, LO, and Beppu, MM (2011), "Natural-based plasticizers and biopolymer films: A review" *European Polymer Journal*, 47(3), 254-263.

Vorum, H, Brodersen, R, Kragh-Hansen, U, and Pedersen, AO (1992), "Solubility of long-chain fatty acids in phosphate buffer at pH 7.4" *Biochimica et Biophysica Acta (BBA)/Lipids and Lipid Metabolism*, 1126(2), 135-142.

Wang, C, Luo, D, Zhang, X, Huang, R, Cao, Y, Liu, G, Zhang, Y, and Wang, H (2022), "Biochar-based slow-release of fertilizers for sustainable agriculture: A mini review" *Environmental Science and Ecotechnology*, 10, 100167.

Wang, S, Li, C, Copeland, L, Niu, Q, and Wang, S (2015), "Starch retrogradation: A comprehensive review" *Comprehensive Reviews in Food Science and Food Safety*, 14(5), 568-585.

Washington, C (1996), "Stability of lipid emulsions for drug delivery" *Advanced Drug Delivery Reviews*, 20(2), 131-145.

Westhuizen, IH (2017), *Stabilising sunflower biodiesel with synthetic antioxidants*, PhD Thesis, University of Pretoria, Pretoria.

World Health, O (2005a), "Guidelines for laboratory and field testing of mosquito larvicides", World Health Organization, Geneva, Switzerland, https://apps.who.int/iris/handle/10665/69101, Document Number: WHO/CDS/WHOPES/GCDPP/2005.13, 31 pages, [Accessed: 2021-12-10].

World Health, O (2005b), "Malaria control in complex emergencies : AN INTER-AGENCY FIELD HANDBOOK*"*, World Health Organization, Geneva, Switzerland, ISBN: 92 4 159389X, https://apps.who.int/iris/handle/10665/43383, 239 pages, [Accessed: 2021-12-10].

World Health, O (2013), "Larval Source Management: A supplementary measure for malaria vector control, An Operational Manual", World Health Organization , Geneva,

Switzerland, ISBN: 978 92 4 150560 4, https://apps.who.int/iris/handle/10665/85379, 128 pages, [Accessed: 2021-12-10].

World Health, O (2019), "World Malaria Report 2019", World Health Organization, Report, Geneva, Switzerland, ISBN: 978-92-4-156572-1, https://www.who.int/publications/i/item/9789241565721, 232 pages, [Acceseed: 2019-12-10].

World Health, O (2020), "Malaria Keyfacts", World Health Organisation, Geneva, Switzerland, https://www.who.int/news-room/fact-sheets/detail/malaria, [Accessed: 2020-07-09].

World Health, O (2021), "World Malaria Report 2021", World Health Organisation, Report, Geneva, Switzerland, ISBN: 978-92-4-004049-6, https://www.who.int/publications/i/item/9789240040496, 322 pages, [Accessed: 2021-12-09].

Xie, Y-Y, Hu, X-P, Jin, Z-Y, Xu, X-M, and Chen, H-Q (2014), "Effect of temperature-cycled retrogradation on in vitro digestibility and structural characteristics of waxy potato starch" *International Journal of Biological Macromolecules*, 67, 79-84.

Xu, ZP, Braterman, PS, Yu, K, Xu, H, Wang, Y, and Brinker, CJ (2004), "Unusual Hydrocarbon Chain Packing Mode and Modification of Crystallite Growth Habit in the Self-Assembled Nanocomposites Zinc- Aluminium- Hydroxide Oleate and Elaidate (cis- and trans-[Zn2Al (OH) 6 (CH3 (CH2) 7CH CH (CH2) 7COO-)] and Magnesium Analogues" *Chemistry of Materials*, 16(14), 2750-2756.

Yaakob, Z, Narayanan, BN, Padikkaparambil, S, Unni K, S, and Akbar P, M (2014), "A review on the oxidation stability of biodiesel" *Renewable and Sustainable Energy Reviews*, 35, 136-153.

Yang, W, Fortunati, E, Dominici, F, Giovanale, G, Mazzaglia, A, Balestra, GM, Kenny, JM, and Puglia, D (2016), "Synergic effect of cellulose and lignin nanostructures in PLA based systems for food antibacterial packaging" *European Polymer Journal*, 79, 1-12.

Yang, WD, Li, S, Wu, DY, Spicer, M, Gutowski, V, Shen, SZ, Selected, prpftsISoAS, and Processing Technology for Materials, NWC (2009), "Synthesis of Carboxylic Acids

122

Intercalated Mg-Al Layered Double Hydroxides by a Modified Reconstruction Method" *Advanced Materials Research*, 66, 218-221.

Ye, C, and Chi, H (2018), "A review of recent progress in drug and protein encapsulation: Approaches, applications and challenges" *Materials Science and Engineering: C*, 83, 233-246.

Ye, H, Liu, S, Yu, D, Zhou, X, Qin, L, Lai, C, Qin, F, Zhang, M, Chen, W, Chen, W, and Xiang, L (2022), "Regeneration mechanism, modification strategy, and environment application of layered double hydroxides: Insights based on memory effect" *Coordination Chemistry Reviews*, 450, 214253.

Yeshi, K, and Wangchuk, P (2022), Chapter 11 - Essential oils and their bioactive molecules in healthcare. *In:* Mandal, SC, Nayak, AK, and Dhara, AK (eds.) *Herbal Biomolecules in Healthcare Applications.* Academic Press, 215-237.

Yonguep, E, Kapiamba, KF, Kabamba, KJ, and Chowdhury, M (2022), "Formation, stabilization and chemical demulsification of crude oil-in-water emulsions: A review" *Petroleum Research*, 7(4), 459-472.

Yukuyama, MN, Kato, ETM, de Araujo, GLB, Löbenberg, R, Monteiro, LM, Lourenço, FR, and Bou-Chacra, NA (2019), "Olive oil nanoemulsion preparation using high-pressure homogenization and d-phase emulsification – A design space approach" *Journal of Drug Delivery Science and Technology*, 49, 622-631.

Zhang, C-W, Li, F-Y, Li, J-F, Li, Y-L, Xu, J, Xie, Q, Chen, S, and Guo, A-F (2018), "Novel treatments for compatibility of plant fiber and starch by forming new hydrogen bonds" *Journal of Cleaner Production*, 185, 357-365.

Zhang, Z, and Hill, GA (1991), "Ternary liquid-liquid equilibria of water, ethanol, and oleic acid" *Journal of Chemical & Engineering Data*, 36(4), 453-456.

Zhao, Y, Li, B, Wang, Q, Gao, W, Wang, CJ, Wei, M, Evans, DG, Duan, X, and O'Hare, D (2014), "NiTi-Layered double hydroxides nanosheets as efficient photocatalysts for oxygen evolution from water using visible light" *Chem. Sci.*, 5(3), 951-958.

Zhou, Q, Verney, V, Commereuc, S, Chin, I-J, and Leroux, F (2010a), "Strong interfacial attrition developed by oleate/layered double hydroxide nanoplatelets dispersed into poly(butylene succinate)" *Journal of Colloid and Interface Science*, 349(1), 127-133.

Zhou, X, Baik, B-K, Wang, R, and Lim, S-T (2010b), "Retrogradation of waxy and normal corn starch gels by temperature cycling" *Journal of Cereal Science*, 51(1), 57-65.

Zuraida, A, Yusliza, Y, Anuar, H, and Mohd Khairul Muhaimin, R (2012), "The effect of water and citric acid on sago starch bio-plastics" *International Food Research Journal*, 19(2), 715-719.

APPENDICES

Annexure 1: Dilutions and concentrations

Initial solution		Aliquot (ml)[a]	Final concentration (PPM) in 100 ml
%	PPM		
1.0	10 000.0	1.0	100.0
		0.5	50.0
		0.1	10.0
0.1	1 000.0	1.0	10.0
		0.5	5.0
		0.1	1.0
0.01	100.0	1.0	1.0
		0.5	0.5
		0.1	0.1
0.001	10.0	1.0	0.1
		0.5	0.05
		0.1	0.01
0.0001	1.0	1.0	0.01
		0.5	0.005
		0.1	0.001
0.00001	0.1	1.0	0.001
		0.5	0.0005
		0.1	0.0001

[a] For 200 ml double the volume of aliquots.

Annexure 2: Bioassays data recording forms

Laboratory evaluation of the efficacy of larvicides against mosquito larvae

Experiment No.: _____ Investigator: _____ Location: _____ Treatment date: _____
Material: _____ Formulation: _____ Temp: _____ Lighting: _____
Species: _____ Larval instar: _____ Larvae/cup or vessel: _____
Water: _____ Tap/distilled _____ Volume of water: _____ ml _____ Food: _____ Date stock made: _____

		No. of dead larvae at various conc. (mg/L) post exposure (hr.):												
		24 hr						48 hr						
Date	**Replicate**	**0.00**						**0.00**						
	1													
	2													
	3													
	4													
	5													
	6													
	7													
	8													
	9													
	10													
	11													
	12													
	Total													
	Ave.													
	% mortality													

LC50 (CL 95 %): _____ LC50 (CL 95 %): _____

LC90 (CL 90 %): _____ LC90 (CL 90 %): _____

LC99: _____ LC99: _____

Slope: _____ Heterogeneity: _____ Slope: _____ Heterogeneity: _____

<u>Insectary supervisor signature:</u> ....

126

Annexure 3: Relative humidity of different salts solutions

|	% Relative Humidity								
Temperature (ᵒC)	Lithium Chloride	Potassium Acetate	Magnesium Chloride	Potassium Carbonate	Magnesium Nitrate	Sodium Chloride	Potassium Chloride	Potassium Nitrate	Potassium Sulphate
0	11.23 ± 0.54		33.66 ± 0.33	43.13 ± 0.66	60.35 ± 0.55	75.51 ± 0.34	88.61 ± 0.53	96.33 ± 2.9	98.77 ± 1.1
5	11.26 ± 0.47		33.60 ± 0.28	43.13 ± 0.50	58.86 ± 0.43	75.65 ± 0.27	87.67 ± 0.45	96.27 ± 2.1	98.48 ± 0.91
10	11.29 ± 0.41	23.28 ± 0.53	33.47 ± 0.24	43.14 ± 0.39	57.36 ± 0.33	75.67 ± 0.22	86.77 ± 0.39	95.96 ± 1.4	98.18 ± 0.76
15	11.30 ± 0.35	23.40 ± 0.32	33.30 ± 0.21	43.15 ± 0.33	55.87 ± 0.27	75.61 ± 0.18	85.92 ± 0.33	95.41 ± 0.96	97.89 ± 0.63
20	11.31 ± 0.31	23.11 ± 0.25	33.07 ± 0.18	43.16 ± 0.33	54.38 ± 0.23	75.47 ± 0.14	85.11 ± 0.29	94.62 ± 0.66	97.59 ± 0.53
25	11.30 ± 0.27	25.51 ± 0.32	32.78 ± 0.16	43.16 ± 0.39	52.89 ± 0.22	75.29 ± 0.12	84.34 ± 0.26	93.58 ± 0.55	97.30 ± 0.45
30	11.28 ± 0.24	21.61 ± 0.53	32.44 ± 0.14	43.17 ± 0.50	51.40 ± 0.24	75.09 ± 0.11	83.62 ± 0.25	92.31 ± 0.60	97.00 ± 0.40
35	11.24 ± 0.22		32.05 ± 0.13		49.91 ± 0.29	74.87 ± 0.12	82.95 ± 0.25	90.79 ± 0.83	96.71 ± 0.38
40	11.21 ± 0.21		31.60 ± 0.13		48.42 ± 0.37	74.68 ± 0.13	82.32 ± 0.25	89.03 ± 1.2	96.41 ± 0.38
45	11.16 ± 0.21		31.10 ± 0.13		46.93 ± 0.47	74.52 ± 0.16	81.74 ± 0.28	87.03 ± 1.8	96.12 ± 0.40
50	11.10 ± 0.22		30.54 ± 0.14		45.44 ± 0.60	74.43 ± 0.19	81.20 ± 0.31	84.78 ± 2.5	95.82 ± 0.45
55	11.03 ± 0.23		29.92. ± 0.16			74.41 ± 0.24	80.70 ± 0.35		
60	10.95 ± 0.26		29.26 ± 0.18			74.50 ± 0.30	80.25 ± 0.41		
65	10.86 ± 0.29		28.54 ± 0.21			74.71 ± 0.37	79.85. ± 0.48		
70	10.75 ± 0.33		27.77 ± 0.25			75.06 ± 0.45	79.49 ± 0.57		
75	10.64 ± 0.38		26.94 ± 0.29			75.58 ± 0.55	79.17 ± 0.66		
80	10.51 ± 0.44		26.05 ± 0.34			76.29 ± 0.65	78.90 ± 0.77		
85	10.38 ± 0.51		25.11 ± 0.39				78.68 ± 0.89		
90	10.23 ± 0.59		24.12 ± 0.46				78.50 ± 1.0		
95	10.07 ± 0.67		23.07 ± 0.52						
100	9.90 ± 0.77		21.97 ± 0.60						

Annexure 4:   SEM images calcined LDH (a), and LDH-oleate (b)
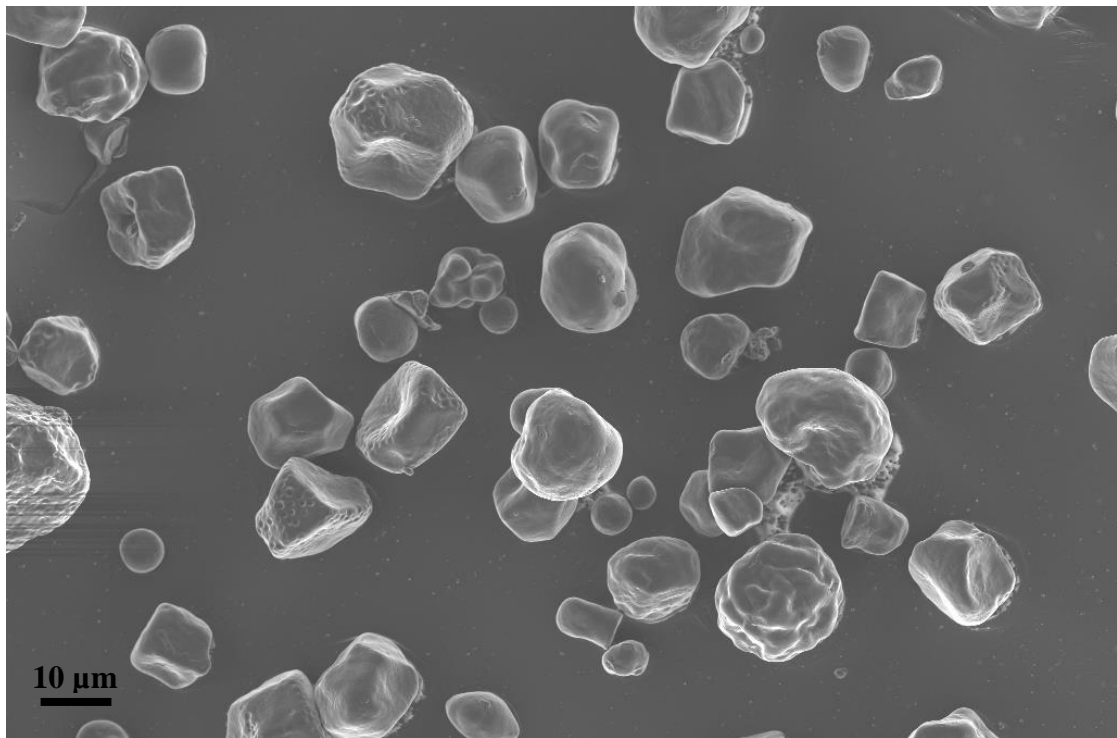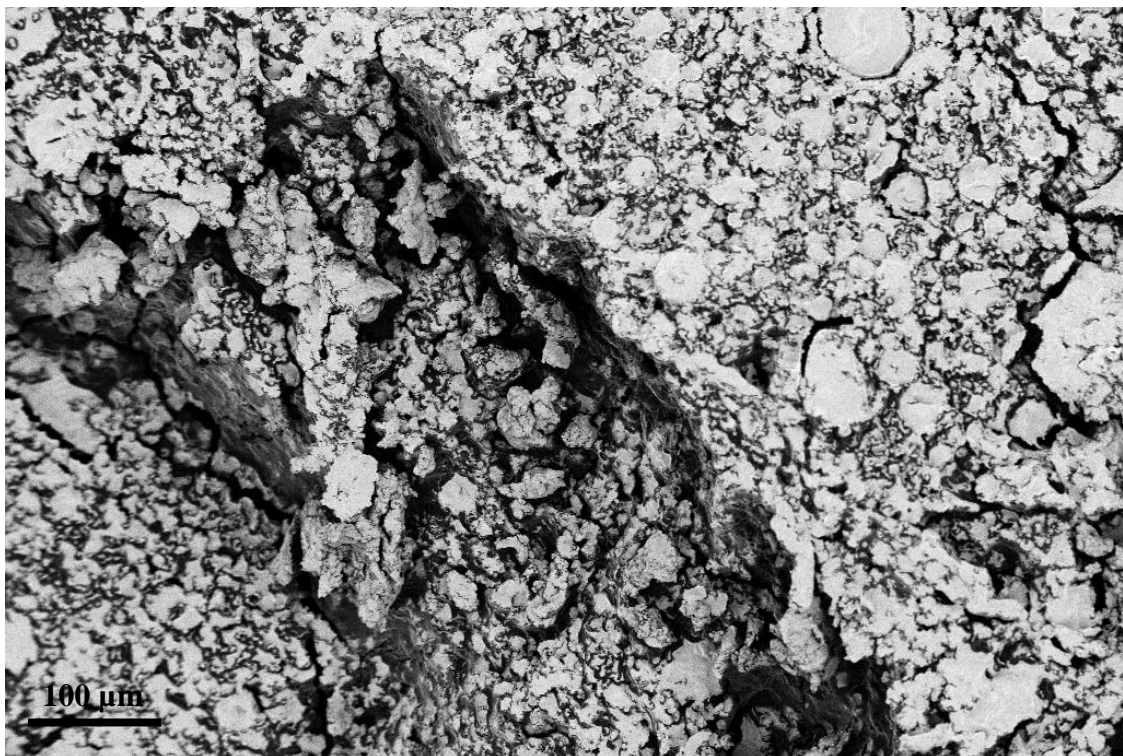
(a)

(b)

128
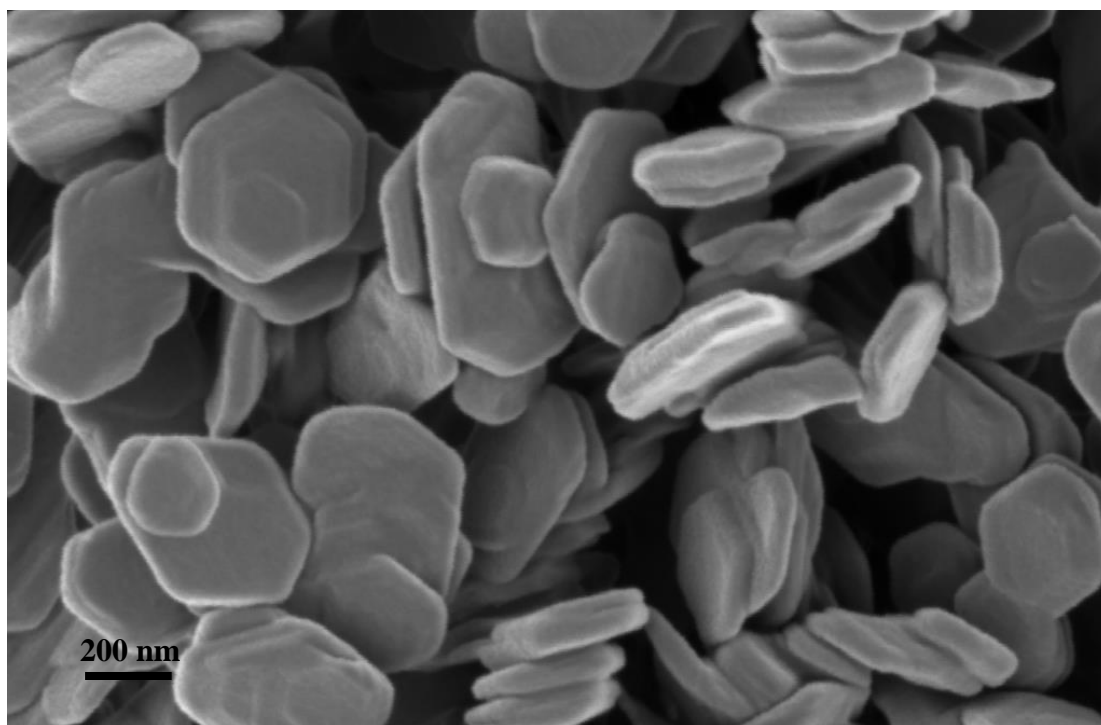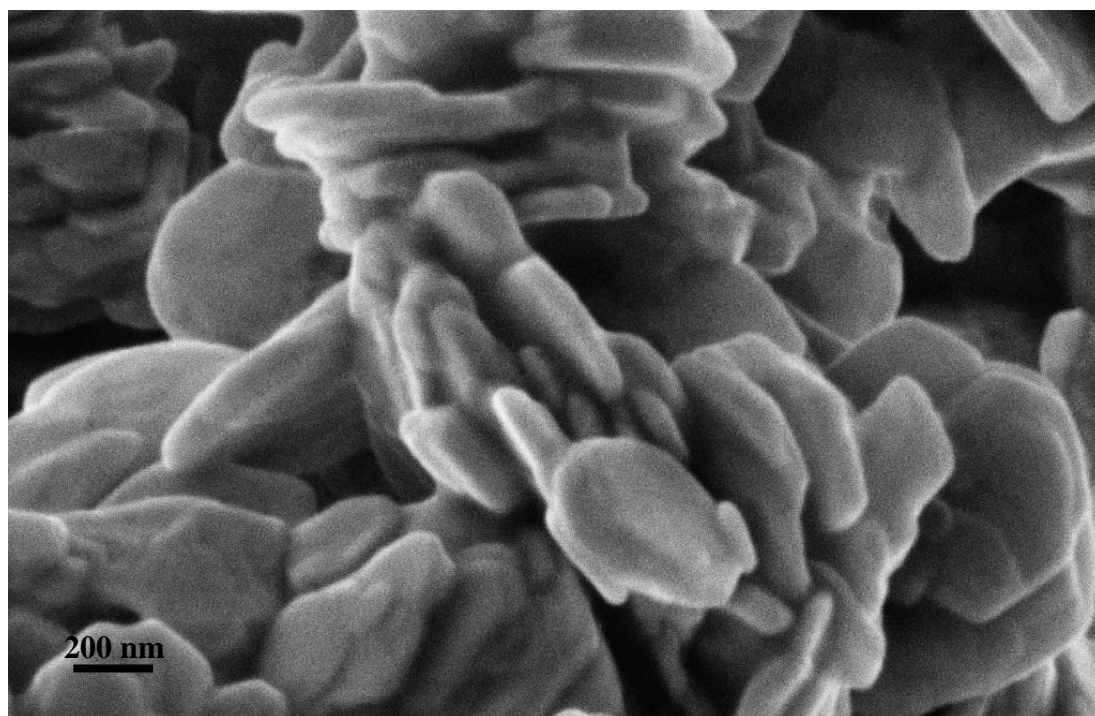
Annexure 5: SEM images dextrin powder (a), oleic acid in starch with 5 wt.% organoclay
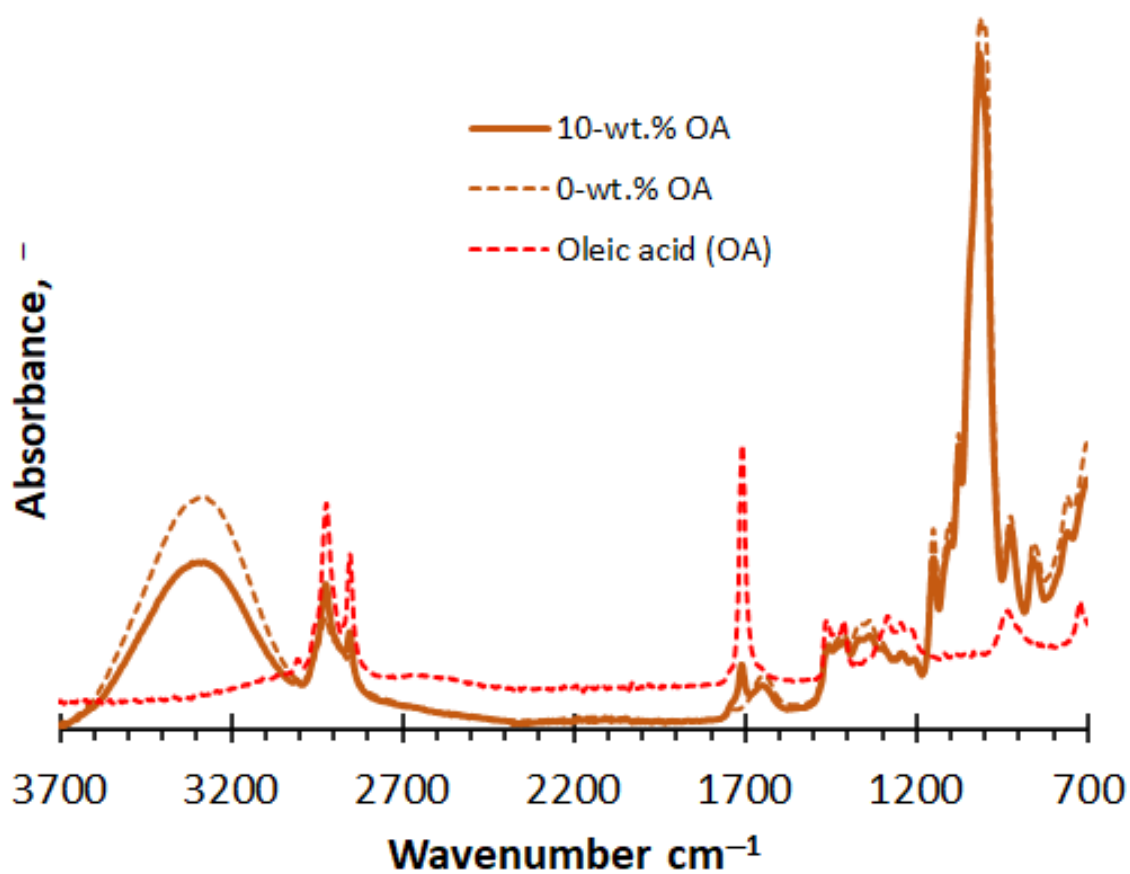
(a)

(b)

Annexure 6: Complete FTIR spectra of pure oleic acid (OA), neat thermoplastic starch and thermoplastic starch with 10 wt.% OA

Annexure 7: Statistical analysis, bioassay results of oleic acid as a free-standing oil

Bioassay Statistical Analysis

M. Theodor Loots
date: "13 December, 2021"

Import Data

```
'data.frame':   168 obs. of  5 variables:
 $ Day        : Factor w/ 3 levels "1","2","3": 1 1 1 1 2 2 2 2 3 3 ...
 $ Replicate  : Factor w/ 4 levels "1","2","3","4": 1 2 3 4 1 2 3 4 1 2 ...
 $ Hour       : Factor w/ 2 levels "24","48": 1 1 1 1 1 1 1 1 1 1 ...
 $ Dosage..ppm: num  0 0 0 0 0 0 0 0 0 0 ...
 $ Proportion : num  0 0 0 0 0 0 0 0 0 0 ...
```

Dose Response Curve

The two dose response curves are considered here, namely, for the 24 and 48 hour curves respectively.

The data is transformed so as to utelise the fact that the observed proportion may be viewed as binomial data. The data is shown below:

Table 4.1: Aggregated data for DRC.

Hour	Dosage	Dead	Total
24	0.0	1	300
24	5.0	22	300
24	7.5	34	300
24	10.0	34	300
24	20.0	58	300
24	30.0	98	300
24	50.0	98	300
48	0.0	4	300
48	5.0	46	300
48	7.5	56	300
48	10.0	110	300
48	20.0	123	300
48	30.0	195	300
48	50.0	222	300

The following six, four-parameter families of distributions were selected, as to specifically restrict the lower limit at zero. These are the four-parameter logistic, Weibull Type I and II, the log-normal, log-logistic and Gompertz.

```
         logLik      IC  Lack of fit
G.4    -61.62074 135.2415 1.242078e-07
L.4    -75.47785 162.9557 1.669243e-11
W2.4  -160.02598 332.0520 2.042789e-04
LL.4  -160.30537 332.6107 1.634249e-04
LN.4  -160.40064 332.8013 1.547902e-04
W1.4  -160.53535 333.0707 1.405549e-04
```

THE AIC was used for model selection, and the model with the lowest AIC was chosen as the best. This turned out to be the Gompertz model. The parameter estimates along with ED/LC 10, 50 and 90 values (with their 95% CI's) are given below:

```
Model fitted: Gompertz (3 parms)

Parameter estimates:

       Estimate Std. Error t-value   p-value
b:24 -0.118441   0.023361 -5.0701 3.976e-07 ***
b:48 -0.107368   0.012862 -8.3477 < 2.2e-16 ***
d:24  0.325624   0.026112 12.4701 < 2.2e-16 ***
d:48  0.723710   0.030885 23.4327 < 2.2e-16 ***
e:24  9.644310   1.288706  7.4837 7.221e-14 ***
e:48  9.896502   0.797521 12.4091 < 2.2e-16 ***
---
Signif. codes:  0 '***' 0.001 '**' 0.01 '*' 0.05 '.' 0.1 ' ' 1
```
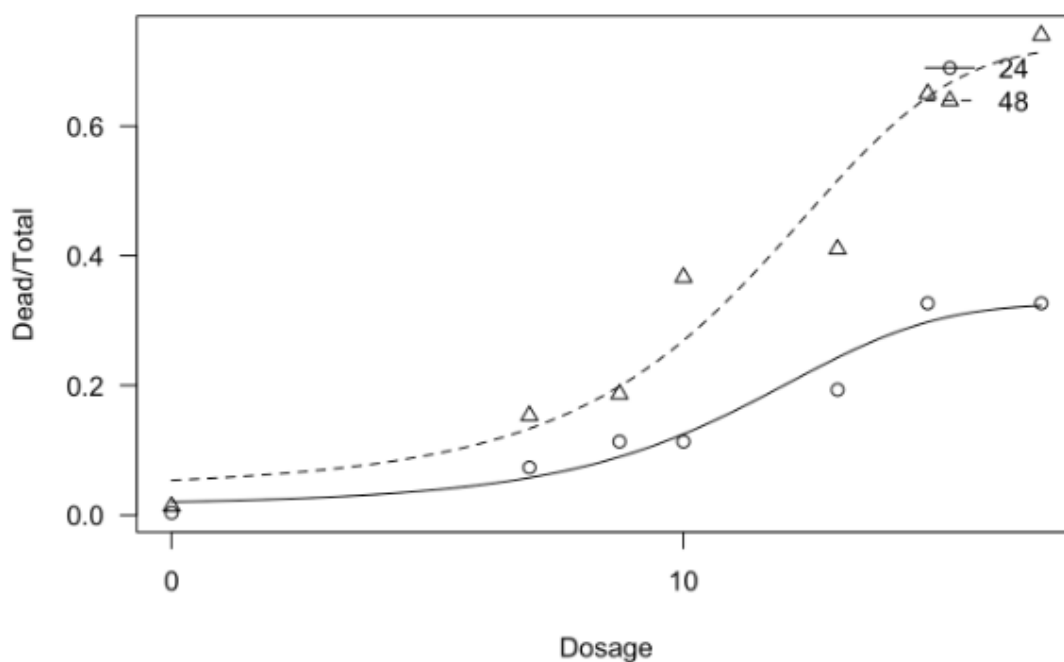


```
Estimated effective doses

         Estimate Std. Error      Lower      Upper
e:24:10   2.60256    2.07220   -1.45888    6.66400
e:24:50  12.73879   23.25370  -32.83763   58.31520
e:24:90  28.64421  139.38622 -244.54777  301.83619
e:48:10   2.12849    1.21320   -0.24933    4.50632
e:48:50  13.31013   15.29531  -16.66813   43.28839
e:48:90  30.85596   98.14084 -161.49655  223.20848
```

A more robust ED/LC estimation may be performed by model averaging the values returned by all 6 models, and are given below.

```
          ED10      ED50      ED90      Weight
G.4   2.6025559 12.73879   28.64421 9.999990e-01
LL.4  3.5976393 24.52882  167.23835 1.386155e-43
L.4   0.7763581 13.86763   26.95890 9.592521e-07
W2.4  2.7235961 15.65064   47.69543 1.832933e-43
W1.4  6.0810870 87.71894 5780.05914 1.101363e-43
LN.4  3.9681852 27.93044  196.59096 1.260189e-43
```

```
          ED10      ED50      ED90      Weight
G.4   2.1284947 13.31013   30.85596 9.999990e-01
LL.4  3.4319284 23.26734  157.74485 1.386155e-43
L.4  -0.3415402 14.43102   29.20357 9.592521e-07
W2.4  2.5968374 16.46467   53.42219 1.832933e-43
W1.4  5.5439163 69.64004 3693.50243 1.101363e-43
LN.4  3.7769884 25.32394  169.79194 1.260189e-43
```

```
          Estimate  Std. Error        Lower        Upper
e:24:10   2.602554    2.183750   -1.6775164     6.882625
e:24:50  12.738787   29.203765  -44.4995401    69.977115
e:24:90  28.644208 1022.102411 -1974.6397068 2031.928123
e:48:10   2.128492    1.414662   -0.6441947     4.901179
e:48:50  13.310129   20.575687  -27.0174759    53.637734
e:48:90  30.855960  665.506938 -1273.5136704 1335.225591
```

Conclusion

The R package "drc" was used for analysing the dose response curves (Christian *et al*, 2015; Ritz & Streibig, 2005).

133

KISUMA CHEMICALS BV   Tel. +31 598 666 766
Billitonweg 7   Fax. +31 598 690 792
9641 KZ Veendam
P.O. Box 400   support@kisuma.com
9640 AK Veendam
The Netherlands

KISUMACHEMICALS DATASHEET

ALCAMIZER 1

Mg-Al Hydrotalcite as heat stabilizer in heavy metal free PVC stabilizer systems

Features:

Suitable for all resins. High heat stability combined with high transparency and no deterioration of the insulating characteristics of PVC. High volume of compounding and good dispersion characteristics. No sulfide polution. Good weatherability and high personal safety.

Specified and Typical Properties:

	Typical value	General specification	
Appearance	Free flowing White powder	-	
Molar ratio MgO/Al_2O_3	4	min 3.7 max 4.6	
Loss on Drying (105C 1 hr)	0.2	max 0.5	w/w%
Specific Surface Area	8	min 5 max 20	m^2/g

Secondary particle size
   Average
 	
   > 5 µm
	0.7	min 0.5
		max 0.8
		0
			µm
			µm
			vol %

Specific Gravity	2.1	-	
Mohs hardness	2.0	-	
Refractive index	1.50	-	
Temp. of commencing dehydration	185	-	^{o}c
Amount of linseed oil absorbed	50	-	ml/100g

KCBV410/0617

134

DELLITE® 43B
Nanoclay for nanocomposites

Description

DELLITE® 43B is a nanoclay deriving from a naturally occurring montmorillonite especially purified and modified with a quaternary ammonium salt (dimethyl benzylhydrogenated tallow ammonium).

DELLITE® 43B is an additive for polymer application, used to improve various physical and thermo-mechanical properties.

Applications

- Polyolefins
- Polyester
- Polystyrene
- Ethylene Vinyl Acetate
- Polyamides
- Epoxy and acrylic resins
- Rubbers and Elastomers
- (...)

Advantages of Dellite® 43B in Polymeric Systems

- Oxygen, CO_2 and water vapour barrier
- Thermal stability
- Stiffness
- Melt fracture reduction
- Solvent/Chemical resistance
- Weight reduction
- Fiberglas reduction
- Rheology control
- UV transmission
- Flame retardant and Antidropping
- (...)

Chemical and physical data

		DELLITE® 43B
Colour		off white
Moisture	%	3 (max)
Loss of ignition	weight %	32 – 35
Particle size (dry)	micron	7-9 (medium)
Particle size after dispersion	nm	1x500 (medium)
Modifier		dimethyl benzylhydrogenated tallow ammonium
Specific weight	g/cc	1.6
Bulk density	g/cc	0.40

Incorporation

- **Thermoplastic Systems**

According to the application the incorporation of Dellite® 43B into a thermoplastic system is usually carried out as follows:

a) Adding up to 50% of Dellite® 43B in a masterbatch and diluting the master in the final compound
b) Adding directly the Dellite® 43B to the compound.

- **Thermoset Systems**

The incorporation of Dellite® 43B into a thermoset system may be obtained using the following methods:

a) Mixing the desired amount of Dellite® with the resin. Then the curing agent and other additives may be added.
b) Mixing the desired amount of Dellite® with the curing agent. Then the resin and other additives may be added.
c) Resin, curing agent and additives are mixed and then Dellite® 43B is added.

Dosage

The typical levels of use are included in the range 1- 5% based on total system weight .

Storage Stability and Packing

Product does not deteriorate in a significant way in a twelve months period.
Storage is advisable in a dry sheltered place in closed bags.
Packing is 25kg net paper bags on wood pallets of 1200kg each. Different packing is possible if required.

All information contained here in is believed to be accurate but is not warranted. It doesn't represent any assurance of properties and fitness for use of the product. Above mentioned specifications may be changed without any notice.

LAVIOSA CHIMICA MINERARIA S.p.A.

I-57123 LIVORNO • Via Leonardo da Vinci, 21
Tel. (+39) 0586 434000 - Fax (+39) 0586 410852
www.laviosa.it • E-mail: additives@laviosa.it

COMPANY
WITH QUALITY SYSTEM
CERTIFIED BY DNV
=ISO 9001/2000=

TongaatHulett
Starch

Certificate of Analysis

Stydex White Dextrin 072012 - 25Kg Bag

Meyerton Mill
Johan Le Roux Road,Meyerton,1961
Phone: 016 3607000
Fax: 016 3607100
AN ISO 9001 Certified Company

Customer	TONGAAT HULETT STARCH HO TECH LAB
Customer No	110039
Order Number	
Material Number	100172
Delivery item	
Date	09.09.2020

Manufacture Date: 16.03.2020
Best Before Date: 16.03.2022
Batch Number   M7652

Approved by **Wallie Walther, on 19.03.2020 at 09:48:51**

Characteristic	Unit	Value	Lower Limit	Upper Limit
Moisture	%	7.0		7.0
Blattman Vi 20% dbs	s	13.0	13.0	18.0
Grits (150 micron)	%	0.0		0.3
NSR		Pass		
pH		2.7	2.5	3.5
Solubility	%	17.8	10.0	20.0
Whiteness Index(Colour-Hunte	hu	82.4	69.0	

Country of Origin: SOUTH AFRICA.

136